Hybrid Torsional Damper for Semi-Active Control of Torsional Vibrations in Rotating Machines

Ehab Mohamed Said Abouobaia

A Thesis

In The Department

of

Mechanical and Industrial Engineering

Presented In Partial Fulfillment of the Requirements

For The Degree of

Doctor of Philosophy (Mechanical Engineering) at

Concordia University

Montreal, Quebec, Canada

November 2014

CONCORDIA UNIVERSITY
SCHOOL OF GRADUATE STUDIES

This is to certify that the thesis prepared

By: Ehab Mohamed Said Abouobaia

Entitled: Hybrid torsional damper for semi-active control of torsional vibrations in rotating machines

and submitted in partial fulfillment of the requirements for the degree of

Doctor of Philosophy (Mechanical Engineering)

complies with the regulations of the University and meets the accepted standards with respect to originality and quality.

Signed by the final examining committee:

_____ Chair
Dr. M.R. Soleymani

_____ External Examiner
Dr. A. Lakis

_____ External to Program
Dr. W.P. Zhu

_____ Examiner
Dr. S. Rakheja

_____ Examiner
Dr. S. Narayanswamy

_____ Thesis Co-Supervisor
Dr. R. Bhat

_____ Thesis Co-Supervisor
Dr. R. Sedaghati

Approved by: _____
Dr. A. Dolatabadi , Graduate Program Director

November 24, 2014 _____
Dr. A. Asif, Dean
Faculty of Engineering and Computer Science

ABSTRACT

Hybrid torsional damper for semi-active control of torsional vibrations in rotating machines

Ehab Mohamed Said Abouobaia, Ph.D.
Concordia University, 2014.

Rotating machinery systems experience torsional vibrations with varying frequencies to some degree during normal operation. These vibrations if not controlled properly may cause severe system performance limitation and reduction of the fatigue life. Attenuation of torsional vibrations in these systems is a challenging engineering problem and raises several important issues in industrial applications.

The present research aims at developing a novel hybrid torsional vibration damper incorporating a conventional Centrifugal Pendulum Vibration Absorber (CPVA) with the Magnetorheological (MR) damper capable of suppressing torsional vibrations at different excitation frequencies. In fact, CPVA and torsional MR damper have been investigated separately in previous research, however, there has been no study reported on integrating the two systems for the attenuation of torsional vibration.

In this research study, first, the governing equations of motion for both horizontal and vertical CPVA have been derived using Lagrange's principle to investigate the effect of gravity on the dynamics and performance of CPVA. Moreover, softening nonlinear behavior of the pendulum absorber and its effect on the natural frequency of the system has been investigated.

Next, a rotary MR damper prototype was optimally designed, manufactured and tested. The design process of the rotary MR damper included several critical factors, particularly, analysis and design of the magnetic circuit of the MR damper. In order to ensure efficient design of the proposed damper, a finite element (FE) model of the rotary MR damper was developed to accurately evaluate the magnetic field distribution in the MR fluid and electromagnet core generated by the built-in electromagnet. The developed FE model enables to verify the effectiveness of the proposed design configuration as well as the selected material for the MR damper components. In addition, the equation of transmitted torque has been derived and utilized to evaluate the MR damper performance. In order to obtain the optimum geometric dimensions of the designed MR damper, an optimization problem has been formulated. The combined Genetic Algorithm (GA) and Sequential Quadratic Programming (SQP) have been employed to accurately capture the global optimum solution.

An experimental test set up has been designed to evaluate the fabricated rotary MR damper performance by measuring the generated damping torque and to validate simulation results obtained from the model.

Subsequently, the hybrid torsional MR damper incorporating both conventional CPVA and rotary MR damper has been proposed. The CPVA has been connected to the cylindrical housing of the MR damper. The governing equations of motion of the system consisting of a rotor with attached hybrid torsional dampers have been derived to evaluate the performance of the system under current off and maximum current applied to the MR damper's electromagnet. The results are also compared with those obtained from rotor systems with only attached CPVA and rotary MR damper.

Finally, a feedback control system using the semi-active skyhook control algorithm has been developed to adaptively control the proposed hybrid torsional damper under varying external excitations. It has been shown that the suggested closed-loop feedback control algorithm can significantly improve the damper performance compared with the open-loop (current off and on) system.

DEDICATION

To my Creator “Allah” hope to be accepted.

To my Mother and Father for providing all tools necessary to achieve my goals.

To my Wife, My Kids, Ziad & Moaaz for their encouragement and support throughout my thesis program.

ACKNOWLEDGMENT

First, I would like to thank Allah the Almighty, for having made everything possible by giving me strength and courage to do this work. We have no knowledge except whatever he has taught us. He is the all-knowing, the all wise.

I would like to thank my supervisors, Professor Rama Bhat and Professor Ramin Sedaghati, who endured this long process with me, for their instructive and expert guidance and assistance at every stage of the thesis process. Their gentle support and their efforts in reviewing and correcting this thesis drafts have been most appreciated.

I would also like to thank my examination committee members, Dr. Wei-Ping Zhu, Dr. S. Narayanswamy and Dr. S. Rakheja for their support and helpful comments.

Likewise, I would like to thank all my professors in Military Technical College, Cairo, Egypt. Their great help and support during my undergraduate and graduate studies really helped me to have a strong academic background and to continue my thesis program to achieve what I aimed for.

Of course, I would not have reached this stage without the continuous help, guidance, support and care of my mother, father and my wife in every single stage of my life. Words alone cannot express the thanks I owe to my family for their encouragement and assistance during this long period. I am also grateful to all my friends in Montréal for their support and their insights that guided and challenged my thinking during my study and special thanks for Capstone team, Guillaume C., Laurent D., Yao F., Dominik H. and Kevin S., for their help in fabricating the rotary MR damper and carrying out my work.

Finally, I dedicate this thesis to my wife, my mother, my father and all my friends and fellow colleagues for their invaluable support during my study. I also dedicate it to my lovely sons Ziad and Moaaz. Their presence in my life was the main motivator for me to work hard on my research and achieve my goals.

TABLE OF CONTENTS

LIST OF FIGURES

LIST OF TABLES

NOMENCLATURE

Notation

A	Cross sectional area, m^2
B	Magnetic field density, T
C_a	Absorber viscous damping coefficient, *N.m.s/rad*
C_r	Shaft viscous damping coefficient, *N.m.s/rad*
G^*	Complex modulus of the MR fluid, *Pa*
G'	Storage modulus of the MR fluid, *Pa*
G''	Loss modulus of the MR fluid, *Pa*
H	Magnetic field intensity, *A/m*
I	Applied electric current *A*
J	Rotor mass moment of inertia, $kg.m^2$
J_d	Disk mass moment of inertia, $kg.m^2$
J_s	Moment of inertia of shaft system including MR damper housing, $kg.m^2$
K	Fluid plastic viscosity, *Pa.s*
L_h	Housing width, *m*
N	Number of turns of the coil
R	Rotor radius, *m*
R_b	Bore diameter of the damper housing, *m*
R_d	Disc radius, *m*
R_h	Outer radius of the damper housing, *m*
R_s	Input shaft diameter, *m*
T	Rotor system kinetic energy, *Joule*
T_o	Amplitude of the excitation torque, *N.m*
T_e	Excitation torque, *N.m*
T_d	Total generated damping torque of MR damper, *N.m*
T_{fric}	Generated torque due to fluid friction in the annular gap, *N.m*
T_{vis}	Generated torque due to fluid viscosity, *N.m*
T_{ye}	Generated torque due to field dependent, *N.m*
V	Rotor system potential energy, *Joule*
b_d	Disc width, *m*
d	Thickness of the MR fluid gap, *m*

d_o	Thickness of the MR fluid annular duct, *m*
g	Gravitational acceleration, m/s^2
h_c	Coil's height, *m*
k_s	Shaft torsional stiffness, *kN.m/rad*
l	Pendulum length, *m*
m	Pendulum mass, *kg*
n	Absorber tuning order
r	Radial distance from the center of the disc, *m*
t	Side thickness of the damper's housing, *m*
t_o	Radial thickness of the damper's housing, *m*
v_m	Velocity of the pendulum mass, *m/s*

Greek Symbols

Φ	Magnetic flux, *Wb*
Ω	Rotational speed of rotor, *rad/s*
θ	Angular displacement of rotor, *rad*
ϕ	Angular displacement of pendulum, *rad*
ϕ_d	Angular displacement of disk, *rad*
ψ	Torsional displacement of system with CPVA, *rad*
ψ_s	Torsional displacement of system with MR damper, *rad*
ξ	Damping ratio of the shaft
ω	Excitation frequency, *rad/s*
ω_n	Absorber natural frequency, *rad/s*
τ	Shear stress, *Pa*
τ_y	Yield stress, *Pa*
η	Post-yield viscosity of MR fluid, *Pa.s*
γ	Shear strain
$\dot{\gamma}$	Shear strain rate, *rad/s*
μ_o	Magnetic permeability of vacuum, *Tm/A*
μ_r	Relative permeability of the material
μ_J	Inertia ratio
λ	The torque ratio of the MR damper
λ_d	The critical design value of the torque ratio

Chapter 1
Introduction

1.1 Background

Torsional vibration is an important issue in many mechanical systems with rotating mechanical components. Excessive torsional vibrations may result in noise, excessive stresses or even fatigue failure if not controlled immediately. Consequently, it should be suppressed to a proper desired level to ensure system's reliability. Some measures have been introduced to reduce torsional vibrations in rotating machinery such as addition of flywheels and tuned vibration dampers [1-6]. However, these methods have some deficiencies. The flywheels increase the system inertia, and results in reduction in system responsiveness, while torsional dampers are effective at only a single frequency [7].

Centrifugal Pendulum Vibration Absorber (CPVA) is also one of the effective passive devices used for reducing torsional vibrations and are widely used in rotating and reciprocating machines to suppress torsional vibrations. These absorbers consist of a pendulum constrained to move in a plane normal to the rotational axis of the machine. CPVAs are simple and reliable torsional vibration absorbers that are expected to be efficient under steady state conditions. However, for unpredictable environmental conditions such as an internal combustion engine where the load, speed, acceleration, braking and road conditions are highly unpredictable, the CPVAs have shown performance limitations.

Recently, MR based torsional absorbers have been considered as of one the most promising new energy absorption devices for semi-active control of torsional vibrations due to their

inherent fail-safe feature, low power requirement and capability to attenuate vibration under unpredictable environmental conditions.

It is noteworthy that the use of active or semi-active vibration control systems overcomes the limitations inherent in the conventional passive systems. However, active control systems are expensive, complicated to design and need large power. Thus, semi-active control systems have emerged as a good compromise between active and passive systems. Compared with conventional semi-active devices, MR based semi-active devices have less moveable parts (thus less wear) and faster response time, thus ideal for real-time vibration control applications.

While application of linear MR dampers have been widely investigated over the past three decades, to the best of our knowledge, relatively fewer research studies have been conducted on rotary MR damper applications which is the main subject of the present research work.

1.2 Aims and objectives

The main goal of this research study is to develop a novel hybrid MR based torsional vibration damper combining conventional CPVA with the rotary MR damper and compare its performance with conventional CPVA and rotary MR damper alone.

To achieve this, the following objectives have been identified:

- Develop an analytical model of the CPVA in both vertical and horizontal planes and investigate the torsional vibration response of the system with and without CPVA and also the effect of gravity on the CPVA's performance.

- Develop a phenomenological based model for the rotary MR damper. Also formulate a design optimization formulation to identify the optimal geometrical parameters of the rotary MR damper to maximize its damping torque capacity.
- Fabricate a proof-of-concept rotary MR damper and design an experimental set up to validate the developed MR damper model.
- Develop an analytical model for the proposed hybrid MR based torsional vibration damper and investigate the torsional vibration response of the system with and without proposed damper in an open-loop current off and on modes. Also compare the performance of the proposed hybrid damper that of CPVA and rotary MR damper alone.
- Develop an efficient semi-active control algorithm for the proposed hybrid torsional vibration damper to suppress vibration effectively in broadband frequency range.

1.3 Thesis organization

The present research dissertation consists of the following seven chapters.

Chapter 1 presents an introduction to the research conducted in this thesis. The research aims and objectives are outlined in this chapter. A summary of the thesis organization is then presented at the end of this chapter.

Chapter 2 presents state of the art of the torsional vibration problems using both CPVA and MR dampers. In addition, some fundamental concepts on CPVA and MR damper technology are presented as well as the semi-active control strategies used for torsional vibration reduction using MR Dampers.

Chapter 3 provides the development of mathematical model for the CPVA. In addition, the effect of gravity on the amplitude of torsional vibration and the softening nonlinear behavior of CPVA are also discussed in this chapter.

Chapter 4 demonstrates modeling and design optimization formulation for the rotary MR damper. The fabricating procedures of the designed MR damper is also discussed. Moreover, experimental test setup as well as steps for measuring the generated damping torque are presented.

Chapter 5 presents the mathematical model of the proposed hybrid torsional damper and the governing equations of motion. The semi-active control algorithm proposed for the hybrid damper is then described.

Chapter 6 provides results and detailed discussions on the torsional vibration response of the system with the proposed hybrid torsional damper in open loop (current off and on modes) and closed-loop (proposed semi-active control algorithm).

Finally, chapter 7 outlines conclusions and contributions as well as future work recommendations.

Chapter 2
Literature Review

This chapter provides a comprehensive literature review summarizing the previous work and contributions relevant to the aims and objectives of the present research. There have been a number of research studies in the field of torsional vibration control. Reported studies on CPVA will be presented in the first section, followed by research studies on MR damper and its application in torsional vibration control.

2.1 History and background of CPVAs

CPVAs have been in use for over half a century and they are widely used in rotating and reciprocating machines to suppress torsional vibrations. As shown in Figure 2-1, these absorbers consist of a pendulum constrained to move in a plane normal to the rotational axis of the machine.

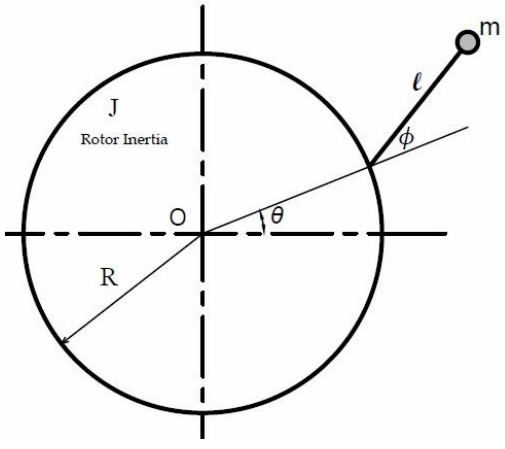

Figure 2-1 Schematic view of CPVA attached to a rotor

CPVAs are tuned absorbers with their natural frequencies varying proportional to the rotational speed of the rotating shaft. Pendulum absorbers have some attractive features for applications; they can be tuned to a given order of rotation rather than to a set frequency and therefore they are effective over a continuous range of rotating speeds [7]. CPVAs were first introduced in 1929 by Ker Wilson [1].

Further, Den Hartog in 1956 [8] presented the linear analysis of the dynamic response of the CPVA and explained briefly the characteristics of its large amplitude nonlinear motion. According to small amplitude vibration theory, the linear tuning order of the CPVA is given by:

$$n = \sqrt{\frac{R}{l}} \tag{2-1}$$

where R is the rotor radius and $\boldsymbol{l}$ is the pendulum length as shown in Figure 2-1.

By proper selection of the optimum suspension point and pendulum effective length, the absorber can be tuned to absorb any desired order of excitation torque. For constant rotor speed, Ω, the linearized natural frequency of the tuned absorber is given by:

$$\omega_n = \Omega \sqrt{\frac{R}{l}} \tag{2-2}$$

It is clear from Eq. (2-2) that the CPVA's natural frequency is directly proportional to the rotor speed, which allows CPVA to suppress torsional vibration over the entire operational range of rotor speed [9]. CPVA could be overtuned (undertuned) when the desired order is adjusted to a value greater (smaller) than the absorber order n.

CPVAs have been used for several decades in light engines and helicopter rotors [10]. In 1991, Borowski et al. [11] have proven their effectiveness to be feasible for automotive applications for vibration suppression. These absorbers not only dissipate very little energy, but they also can often be designed without adding any mass or rotating inertia to the crank shaft as achieved by Nester et al. [12] in automotive applications by replacing existing counterweights by CPVAs, which then serve for both balancing and torsional vibration reduction.

The operating envelope of CPVA depends on the amount of the mass of the absorber. Often in some applications, the mass must be minimized as in aerospace applications. Haddow and Shaw [13] established a rigid rotor fitted with several point mass absorbers that move along prescribed paths relative to the rotor. An external excitation torque is applied to the rotor that fluctuates at a given order of rotation and the absorber's paths are selected such that their motion counteracts the applied torque.

It is noteworthy that until around 1980 all designs related to CPVA employed simple circular paths for the absorbers [7]. Absorbers with circular paths work fine at small amplitudes; however, their nonlinear behavior due to amplitude dependent frequency limits their effectiveness. Absorbers with circular paths exhibit softening nonlinear behavior in which rate of change of their natural frequency decreases as the amplitude increases. To overcome this shortcoming in the circular path absorbers, a small mistuning should be intentionally used to ensure stable and reliable operation of the CPVA.

Subsequently, various kinds of pendulum with non-circular path have been designed. In 1992, Denman [14] introduced other paths that offer improved performance for the absorbers at large amplitudes. Cycloidal path absorbers exhibit hardening nonlinear behavior; that is, the absorber natural frequency increases as the amplitude increases. Accordingly, cycloidal absorbers offer improved performance at large amplitudes than that of a circular path absorber. Another special absorber path is the epicycloidal path, since it maintains a constant frequency for the absorber over all amplitudes, thus keeping the absorber as linear as possible over a large operating range; this type is typically used in automotive engines [15].

Ryan and Shaw [16] studied the transient response characteristics of a single absorber mounted on a rotor which is subjected to engine order torsional excitation. Two types of absorbers have been considered: Circular path and Tautochronic absorber. An approximate analytical method was developed for predicting the transient overshoot of CPVA when the rotor is subjected to near resonant torsional excitation.

In order to overcome limitation of passive vibration absorbers, Chen et al. [17] developed an active dynamic absorber to retain the advantages of the conventional CPVA. The active pendulum absorber is simply a CPVA connected to a torque motor that acts as an actuator to drive the pendulum at adequate oscillatory amplitude. It has very wide range of operating frequencies. This active absorber can be tuned according to the system characteristics to meet desired requirements. Genetic Algorithm controller for the active pendulum absorber was presented by Liang and Tung [18]. The proposed algorithm estimates an appropriate value for the torque of the active pendulum that is capable of suppressing the torsional vibration of the carrier.

Although significant research work has been done in CPVA, previous works have mainly focused on analysis of CPVA operating in horizontal plane in which the gravity effect has not been considered. In this research study, the rotor system integrated with the pendulum absorber has been investigated in both vertical and horizontal planes in order to assess the effect of gravity.

2.2 Magnetorheological (MR) dampers

2.2.1 Magnetorheological fluids

MR fluids are suspensions of non-colloidal (0.05-10 μm) and magnetically soft particles in organic or aqueous liquid with low viscosity [19]. The discovery of MR fluids is credited to *Jacob Rabinow* in 1949 [20]. Magnetorheology is a branch of rheology that deals with the flow and deformation of the MR fluids (elasticity, plasticity, or viscosity).

MR fluids respond to an applied Magnetic field, instantly, with a drastic change in rheological behavior and thus consequently in the damping and stiffness properties. In their off state, MR fluids behave like Newtonian fluids. The most fundamental characteristic of these fluids is their ability to reversibly change from free-flowing, linear, viscous liquids to semisolids having controllable yield strength in milliseconds when exposed to a magnetic field. This is basically associated with the formation of chains of polarizable particles in the direction of the applied field as shown in Figure 2-2, which causes resistance to the movement of the fluids and consequently development of the yield stress [21].

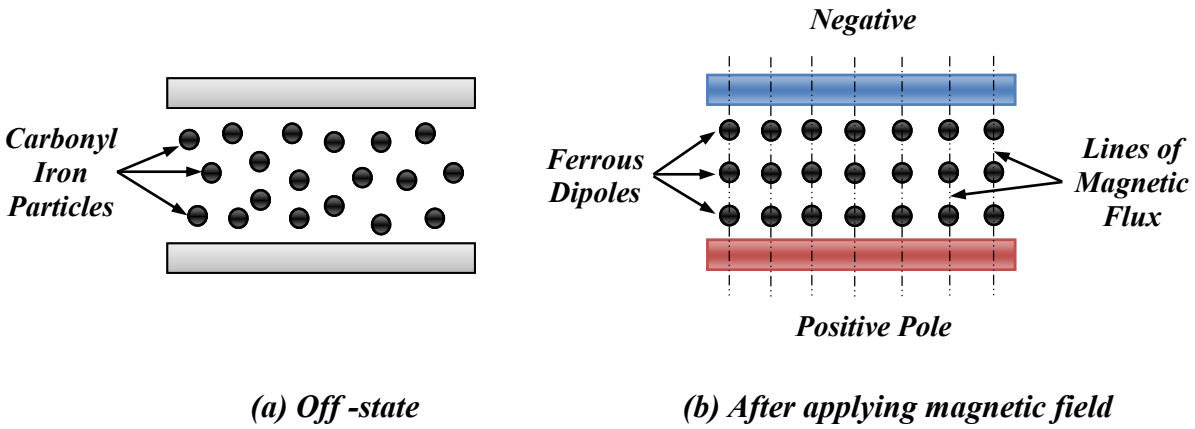

Figure 2-2 Effect of applied magnetic field on MR fluid Particles

MR fluid develops a yield stress based on the amount of mechanical energy required to establish the ferrous dipole chains. MR fluids demonstrate a much greater increase in viscosity (and thus yield strength) than their Electrorheological (ER) fluid counterparts (20-50 times) when the field is induced. An yield stress of nearly 100 kPa can be obtained in MR fluids with magnetic suspensions containing carbonyl iron powder [22]. Moreover compared with ER fluids, MR fluids can operate under wide variations in temperature ranges from -40°C to 150°C with slight change in yield stress and have the ability to use low voltage power supply 12 volt [23].

In the off state, the apparent viscosity of the MR fluids is found to be (0.1 to 1 Pa.s at low shear rates). However, when the magnetic field is applied the apparent viscosity of the MR fluids increase significantly (105 – 106 times) within a few milliseconds [19]. This rapid increase in the viscosity is completely reversed as soon as the magnetic field is removed. For this reason, MR fluids play a key role for various semi-active damping control applications. Although ER/MR fluids are considered as smart controllable fluids, ER fluids have some drawbacks compared with MR fluids, since they have low yield strength, need

high voltage power supplies (5000 volts), high sensitivity to common impurities and they often lose their strength as their temperature increases [23]. Some properties of typical ER/MR fluids are provided in Table 2-1.

Table 2-1 Typical properties of MR and ER fluids

Property	***MR Fluid***	***ER Fluid***
Response time	milliseconds	milliseconds
Plastic Viscosity	0.1 to 1.0 Pa.s	0.1 to 1.0 Pa.s
Temperature Range	-40 to 150 ^{o}C	+10 to 90 ^{o}C
Stability	Unaffected by most impurities	Cannot tolerate impurities
Max. field	~250 kA/m	~4 kV/mm
Max. yield stress	50 – 100 kPa	2 – 5 kPa
Density	3 – 4 g/cm^3	1 – 2 g/cm^3
Max. energy density	0.1 J/cm^3	0.001 J/cm^3
Power supply	2 to 25 V & 1 to 2 A	2 to 5 kV & 1 to 10 mA

2.2.2 Operating modes of MR fluid

In various semi-active vibration control applications, MR fluids can be used in three principal modes of operation as shown in Figure 2-3, namely, flow mode, shear mode, their combination and squeeze film mode [22].

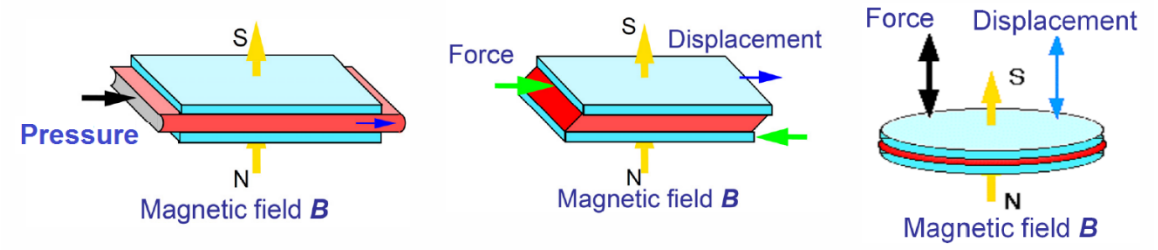

(a) Flow Mode ***(b) Shear Mode*** ***(c) Squeeze-film Mode***

Figure 2-3 Basic operating modes for MR fluids [24]

In flow mode, a pressurized flow of MR fluid moves between two stationary plates while the magnetic field direction is perpendicular to the direction of the fluid motion. Flow mode is typically used for developing a controllable damping force in shock absorbers as in vehicle suspensions [25]. In shear mode, the two plates containing the MR fluid move relative to each other causing the MR fluid to shear. Here also magnetic field direction is perpendicular the relative motion of the plates or the shear direction. Shear mode is commonly used in clutches and brakes in which resistance to rotational motion is required [26]. Squeeze-film mode involves a layer of MR fluid, which is squeezed between the two plates. In this mode, the direction of the magnetic field is along the relative motion of the plates. Squeeze-film mode is used for introducing support flexibility and damping in the bearing/support structure [27].

2.2.3 Mathematical models of MR fluids.

In order to effectively utilize MR fluids in MR based devices, their rheology behavior should be properly characterized. The MR fluid characteristics have been described based on measured shear stress-strain properties in two regions, pre-yield and post-yield. MR fluid displays viscoelastic behavior in the pre-yield region. Further, the shear stress and shear strain are proportional in terms of the complex modulus G^* [28] described as:

$$G^* = G' + i\,G'' \tag{2-3}$$

where G' is the storage modulus of the MR fluid, which is related to the energy stored per unit volume of the material during a deformation cycle and G'' is the loss modulus, which is a measure of the energy dissipated per unit volume of the material over a deformation cycle. Hence, the shear stress-strain relationship in pre-yield region can be expressed as:

$$\tau = G^* \gamma \tag{2-4}$$

where τ is the shear stress and γ is the shear strain.

Post-yield region is considered as the dominant mode of operation in most devices such as dampers, brakes and clutches. Bingham plastic model developed by Phillips in 1969 [29] is the most popular model to characterize the post-yield behavior of MR fluids. According to this model, MR fluid behaves as a rigid body at stresses below the yield shear strength of the material (pre-yield region) and flows like a Newtonian fluid with constant viscosity at shear stresses above the shear yield strength (post-yield region). The relation for shear stress-strain rate for this model can be described as:

$$\tau = \tau_y(H) + \eta\dot{\gamma} \qquad \tau \geq \tau_y \tag{2-5}$$

$$\tau = 0 \qquad \tau \leq \tau_y \tag{2-6}$$

where τ_y is the apparent yield shear strength which depends on the applied magnetic field (H), η is the Newtonian post-yield viscosity independent of the applied magnetic field and $\dot{\gamma}$ is the shear strain rate.

It should be noted that in the post-yield region, under high shear strain rate, MR fluids may undergo shear thinning or shear thickening and thus behave in nonlinear fashion as shown in Figure 2-4. Shear thinning refers to the reduction of the apparent viscosity of the MR fluid at high shear strain rates while shear thickening is the increase in dynamic viscosity corresponding to the increment of the shear strain rate. To address this behavior, Herschel-Bulkley model has been developed which can be described as [30, 31] :

$$\tau = \left(\tau_y(H) + K|\dot{\gamma}|^{\frac{1}{m}}\right) sgn(\dot{\gamma}) \tag{2-7}$$

where *K is* the fluid plastic viscosity and *m* is the flow behavior index. For $m > 1$, Eq. (2-7) represents a shear thinning fluid, while shear-thickening fluids are described by $m < 1$. It is noted that for $m = 1$ and $K = \eta$ the Herschel–Bulkley model reduces to the Bingham plastic model as shown in Figure 2-4.

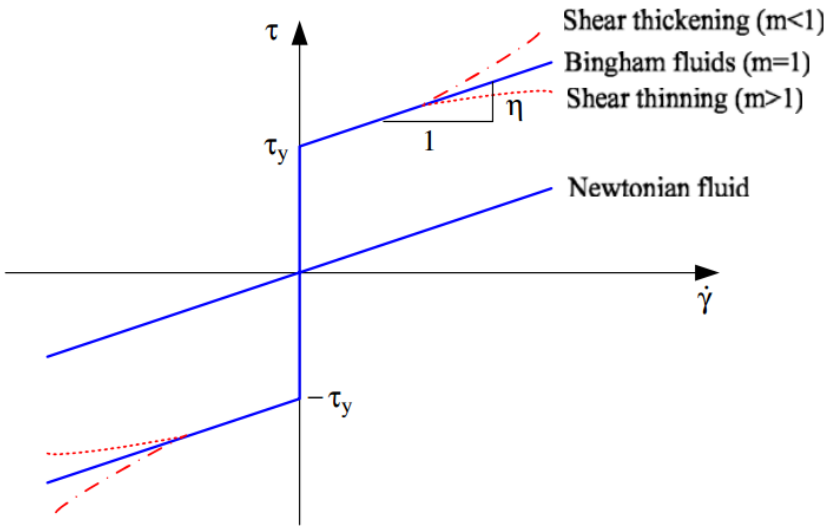

Figure 2-4 Viscoplastic models describe MR fluid [31]

Several phenomenological models have been developed to accurately describe the dynamic behaviors of MR dampers such as simple Bouc-Wen model as shown in Figure 2-5 [32], modified Bouc-Wen as shown in Figure 2-6 [32], equivalent viscous damping model [33], nonlinear bi-viscous model [34] and nonlinear hysteretic bi-viscous [33].

It is noted that MR fluid dampers experience hysteresis behavior in which the output (damping force or torque) depends on not only instantaneous value of the input (velocity or electrical current), but also on the history of the output [35].

The above-mentioned phenomenological models have shown to properly characterize the hysteresis behavior of MR dampers.

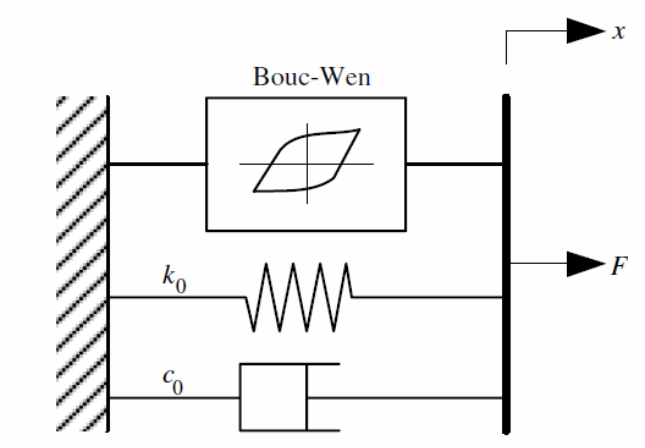

Figure 2-5 Simple Bouc–Wen model [32]

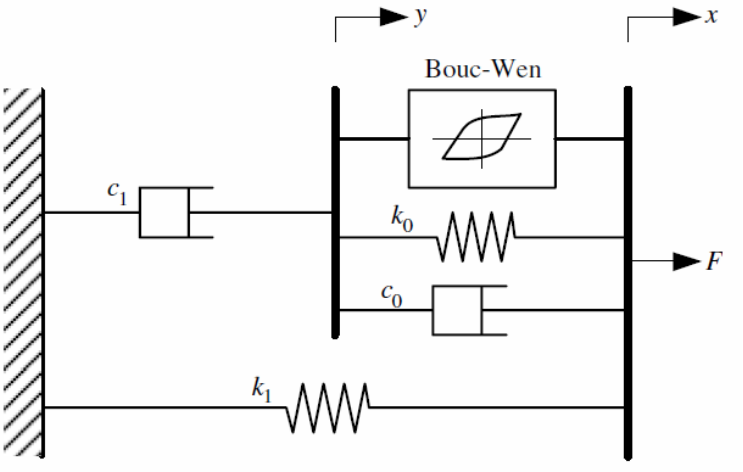

Figure 2-6 Modified Bouc–Wen model [32]

2.3 MR fluid dampers

MR dampers are semi-active adaptive devices that have received considerable interest of designers and researchers due to their variable damping feature, mechanical simplicity, high dynamic range, low power consumption, large force capacity, fast response and robustness. MR dampers are categorized in two main types: Linear MR dampers and Rotary MR dampers.

2.3.1 Linear MR dampers

MR fluid has been used in shock absorbers as a working fluid rather than the conventional fluid due to its adjustable viscosity property that makes it ideal for adaptive vibration control. A typical linear MR damper, which operates in flow mode, is shown in Figure 2-7

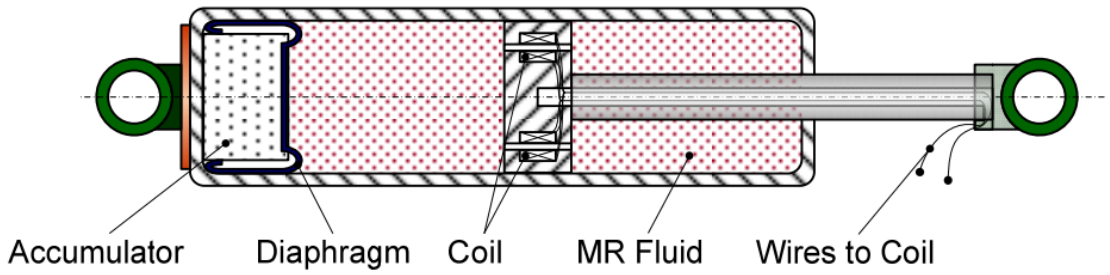

Figure 2-7 Cross-section of typical linear MR fluid damper [36]

As the piston rod enters the housing, the MR fluid flows from the high-pressure chamber to the low-pressure chamber through orifices in the piston head. The accumulator contains a compressed gas (usually nitrogen) and its piston provides a slightly moveable barrier between the MR fluid and the gas.

The accumulator provides a degree of softening by providing an extra allowance for the volume changes that occur when the piston rod enters the housing; in addition, it prevents the creation of vacuum in the housing and cavitation of the damper. The magnetic coil is built in the piston or on the housing. When a current is supplied to the coil, polarizable chains will be developed and the fluid changes from the liquid state to the semi-solid state within milliseconds. Consequently, a controllable damping force is produced. Thus, linear MR damper, in contrast to conventional linear hydraulic damper, has the capability to change its damping force by varying the magnetic field strength inside the damper. This provides a unique opportunity for adaptive vibration control applications.

2.3.2 Rotary MR dampers

While the development of the rotary MR dampers are not as extensive as the linear MR dampers, many types and classes of rotary MR dampers have been developed for different purposes. The term MR brake was more commonly used than rotary MR damper since the early intentions of the device development were only as a braking device [37].

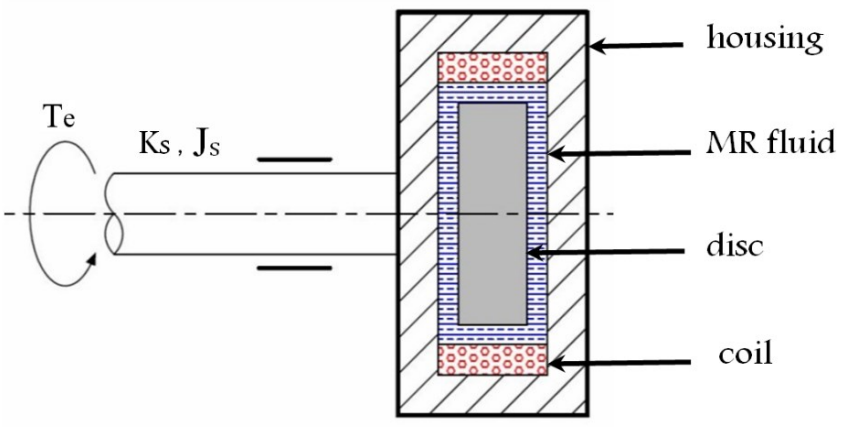

Figure 2-8 Configuration of MR damper

As shown in Figure 2-8, MR brake consists of a disc placed inside the cylindrical cavity filled with MR fluid and allowed freely to rotate relative to the housing. This provides a controllable damping torque capable of reducing the torsional vibration of the system. The housing of the MR damper is typically fixed to the shaft and rotating together with the same speed. The vibration energy of the shaft system is then absorbed by the disc, i.e., it is converted into vibration energy of the disc through the frictional torque of the damper. The controllable friction torque of the damper is achieved by the current applied to the coil that is wound circumferentially inside damper housing.

MR brake operates in shear mode and its damping torque depends on several parameters in the effective area, such as magnetic field strength, clearance gap and working speed. Since normally the clearance gap and working speed are part of the design constraints, manipulating magnetic field strength in the effective area is the only way to operate and control the MR brake [37]. According to the location where the shear mode occurs, MR brake can be divided into two basic types: drum type and disc type MR brake. The basic configuration of both types is shown in Figure 2-9.

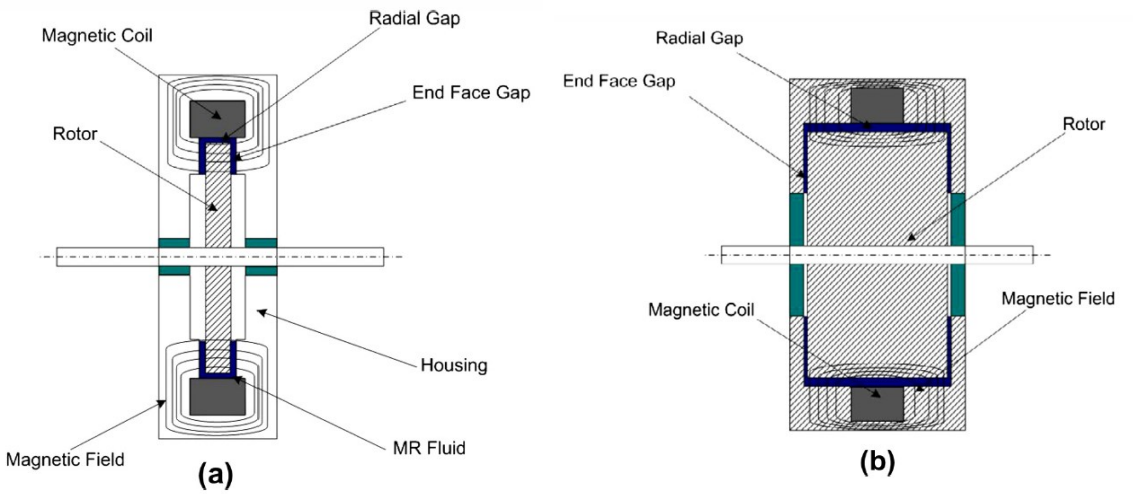

Disc Type ***Drum Type***

Figure 2-9 Typical structure configuration of MR Brake [37]

As can be seen from Figure 2-9 (a), in disc type MR brake, the magnetic field effective area is the end face gaps of rotor at which the shear mode takes place and magnetic flux is perpendicular to the shear direction. While in the drum type MR brake, shown in Figure 2-9 (b), the effective area of the magnetic field is the radial gap of rotor at which the shear mode takes place.

2.4 Semi-active control techniques for MR damper

This section presents a brief review of the control strategy used in both damper and system controllers for semi-active vibration control of rotating shaft systems.

A semi-active or active system controls the system dynamics to achieve optimized conditions. Semi-active control system incorporating MR dampers needs two controllers, a system controller and a damper controller. The system controller generates the desired damping torque according to the dynamic responses of the system while the damper controller is used to regulate the command voltage to the current driver to track the desired

damping torque determined by the system controller based on the desired and the actual damping torque. The damping torque of the MR fluid damper should be monitored and fed to the damper controller to generate the command voltage according to the desired damping torque generated by the system controller [31]. In the following subsections, both damper controller and system controller are described in some detail.

2.4.1 MR damper controller

In semi-active systems incorporating MR dampers, a damper controller is used to allow the MR fluid damper track the desired damping torque determined by the system controller. There are two key factors have great influence in controlling the damping force or torque when designing the damper controller: (1) tracking ability of damping force or torque, and (2) energy requirement for MR damper. The term tracking ability can be defined as the ability of the controlled damping force or torque to follow the desired force or torque produced by the system controller. The tracking ability can be evaluated by the damping force or torque error between the controlled and the desired damping forces. However, the term energy requirement defines the amount of energy required for powering the MR fluid damper. Although the MR damper requires low voltage source, energy consumption by MR fluid damper on moving carriers, like automobiles or railway vehicles, is an issue of concern for MR based semi-active systems. Furthermore, less energy consumption will extend the effective life of the power supply and hence extend the lifetime of the MR damper.

Having discussed the functioning of MR damper controller, now types of MR damper controllers used in MR based semi-active systems will be discussed. Various damper controllers for MR based semi-active systems have been developed.

Heaviside Step Function (HSF) controller has been widely used in semi-active systems [38-41]. HSF was introduced by Dyke et al. in 1996 [42], and it is identified as " on-off " controller, where the applied voltage is either zero value or maximum. In [40], a half car suspension model is developed and the HSF is utilized to control two MR dampers in the proposed two degrees of freedom system. The applied voltage is altered between zero and maximum (2 volts) depending on the value of the desired damping force.

In the modified HSF algorithm known as Signum Function (SF), the applied voltage is altered in a discrete way as described in [41, 43]. In this approach, the command voltage under certain conditions varies to a certain value between zero and maximum. A comparison of the two approaches reveals that the SF has a better tracking ability and less energy requirement than that for the HSF [41]. However, in both controllers, the command voltage is still displayed in discrete values.

Unlike previous controllers, the continuous state (CS) algorithm operates in different manner. In this approach, the command voltage varies continuously between zero and maximum. CS algorithm was introduced in [44] with ER based semi-active system and applied also in [38, 45] as MR based semi-active system.

Non-parametric control algorithms such as polynomial function control algorithm [46] and recurrent neural network (RNN) algorithm [47] are used as MR damper controller. In the polynomial approach, a polynomial function is used to express the damping force as a

function of relative velocity and thus hysteresis behavior of MR damper. The polynomial coefficients in this approach are linearized with respect to the input current. One of the benefits of this approach is that it is an invertible model, i.e., it is possible to obtain the input current for a given velocity and a desired damping force.

RNN algorithm is another controller approach that is commanding a continuous voltage signal to the MR damper. Due to the inherent nonlinear behavior of MR dampers, the RNN is used to match the nonlinearity in controlling the damping force through learning methods of the dynamic neural network models for MR damper [48].

2.4.2 System controller

Unlike the damper controller, the system controller generates the desired damping torque according to the dynamic response of the system to achieve optimized operation condition. Various types of system controllers have been introduced among which Skyhook controller has been widely used. Skyhook control is a popular and effective vibration control method because it can dissipate system energy at a high rate. Several studies were presented with a comprehensive analysis of semi-active systems incorporating skyhook scheme control [49-52]. The name skyhook is due to the fact that the controllable damper is hooked between the body (sprung) mass and the sky, as illustrated in Figure 2-10. The basic concept of skyhook control is to reduce the transmissibility of the sprung mass.

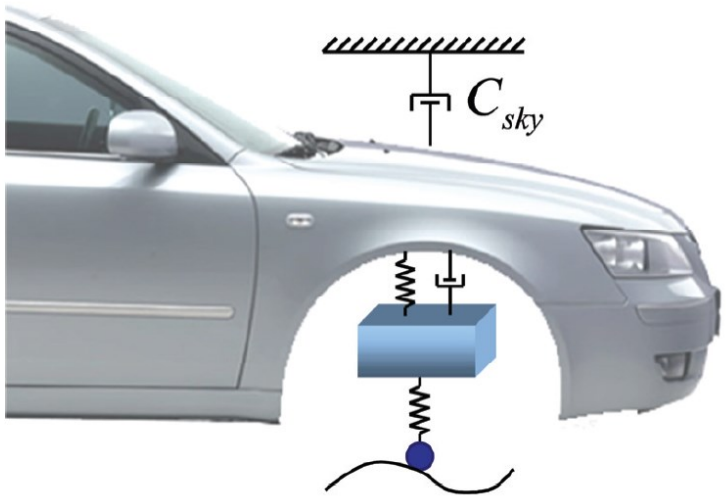

Figure 2-10 Skyhook control scheme [53]

In [50] a skyhook controller was designed and incorporated with the hardware-in-the-loop simulation for controlling a full car suspension system featuring four MR dampers. The results obtained through experimental tests showed that the intended skyhook control substantially improves both ride comfort and steering stability for the proposed semi-active suspension system.

H-infinity control is another system controller that has been successfully implemented [54-59]. In this method, the control problem is expressed as a mathematical optimization problem to find the optimal controller's gain. A quarter car suspension system model with a MR damper is considered in [59] and a semi-active static feedback H-infinity control has been considered. The intended control scheme utilized the measurable suspension deflection and sprung mass velocity as feedback signals for active vehicle suspension. The proposed scheme is validated by numerical simulation under random excitation in the time domain and simulation results showed a significant improvement in suspension performance.

Linear Quadratic Regulator (LQR) control has also been used for vehicle suspension system with MR damper [60, 61]. LQR control is employed in [60] to study an active vibration control scheme for controlling torsional vibration of a rotor shaft due to electromagnetic disturbances or unsteady flow in large steam turbine generator sets. The proposed optimal LQR control scheme solved for each time interval with the weighting matrices, through the Ricatti equation to obtain the time varying gain matrices. Simulation results showed good reduction in torsional vibration response.

Another robust system controller is the sliding mode controller that has been recently used in MR based systems [38, 45, 62, 63]. In addition to the fact that the system can be designed to be robust with respect to modelling imprecision, sliding mode control can be synthesized for the nonlinear semi-active system adequately [45]. This control scheme is effectively used in [45] for considering loading uncertainties for an automotive suspension system with MR damper. For evaluation of the controller performance, two kinds of excitation (bump and random) were created through a computer simulation in both time and frequency domains. The planned control policy showed its ability to reduce both peak and root mean square responses in comparison with the passive suspension system. In [63], Wereley and Choi demonstrated the feasibility and effectiveness of ER and MR Fluid-based landing gear systems on attenuating dynamic load and vibration due to the landing impact. A theoretical model of ER/MR landing gear system was constructed, and its governing equation was derived. In this study, a sliding mode controller is formulated to attenuate the acceleration and displacement of the landing gear system during touchdown of the aircraft. It was shown that the acceleration and the displacement are attenuated regardless of parameter variations such as upper vehicle mass, viscous damping, etc.

2.5 Semi-active torsional vibration control systems

From the available literature, unlike the MR brakes, the linear MR damper are among the most popular MR fluid devices. Although there have been a number of reported studies in automotive suspension system utilizing linear MR dampers, there are fewer studies in semi-active control strategies with the application of MR brake, due to complexity in design, difficulties in measuring torque signals and difficulties in dealing with the torsional vibration response of a given system. This section gives an overview of the highlights on the relevant research in semi-active torsional vibration control strategies.

One of the early studies in torsional vibration control was introduced by Den Hartog & Ormondroyd [64]. They related the constant optimal friction torque to the excitation torque applied to the main system, thus providing the optimum damping required for controlling the torsional vibration of the primary system. Based on this theory, Ye and Williams [65] developed an exact form of steady-state solution for a rotational friction damper, and a numerical method was used to determine the optimum friction torque.

Subsequently, analytical and experimental investigations were carried out by Ye and Williams [66, 67] on the use of MR brake absorber for controlling torsional vibrations in rotating systems. In [51] two different strategies were examined for controlling the braking torque of the MR absorber. First, MR brake was implemented as an open-loop passive friction damper with variable friction torque by applying a constant current to the coil of the MR brake absorber. In the second strategy, the MR brake was implemented in a closed loop feedback control using skyhook damping control approach. In this approach, the damping torque in the MR absorber was adjusted by comparing the sign of the absolute

angular velocity of the primary system and that of the relative angular velocity between the MR brake and the primary system in order to apply the effective damping to the system. Experimental results in both control implementations showed a significant reduction in torsional vibration amplitude of the primary system. However, a high cost control system is required since both the absolute velocity of the primary system and the velocity of the floating disc inside the MR brake housing are required.

More recently, Nguyen and Choi [68, 69] presented an optimal design of a MR absorber for torsional vibration control of a rotating shaft system. A configuration of a MR brake absorber for torsional vibration control of a rotor system was proposed and the braking torque of the MR brake absorber was derived based on the constitutive Bingham plastic model of the MR fluid [69].

2.6 Summary

This chapter provides a literature review of the recent research studies showing the most important and relevant studies that are closely related to the field of torsional vibration control. Reported studies on both CPVA and MR damper have been presented as well as their various applications in reducing torsional vibrations. In the next chapter, mathematical modeling of CPVA will be addressed. In addition, the effect of gravity on the torsional response amplitude of the rotor system at different operating speeds will be investigated and obtained results for different cases will be illustrated.

Chapter 3
Modeling and Analysis of CPVA Considering Gravity Effect Investigations

3.1 Introduction

In this chapter, the mathematical model for the rotor system attached to CPVA is developed based on the differential equations that describe its physical behavior. Although much work has been done in this field, past research has focused mainly on analysis of absorbers operating in horizontal plane, which does not experience the gravity effect. In the present study, the rotor system integrated with the pendulum absorber has been investigated in both vertical and horizontal planes in order to assess the effect of gravity, using an appropriate term in the potential energy. In this research, a CPVA with circular path is considered, in order to demonstrate the dynamical features of interest.

The system under investigation is modeled as a rotating disk attached with CPVA in which the disk is subjected to an external harmonic torque. Mathematical modeling of a CPVA has been formulated using Lagrange's principle, resulting in two coupled nonlinear differential equations of motion for both rotor and the pendulum. Then, the Simulink toolbox within the MATLAB environment is used to formulate the block diagrams of the model equations. Three different cases have been investigated in this chapter. First case considers the absorber operating in vertical plane where the gravity effect is considered, the second case considers the absorber operating in horizontal plane in which there is no contribution of the potential energy due to gravity except for the torsional stiffness of the rotor, and in the third case the rotor system is operated without absorber.

The results obtained from numerical analysis for both rotor and absorber responses are illustrated for each case and compared against one another. In addition, softening nonlinear behavior of the pendulum and its effect on the natural frequency of the system has been investigated.

3.2 Mathematical modelling of rotor/absorber system

A schematic of the rotor system with a pendulum absorber of length l and point mass m attached to it is shown in Figure 3-1. The pendulum is fixed to the rotor at point A, θ is the rotor angle and ϕ is the pendulum angle. The rotor has a rotary inertia J about the point O.

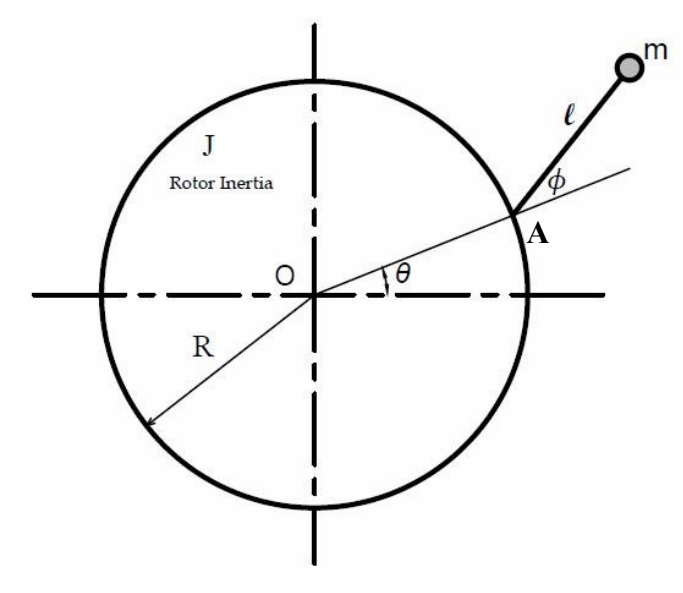

Figure 3-1 Schematic view of CPVAs attached to a rotor of inertia J

Lagrangian formulation is used to model the rotor integrated with CPVA in which two coupled nonlinear equations are derived for the rotor and the pendulum.

First step is to develop expressions for both kinetic and potential energy. The kinetic energy for the rotor and CPVA system shown in Figure 3-1 is given by:

$$T = \frac{1}{2} m\, v_m^2 + \frac{1}{2} J\, \dot{\theta}^2 \tag{3-1}$$

where v_m is the velocity of the pendulum and J is the mass moment of inertia of the rotor. The total potential energy due to the gravity and shaft strain energy can be written as:

$$V = mg\,[R \sin\theta + l \sin(\theta + \phi)] + \frac{1}{2} k_s \psi^2 \tag{3-2}$$

where k_s is the shaft torsional stiffness, ψ is the torsional displacement of the shaft. The total velocity of the pendulum with respect to the point O is obtained as:

$$v_m^2 = 2\, l\, (R \cos\phi + l)\dot{\theta}\dot{\phi} + (R^2 + l^2 + 2\, R\, l \cos\phi)\dot{\theta}^2 + l^2\, \dot{\phi}^2 \tag{3-3}$$

Substituting Eq. (3-3) into Eq. (3-1) yields:

$$T = \frac{1}{2} m\left[2l(R \cos\phi + l)\dot{\theta}\dot{\phi} + (R^2 + l^2 + 2Rl \cos\phi)\dot{\theta}^2 + l^2\dot{\phi}^2\right] + \frac{1}{2} J\dot{\theta}^2 \tag{3-4}$$

The total rotation (θ) of the rotor system consists of two parts, a steady rotation ($\Omega\, t$) due to rotation at a constant angular speed (Ω), and a small torsional oscillation $\psi\ (t)$ superimposed over this rotation and is given by:

$$\theta = \Omega\, t + \psi\,(t) \tag{3-5}$$

Substituting the value of (θ) from Eq. (3-5) into Eq. (3-4), the kinetic energy becomes:

$$T = \frac{1}{2} m\left[2l(R \cos\phi + l)(\Omega + \dot{\psi})\dot{\phi} + (R^2 + l^2 + 2Rl \cos\phi)(\Omega + \dot{\psi})^2 + l^2\dot{\phi}^2\right] + \frac{1}{2} J(\Omega + \dot{\psi})^2 \tag{3-6}$$

Now substituting Eq. (3-5) into Eq. (3-2), the total potential energy becomes:

$$V = mg\,[R \sin(\Omega t + \psi) + l \sin(\Omega t + \psi + \phi)] + \frac{1}{2} k_s \psi^2 \tag{3-7}$$

The Lagrangian [$L = T - V$] in terms of the two generalized coordinates ψ and ϕ can now be described as:

$$L = \frac{1}{2}J\left(\Omega + \dot{\psi}\right)^2 + \frac{1}{2}m\left[2l(R\cos\phi + l)\left(\Omega + \dot{\psi}\right)\dot{\phi} + (R^2 + l^2 + 2Rl\cos\phi)\left(\Omega + \dot{\psi}\right)^2 + l^2\dot{\phi}^2\right] - mg\,[R\sin(\Omega t + \psi) + l\sin(\Omega t + \psi + \phi)] - \frac{1}{2}k_s\psi^2 \quad (3\text{-}8)$$

The equations of motion are given by:

$$\frac{d}{dt}\left(\frac{\partial L}{\partial \dot{\psi}}\right) - \frac{\partial L}{\partial \psi} = T_e - c_r\dot{\psi} \quad (3\text{-}9)$$

$$\frac{d}{dt}\left(\frac{\partial L}{\partial \dot{\phi}}\right) - \frac{\partial L}{\partial \phi} = -c_a\dot{\phi} \quad (3\text{-}10)$$

where T_e is the excitation torque, C_r and C_a are viscous damping coefficients for shaft system and absorber, respectively.

Substituting Eq. (3-8) into Eqs. (3-9) and (3-10) results in the following governing equations of motion:

$$(J + ml^2 + mR^2 + 2mRl\cos\phi)\ddot{\psi} + (ml^2 + mRl\cos\phi)\ddot{\phi} - (2mRlsin\phi)\left(\dot{\psi} + \Omega\right)\dot{\phi} - (mRl\sin\phi)\dot{\phi}^2 + mg[Rcos\,(\psi + \Omega t) + l\cos(\psi + \Omega t + \phi)] + k_s\psi = T_e - C_r\dot{\psi} \quad (3\text{-}11)$$

$$(ml^2 + mRl\cos\phi)\ddot{\psi} + ml^2\ddot{\phi} + mRl\sin\phi\,(\dot{\psi} + \Omega)^2 + mgl\cos(\psi + \Omega t + \phi) = -C_a\dot{\phi} \quad (3\text{-}12)$$

It should be noted that when the absorber operates in the horizontal plane, there is no gravity effect. Hence, the potential energy in Eq. (3-7) will be due to the shaft strain energy alone as follows:

$$V = \frac{1}{2} k_s \psi^2 \tag{3-13}$$

The Lagrangian [$L = T - V$] for the two generalized coordinate ψ and ϕ will then become:

$$L = \frac{1}{2} J\left(\Omega + \dot{\psi}\right)^2 + \frac{1}{2} m \left[2l(R\cos\phi + l)\left(\Omega + \dot{\psi}\right)\dot{\phi} + (R^2 + l^2 + 2Rl\cos\phi)\left(\Omega + \dot{\psi}\right)^2 + l^2\dot{\phi}^2\right] - \frac{1}{2} k_s \psi^2 \tag{3-14}$$

Substituting Eq. (3-14) into Eqs. (3-9) and (3-10) results in two governing equations of motion, similar to Eqs. (3-11) and (3-12) without the terms containing (g) which are valid when the absorber operates in the horizontal plane.

Neglecting the coupling terms between the shaft and the pendulum, and assuming small oscillations of the pendulum ($\sin\phi \approx \phi$, $\cos\phi \approx 1$), the undamped free vibration equations for the shaft and pendulum can be described as [9]:

Shaft: $$J\ddot{\psi} + k\,\psi = 0 \tag{3-15}$$

Absorber: $$\ddot{\phi} + \left(\frac{R}{l}\,\Omega^2\right)\phi = 0 \tag{3-16}$$

Using Eqs. (3-15) and (3-16), shaft system natural frequency (ω_{rn}) and absorber natural frequency (ω_n) can be written as:

$$\omega_{rn} = \sqrt{\frac{k}{J}} \tag{3-17}$$

$$\omega_n = \Omega \sqrt{\frac{R}{l}} \tag{3-18}$$

It is important to investigate the rotor system behavior when operating at the critical speed at which the rotor speed coincides with the system natural frequency. At this condition, the system has the maximum vibration amplitude. Hence, numerical simulation of the rotor system should be modeled such that

$$\Omega = \sqrt{\frac{k}{J}} \tag{3-19}$$

Also the shaft system is set to be excited with an excitation frequency equal to the system natural frequency:

$$\omega = \sqrt{\frac{k}{J}} \tag{3-20}$$

Applying the resonance tuning condition in order to achieve the best effective inertia of the pendulum, the pendulum design parameters must meet the following requirement [9]:

$$\omega^2 = \omega_n^2 = \Omega^2 \frac{R}{l} \tag{3-21}$$

From Eqs. (3-19) - (3-21), the absorber should be designed such that:

$$\mathrm{R} = l \tag{3-22}$$

3.3 Solution of the nonlinear equations for the 2 DOF systems

In this section, rotor system's natural frequencies are obtained for each case discussed in Section 3.1 and then compared against one another.

Required data related to the shaft, disk, pendulum and excitation torque are provided in Table 3-1. It should be noted that the pendulum length is obtained based on the resonance tuning condition given in Eq. (3-22) in order to achieve the best effective inertia of the pendulum. Also, the excitation torque for all considered cases was assumed to be:

$$T_e = T_o \sin \omega t \tag{3-23}$$

Table 3-1 Specific values used in the analysis

Name	Parameter	Unit	Value
Disk radius	R	cm	17
Pendulum mass	m	kg	1.0
Pendulum length	l	cm	17
Rotor mass moment of inertia	J	$kg.cm^2$	500
Shaft damping ratio	ζ	-	0.01
Shaft diameter	d	cm	3.5
Amplitude of the excitation torque	T_o	$N.m$	50
Shaft torsional stiffness	k_s	$kN.m/rad$	23.57
Shaft system natural frequency	ω_{rn}	Hz	109

3.3.1 Absorber operating in vertical plane

Eqs. (3-11) and (3-12) corresponding to the absorber operating in the vertical plane with $T_e = 0$ (free vibration) are solved numerically considering an initial angular velocity for the shaft system as $\dot{\psi} = 15$ rad/s. Table 3-1 provides the numerical values assigned to the other parameters. The FFT of the rotor response shown in Figure 3-2, clearly illustrates the two damped natural frequencies of the system, $\omega_1 = 19$ Hz and $\omega_2 = 113$ Hz, as the absorber operates in the vertical plane.

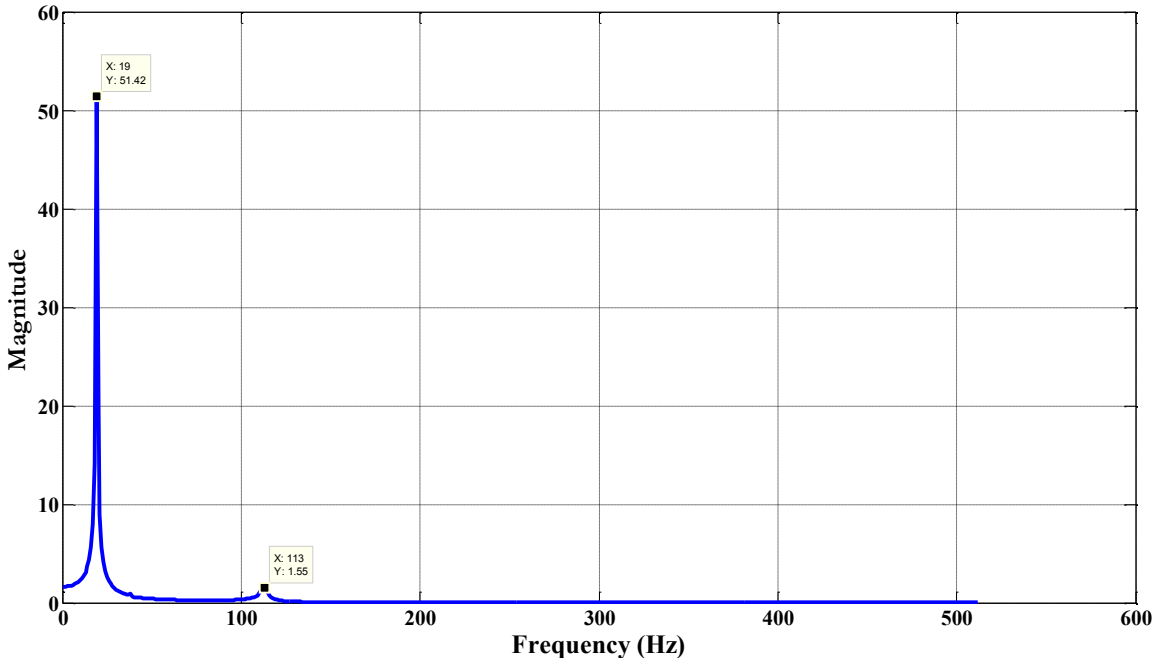

Figure 3-2 Rotor FFT response when CPVA is operating in vertical plane

3.3.2 Absorber operating in horizontal plane

Eqs. (3-11) and (3-12) without (g) terms corresponding to the absorber operating in the horizontal plane with $T_e = 0$ (free vibration) are also solved numerically. The FFT of rotor response shown in Figure 3-3 also illustrates the two damped natural frequencies, $\omega_1 = 20$ Hz and $\omega_2 = 112$ Hz, as the absorber operates in the horizontal plane. By comparing the results obtained for the rotor system natural frequencies in both vertical and horizontal planes, it can be realized that the effect of the gravity has a small contribution on the system natural frequencies.

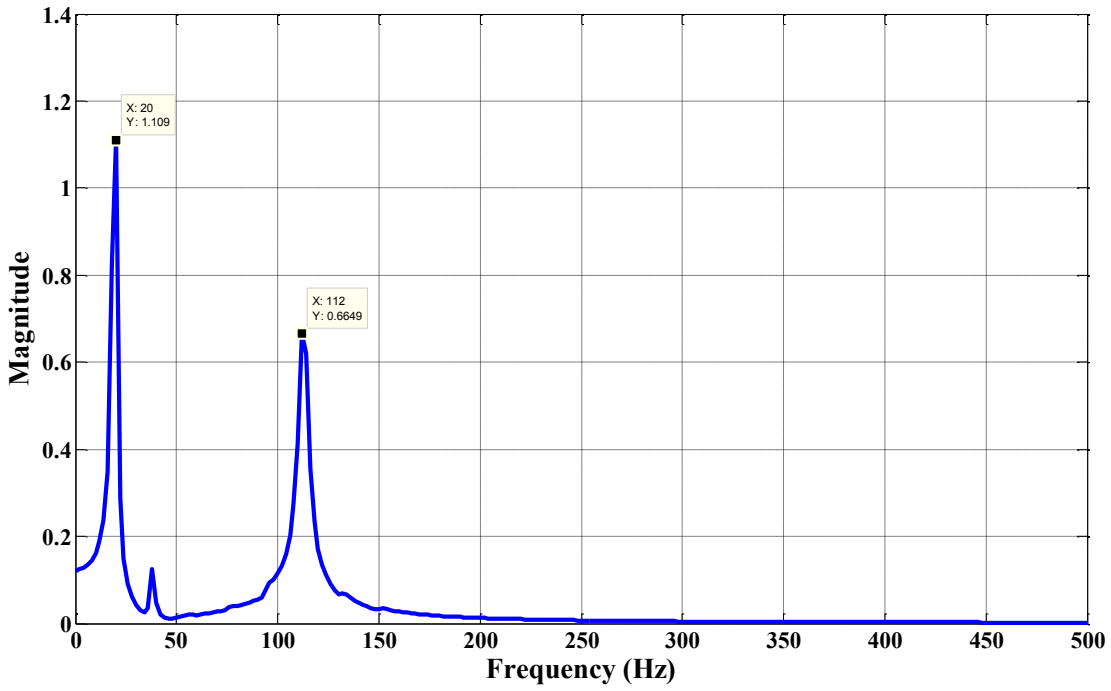

Figure 3-3 Rotor FFT response when CPVA is operating in horizontal plane

3.4 Investigating rotor torsional response

In this section, rotor torsional response is investigated in three different cases. First, when the absorber is operating in the vertical plane at which the gravity effect is considered. Second, when the absorber is operating in horizontal plane with no contribution of the gravity effect. Third case considers the rotor system when it is operating without absorber.

3.4.1 Rotor system with absorber operating in vertical plane

Solving the two nonlinear differential Eqs. (3-11) and (3-12) numerically using Matlab Simulink, the shaft system torsional response when absorber is operating in the vertical plane is obtained and is shown in Figure 3-4. To have a close look at the response amplitude, Figure 3-5 shows a zoom for the steady state response illustrated in Figure 3-4.

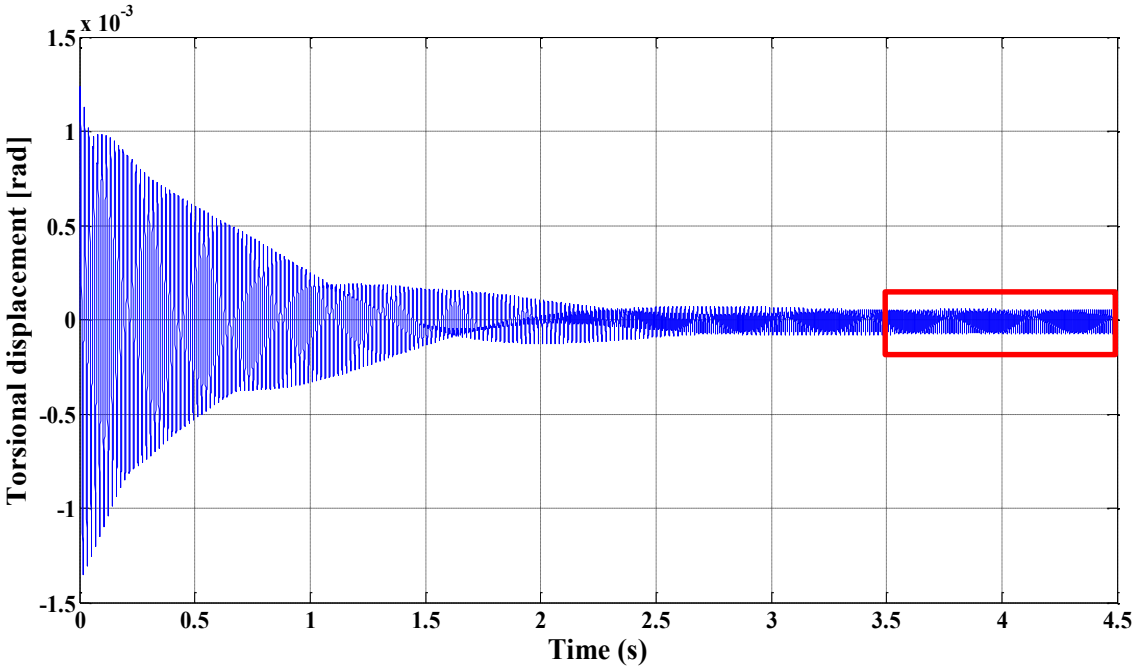

Figure 3-4 Torsional response of the rotor when CPVA is operating in vertical plane

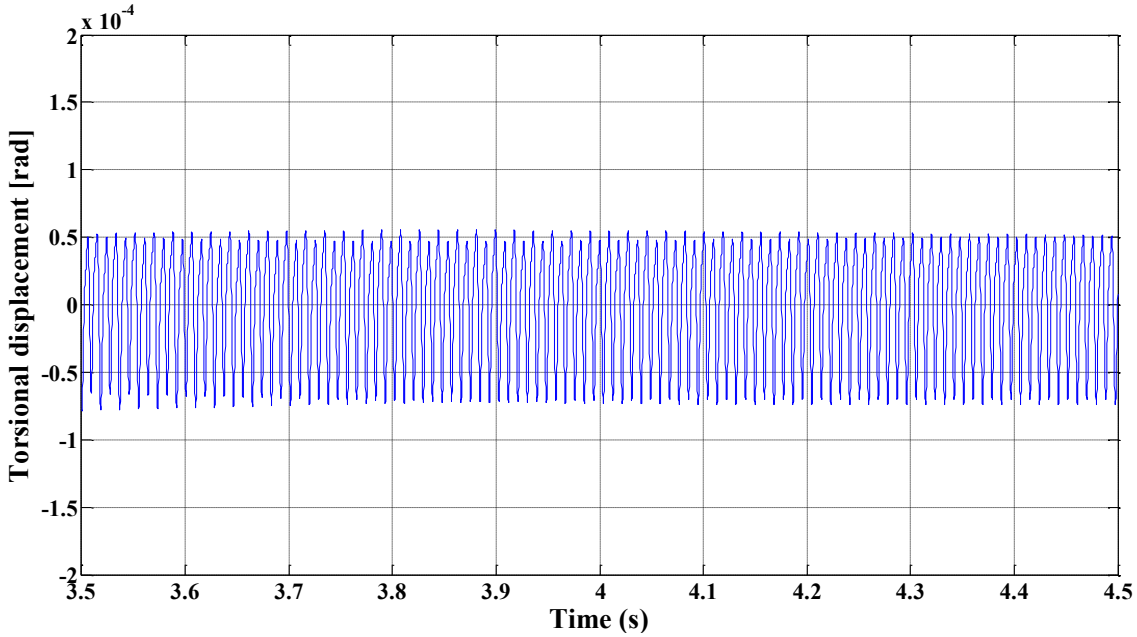

Figure 3-5 Steady state response of the rotor when CPVA is operating in vertical plane

The angular displacement response of the pendulum for this case is also shown in Figure 3-6.

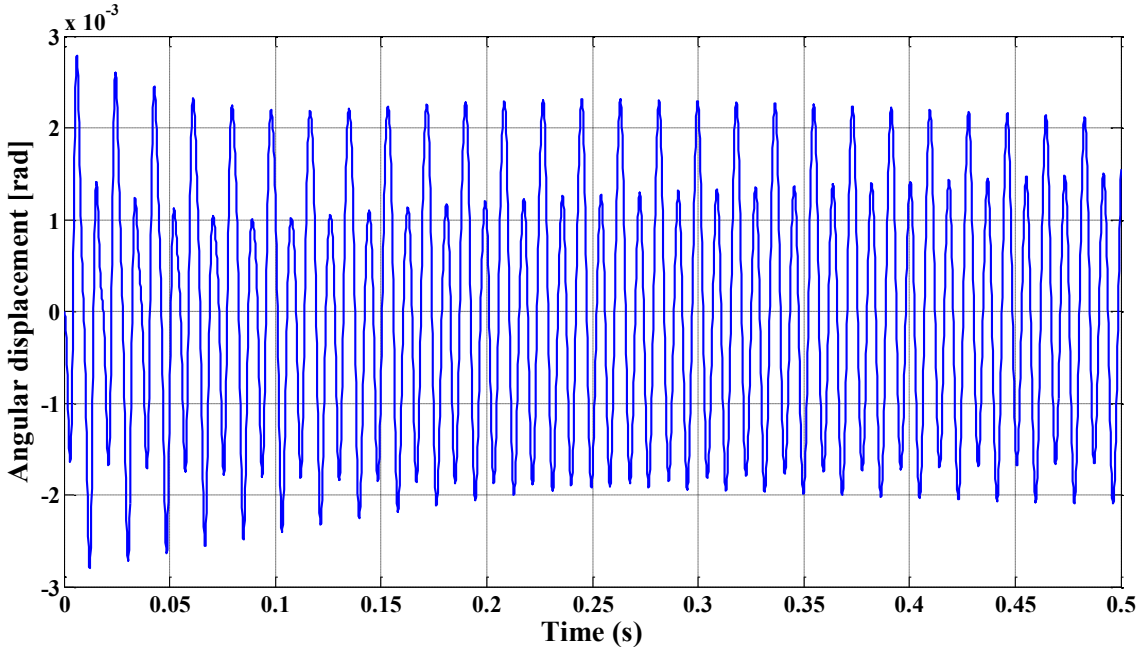

Figure 3-6 Pendulum angular displacement when it is operating in vertical plane

3.4.2 Rotor system with absorber operating in horizontal plane

Now consider the rotor system with the absorber operating in the horizontal plane. By solving Eqs. (3-11) and (3-12) without (g) terms, the system torsional response can be obtained as shown in Figure 3-7 when absorber is operating in the horizontal plane.

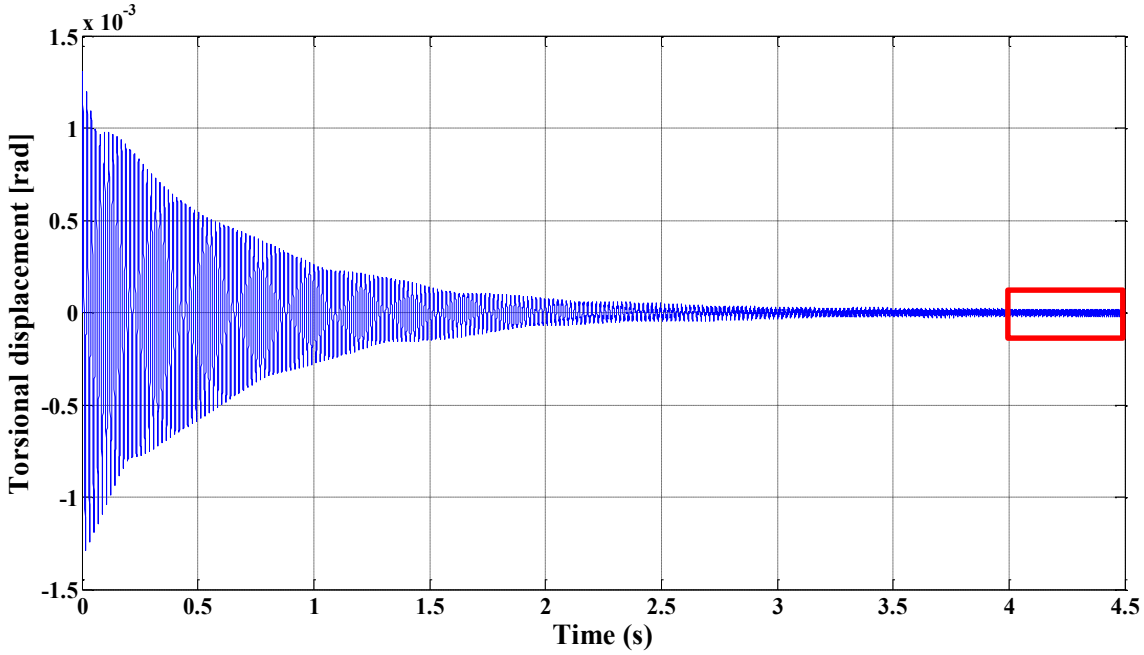

Figure 3-7 Torsional response of the rotor when CPVA is operating in horizontal plane

As in the previous illustration, Figure 3-8 shows a zoom of the steady state response region in order to have a close look at the response amplitude.

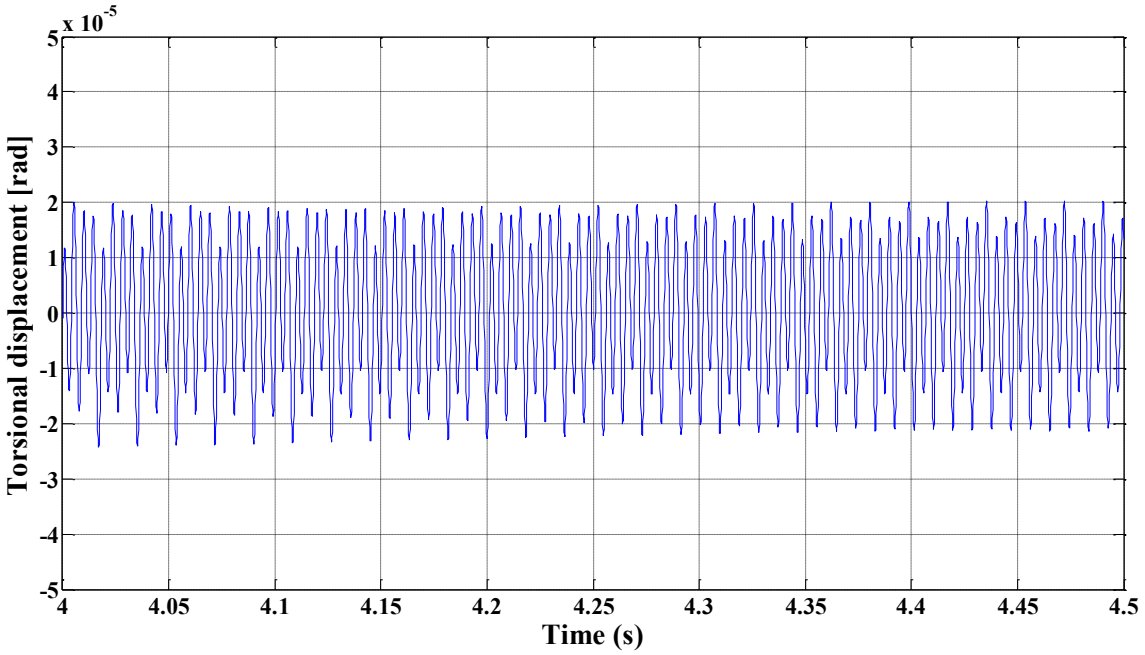

Figure 3-8 Steady state response of the rotor when CPVA is operating in horizontal plane

The pendulum angular displacement response when absorber is operating in horizontal plane is also shown in Figure 3-9.

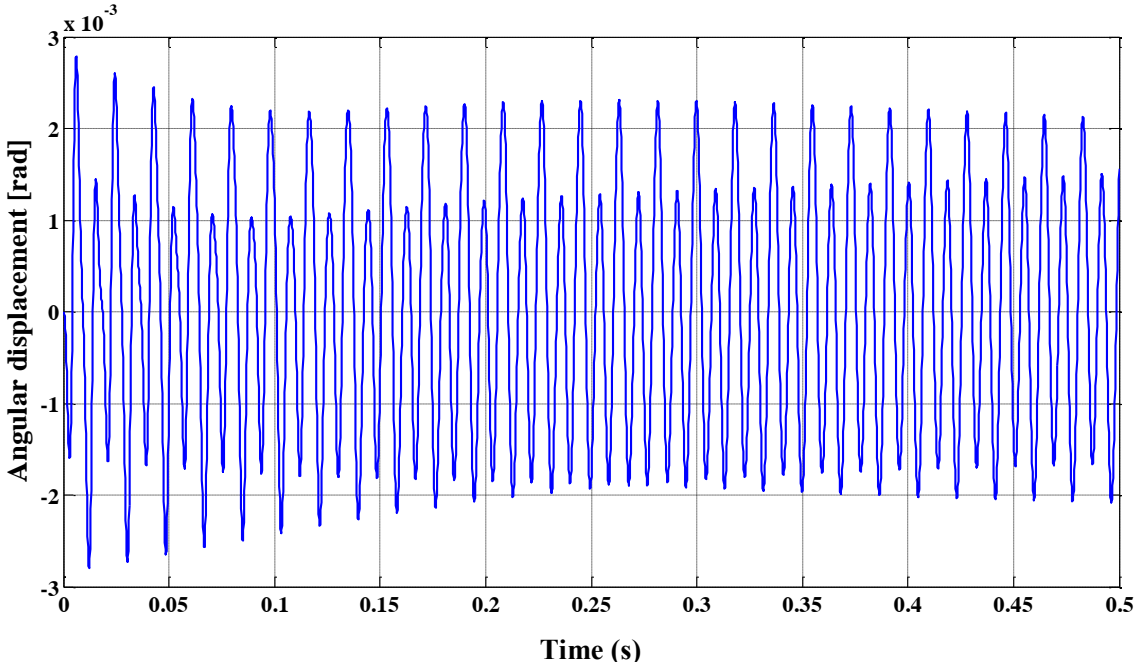

Figure 3-9 Pendulum angular displacement when it is operating in horizontal plane

3.4.3 Rotor system without absorber

In the case of the shaft system operating without the absorber, the equation of motion will be as follows:

$$J\ddot{\psi} + c_r\dot{\psi} + k\,\psi = T_e \tag{3-24}$$

In Figure 3-10, the shaft system torsional vibration responses in both time and frequency domains when operating without absorber are illustrated.

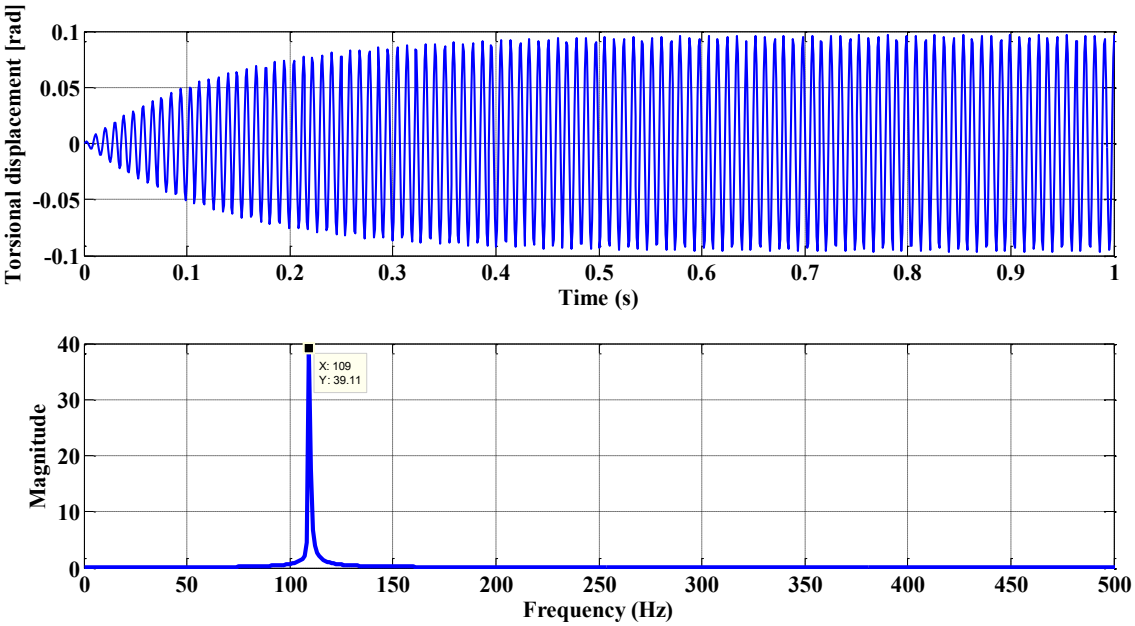

Figure 3-10 Rotor torsional response operating without absorber

Figure 3-4, 3-7 and 3-10 show the shaft torsional response when the rotor system operates in vertical plane, horizontal plane and operates without absorber, respectively. The shaft steady state response amplitude shown in Figure 3-5 is (5×10^{-5} rad) as the absorber operates in vertical plane while as shown in Figure 3-8, it is (2×10^{-5} rad) when the absorber operates in the horizontal plane.

The large difference (almost 60%) in the shaft torsional responses in the two cases is due to the gravity effect when the absorber operates in vertical plane; hence, the pendulum weight contributes to the potential energy term, and results in an additional torsional load on the rotor, which appears clearly in the shaft steady state response in Figure 3-5. Consequently, gravity effect is an important consideration in defining the operational reliability in some important applications such as in aerospace applications.

In contrast, pendulum angular displacement amplitude when operating in both vertical and horizontal planes illustrated in Figure 3-6 and Figure 3-9, show that there is no change in both amplitudes when the absorber is operating either in vertical or horizontal plane.

As shown in Figure 3-10, the rotor steady state torsional response amplitude approaches nearly 0.1 rad as the shaft system operates without absorber. When the absorber is attached to the rotor system, the amplitude is significantly reduced to 2×10^{-5} rad when operating in horizontal plane and 5×10^{-5} rad when operating in vertical plane. This clearly shows that the absorber can effectively reduce large torsional vibrations of the shaft system especially when the absorber is tuned correctly to the resonance tuning condition.

3.5 Rotor torsional amplitudes at different operating speeds

Here, rotor torsional response is investigated over the normal operating speed range of (0 - 120 Hz) in both vertical and horizontal planes. As shown in Figure 3-11, at low operating speed range (0 - 30 Hz), the shaft system operating in vertical plane has torsional vibration amplitude much larger than that when operating in horizontal plane.

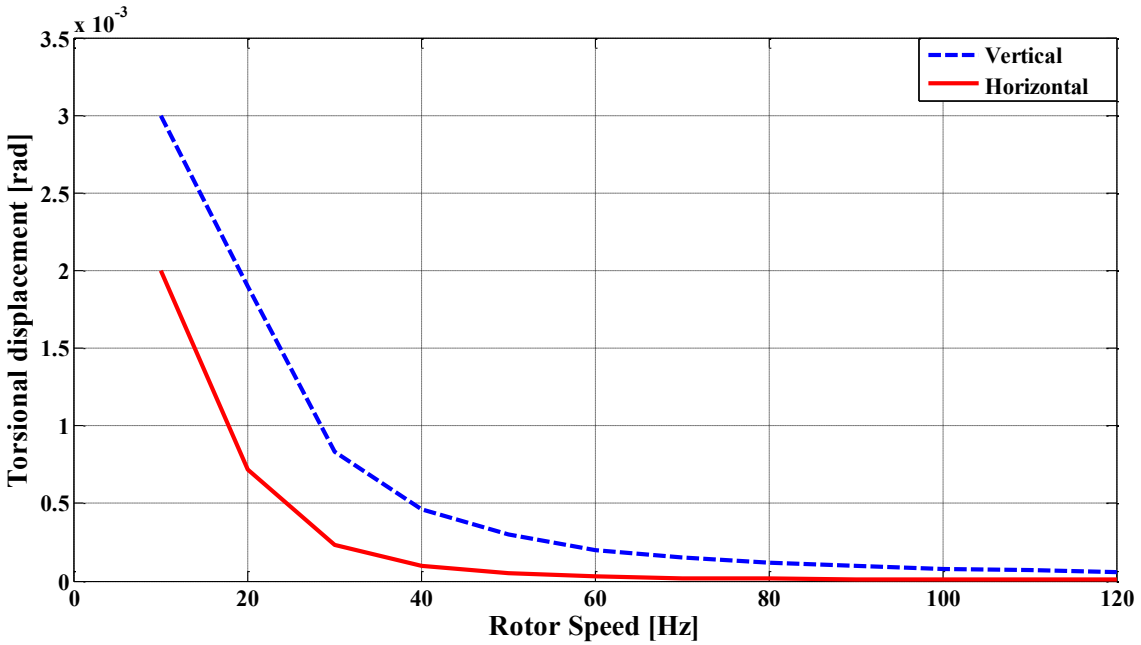

Figure 3-11 Rotor torsional response variation with rotor speed

However, as the rotor operating speed increases, the difference between both amplitudes decreases. In automotive applications, the obtained results serve as important guidelines at the design stage since at low operating speed torsional vibrations transmitted from cylinders at every power stroke results in serious fatigue failure of the crank as well as significant side effect on other mechanisms if not effectively controlled. Consequently, it is important to take into account the gravity effect especially when the rotor system is operating at low speeds.

3.6 Softening behavior of the nonlinear pendulum

As discussed before, for the optimal vibration control, the excitation frequency, ω, should be equal to the natural frequency of the absorber. This requirement results in equal rotor radius, R, and pendulum length, l, when the excitation frequency coincides with the rotation speed, Ω, which is one of the concern here. Figure 3-12 clearly shows that for the rotor speed of 10 Hz, the pendulum natural frequency is also 10 Hz.

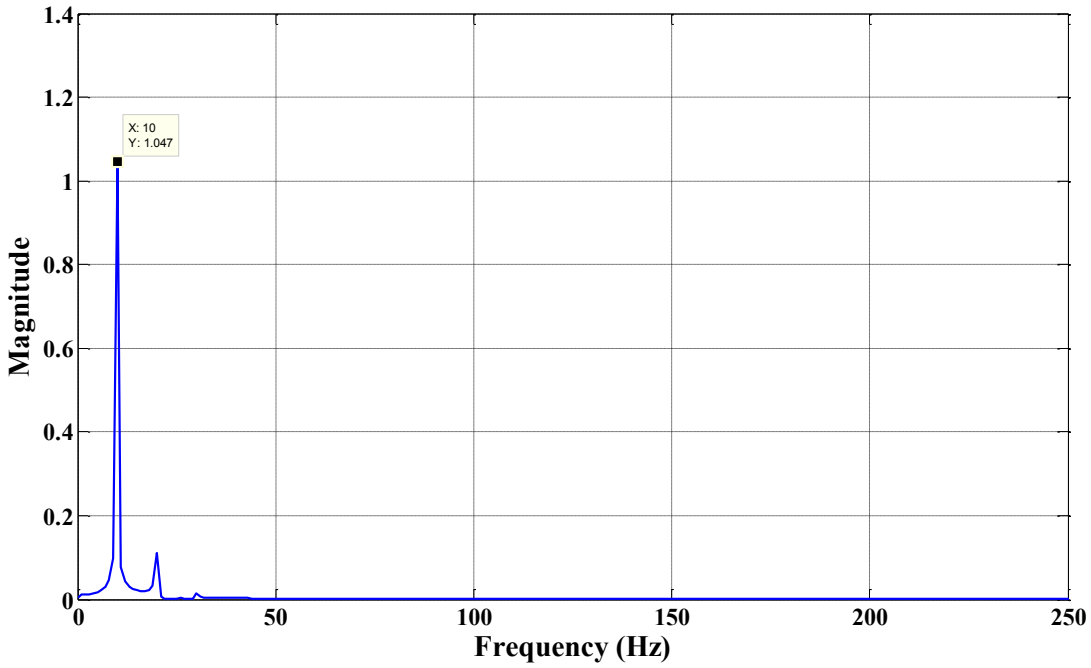

Figure 3-12 Pendulum natural frequency at rotor speed 10 Hz

However, it is found that the pendulum natural frequency deviates from the rotor speed as rotor speed increases. For instance at rotor speed of 50 Hz, the pendulum natural frequency is found to be 40 Hz, as shown in Figure 3-13. To investigate this further, pendulum absorber's natural frequency at different rotor speeds are plotted in Figure 3-14. As it can be realized, the natural frequency of pendulum decreases as the rotor speed increases.

This phenomenon is attributed to the softening nonlinear behavior of the pendulum absorber with circular path [7].

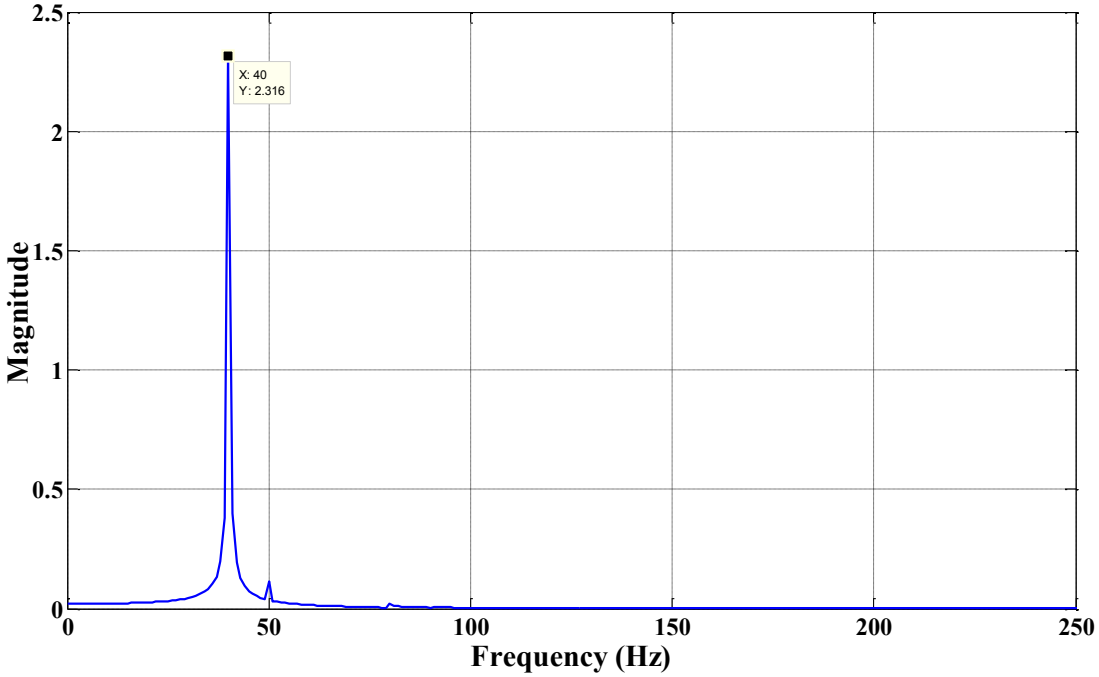

Figure 3-13 Pendulum natural frequency at rotor speed 50 Hz

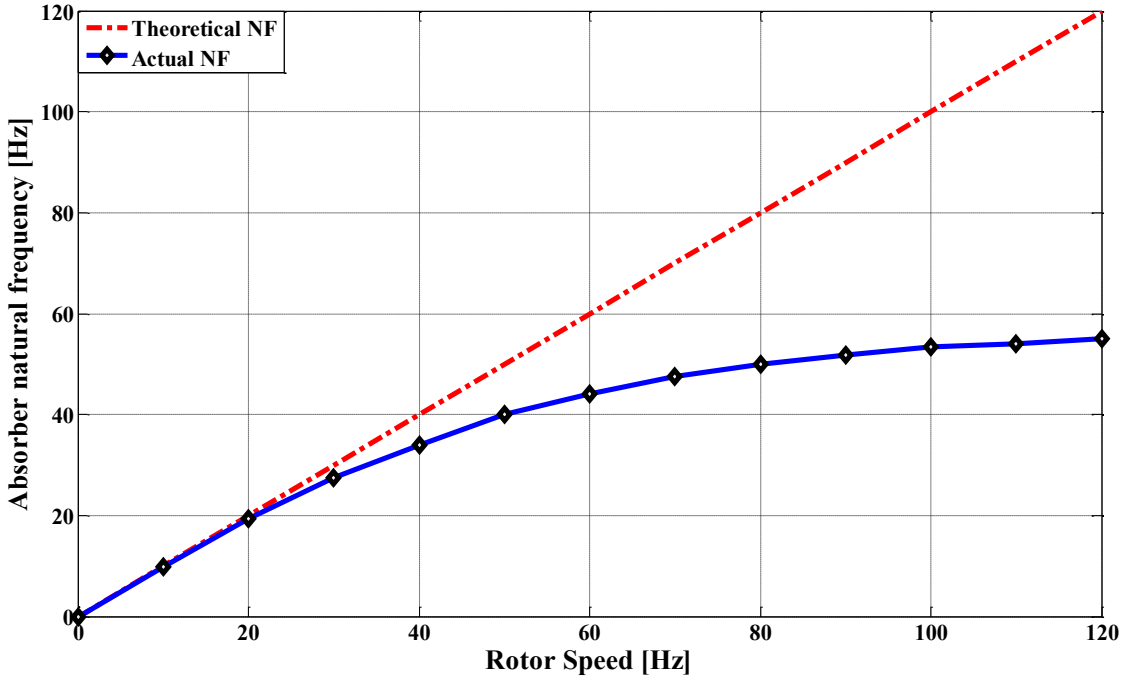

Figure 3-14 Pendulum natural frequency variation with rotor speed

Hence, absorbers with circular paths exhibit softening nonlinear behavior in which their frequency decreases as the amplitude increases. To overcome this shortcoming in the circular path absorbers, a small mistuning must be intentionally introduced to ensure stable and reliable operation of the CPVA.

3.7 Summary

In this chapter, a mathematical model for the rotor system with the pendulum absorber has been developed and the governing equations of motion for the whole system have been derived. Unlike in the past research, the rotor system with pendulum absorber was investigated in both vertical and horizontal planes in this study, in order to assess the effect of gravity. The pendulum absorber with circular path has been considered in this analysis. Three different cases have been investigated. The rotor system torsional responses have been illustrated when the absorber is operating in vertical plane, horizontal plane and when the system is operating without absorber. Results obtained from each case have been illustrated and compared against one another. Moreover, the softening nonlinear behavior of the pendulum with circular path has been investigated over the range of the operating speed.

Chapter 4
Modeling, Design Optimization and Fabrication of Torsional MR Damper

4.1 Introduction

Magnetorheological (MR) fluid based dampers have been considered as one of the most promising devices for semi-active control of torsional vibration due to their variable damping feature, fast response, low power consumption and capability to attenuate vibration under unpredictable environmental conditions [70-72]. Furthermore, MR dampers are inherently fail-safe devices in view of the inherent viscosity of the MR fluid. This implies that when there is a fault within the system, the MR damper could operate as a passive damping device within certain performance parameters. Over the past few decades, there have been many experimental and analytical studies that demonstrated the enhanced potentials of MR dampers in realizing variable damping with desired response time [73, 74].

Potential applications of MR dampers extend to Automotive and Aerospace industries, train suspensions, seismic protection of bridges and buildings [75-79]. Since MR fluids demonstrate highly nonlinear behavior due to the applied magnetic field, a great effort is spent in characterizing the nonlinear properties of MR dampers as well as developing accurate models featuring dynamic behavior of such devices.

In this chapter, a mathematical modelling of the rotary MR damper is carried out to predict its dynamic performance. MR fluids are modeled based on the constitutive Bingham plastic model that is suitable in the initial design phase.

Furthermore, a design optimization methodology is proposed to identify the optimal dimensions of the rotary MR damper in order to maximize the generated damping torque while minimizing damper size and weight.

4.2 Mathematical model of rotary MR damper

A large number of analytical models have evolved in recent years to describe the nonlinear characteristics of MR fluids, including the Bingham plastic model [29, 80], the biviscous model [34] and the Herschel-Bulkley model [30, 81]. For accurate modeling of rotary MR damper with a given specification, one must establish a governing relationship between the critical geometrical parameters of the damper, MR fluids rheological properties, magnetic field density and generated damping torque.

4.2.1 Classification of rotary MR damper

Several types of rotary MR dampers have been introduced in the past decade. Rotary MR dampers can generally be divided into two main types, depending on the location where the shear mode occurs, and a combination of them. First is the disk type MR damper, in which the effective area of shear mode takes place in the end face gaps of the rotating shaft, as shown in Figure 4-1. Thus, the performance of disc type damper can be improved by increasing the effective area of shear mode. Two approaches have been considered in order to achieve such an increase in the effective area such as by increasing the radius of the rotating disc or by using multiple discs. Obviously, it was shown that multiplying the number of discs in MR dampers is better than implementation of large rotating disc, which significantly increases the size of MR damper [37].

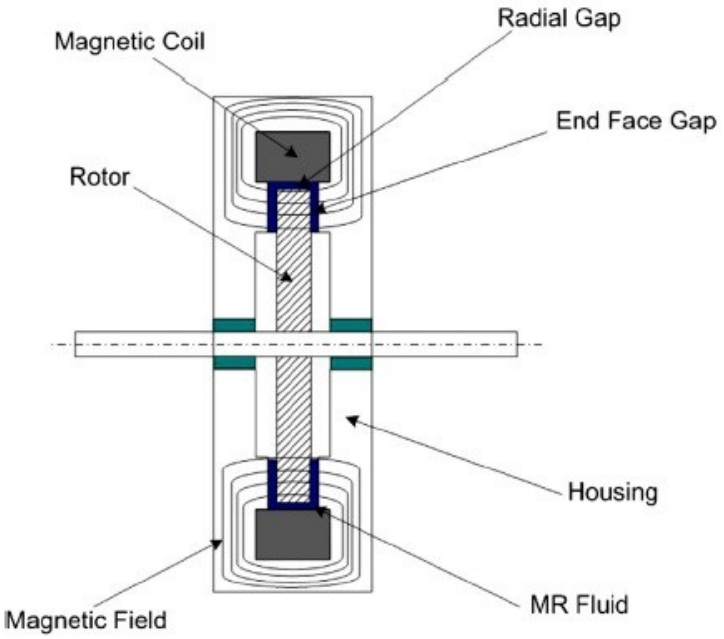

Figure 4-1 Disc type rotary MR damper [37]

Second type is the drum type damper, in which the effective area of shear mode takes place in the circumferential gap of rotating shaft as shown in Figure 4-2. These types can offer very large torques especially in the case where the damper diameter is limited, since their effective surface area is larger than that in disc type dampers. Their design and advantages make them more suitable for braking applications rather than damping [82]. There are several structural designs and magnetic circuit configurations that have been proposed to improve the damper performance by increasing the effective surface area or by optimizing the strength of the magnetic field density [83-86].

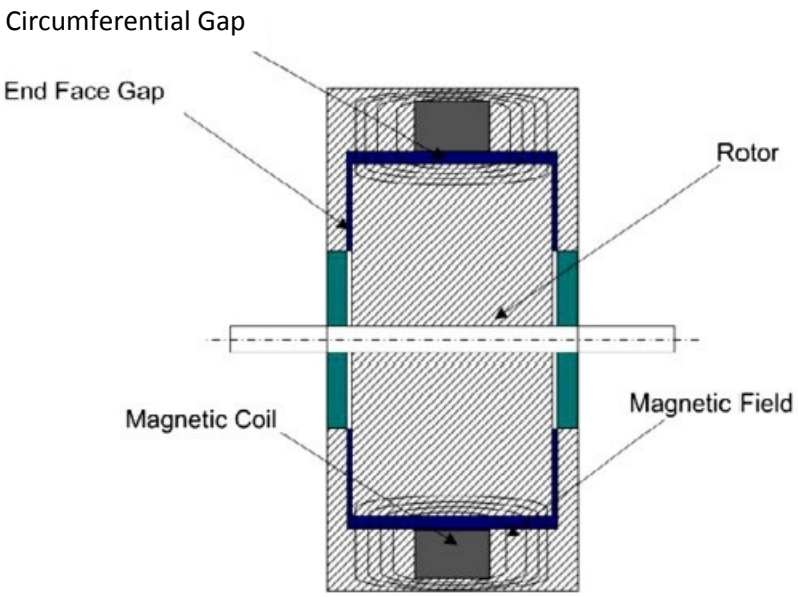

Figure 4-2 Drum type rotary MR damper [37]

Another type of rotary MR damper is the T-shaped design, which is a combination of both disk and drum types but more complex, in which a T-shaped rotor is spinning instead of a simple disk, as shown in Figure 4-3.

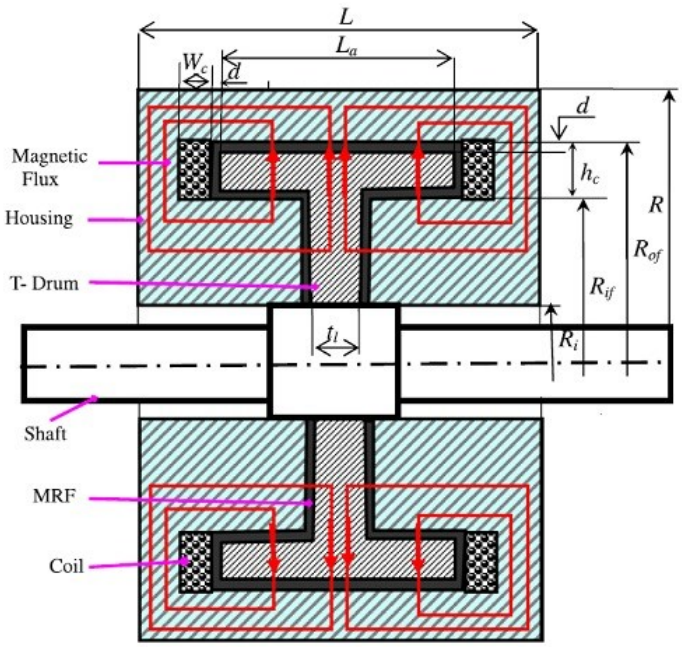

Figure 4-3 T-shaped rotary MR damper [87]

T-shaped configuration, as shown in Figure 4-3, is more effective than other designs, since it has multiple effective areas; hence, the generated damping torque is multiplied. However, they are more complicated in their design and manufacturing [87].

Taking into consideration time for cost and simplicity of manufacturing, disk type damper has been selected as the preferred configuration for the proposed MR damper.

4.2.2 Characteristic equations of a rotary MR damper

MR damper is operated in the shear mode in which the disc is rotating relative to the housing and the MR fluid fills the gap between disc and the housing. Since the MR fluid gaps are very small, the essential magnetic field dependent fluid characteristics of MR fluids can be described by the constitutive Bingham plastic model [88] which is suitable in the initial design phase [70]. The Bingham plastic model is also widely used as a basis in linear and rotary MR damper modelling [37]. In the Bingham plastic model the rheological behavior of MR fluid is described in pre-yield region as rigid while in post-yield region as Newtonian [81].

In order to model the MR damper, the behavior of the MR fluid under magnetic field application has to be modeled. The Lord Corporation's MRF-132DG is used as the working fluid in this research study. The stress-shear strain rate behavior of this fluid in the absence of magnetic field is provided by the Lord Corporation and is shown in Figure 4-4 [89]. As it can be realized, the behavior of the fluid can be well approximated by the Bingham plastic model.

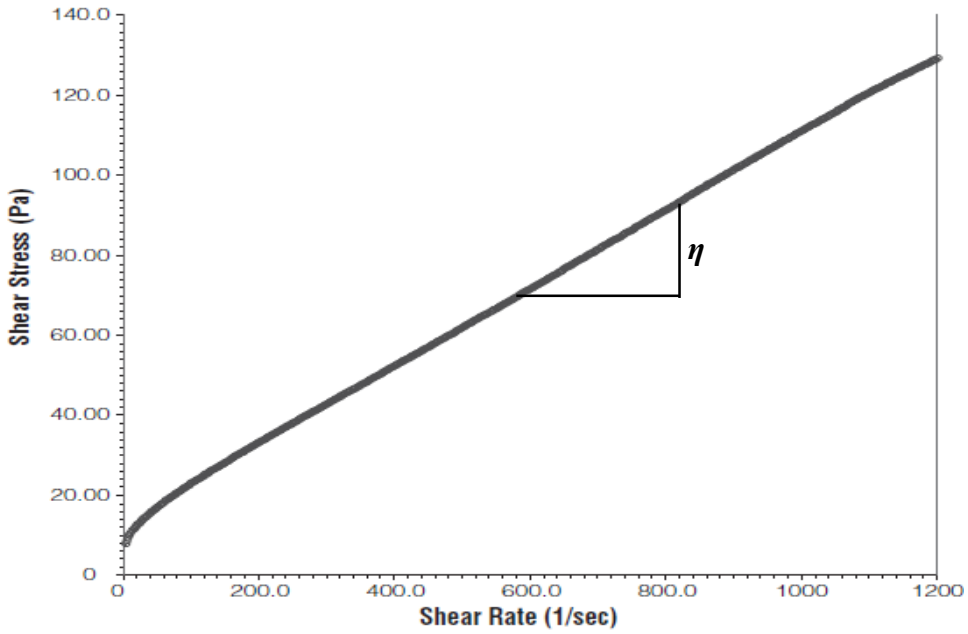

Figure 4-4 Shear stress as a function of shear-strain rate at zero-field for MRF-132DG

As discussed in Chapter 2, the total shear stress using Bingham plastic model can be described as:

$$\tau = \tau_y(H) + \eta\dot{\gamma} \tag{4-1}$$

where τ_y is the induced yield stress controlled by the applied magnetic field H, η is the post yield viscosity of the MR fluid that is assumed to be independent of the applied magnetic field and $\dot{\gamma}$ is the shear strain rate. As shown in Figure 4-4, the post yield viscosity is defined as the slope between the shear stress and shear-strain rate. The variation of the yield stress versus applied magnetic field intensity for MRF-132DG obtained experimentally, provided by Lord Corporation, is shown as solid squares in Figure 4-5 [89]. As it can be seen, the MR fluid saturates at high applied magnetic field intensity. Based on Figure 4-5, a mathematical relation can be easily constructed to describe the

variation of the yield stress versus applied magnetic field intensity. Here, the following cubic polynomial function has been suggested [69]:

$$\tau_y = x_0 + x_1 H + x_2 H^2 + x_3 H^3 \qquad (4\text{-}2)$$

It is noted that, the unit of the yield stress is kPa while that of the magnetic field intensity is kAm^{-1}. The coefficients x_0, x_1, x_2 and x_3 have been determined from least square method to minimize the error between the function and experimental values and they are found to be x_0 = - 0.3641, x_1 = 0.3766, x_2 = - 8E-04 and x_3 = 4E-07. The variation of yield stress versus applied magnetic field intensity using Eq. (4-2) is shown as a solid curve in Figure 4-5 as well. It can be seen that the predicted yield stresses using Eq. (4-2) agree very well with those experimental values.

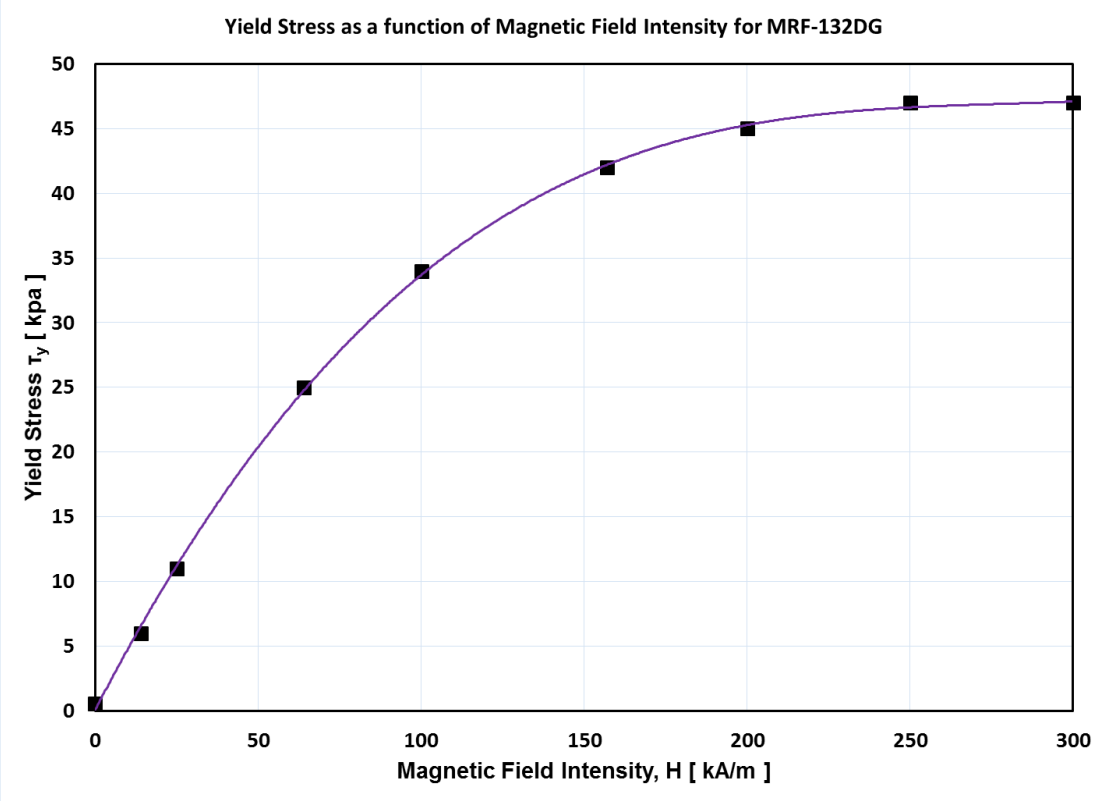

Figure 4-5 Yield stress of MR fluid as a function of magnetic field intensity [89]

Figure 4-5 shows that when the magnetic field intensity is nearly above 275 kA m^{-1}, the MR fluid reaches to a saturation state and the saturated yield stress is almost 48 kPa.

Here, disk type rotary MR damper has been selected to derive the damping torque. A simple sketch of configuration of disk type rotary MR damper mounted on a rotating shaft is shown in Figure 4-6.

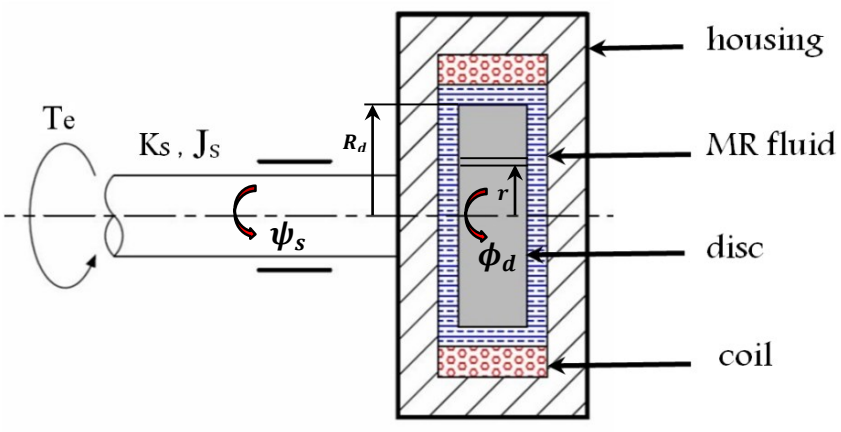

Figure 4-6 Configuration of MR damper

The damping torque generated within the rotary MR damper at end faces can be defined as follows:

$$T_{d_1} = 2\int_A \tau\, r dA = 4\pi \int_0^{R_d} \tau\, r^2 dr \tag{4-3}$$

where A is the working surface area where the fluid is activated by the applied magnetic field, R_d is the disk radius and r is the radial distance from the center of the disk. Since the MR fluid gap is very small, it is reasonable to assume a linear shear rate distribution of the MR fluid in the gaps. Thus, the shear rate can be obtained by:

$$\dot{\gamma} = \frac{r\omega}{d} \tag{4-4}$$

where ω is the angular velocity of the disk and d is the thickness of the MR fluid gap at end faces of the disk. By substituting Eq. (4-4) into Eq. (4-1) and then Eq. (4-1) into Eq. (4-3), the field dependent damping torque can be expressed as:

$$T_{d_1} = 4\pi \int_0^{R_d} \left(\tau_y(H) + \eta \frac{r\omega}{d}\right) r^2 dr \tag{4-5}$$

Therefore,

$$T_{d_1} = \frac{4}{3}\pi\tau_y R_d^3 + \frac{\pi\eta\omega}{d} R_d^4 \tag{4-6}$$

It should be noted that the first term in Eq. (4-6) represents the damping torque due to field dependent yield stress (T_{ye}) while the second term represents damping torque due to fluid viscosity (T_{vis}). The MR fluid located in gap, at the circumferential surface of the disk is not exposed intensely to the magnetic flux and thus the damping torque generated on this surface due to friction can be described as:

$$T_{d_2} = (2\pi R_d b_d) R_d \tau_o = 2\pi R_d^2 b_d \left(\tau_{yo} + \eta_o \frac{\omega R_d}{d_0}\right) \tag{4-7}$$

where b_d is the thickness of the disc and d_o is the thickness of the annular duct encapsulating the MR fluid. τ_o is the shear stress experienced in the MR fluid in the absence of magnetic field and subsequently η_o and τ_{yo} are, respectively, the post-yield viscosity and yield stress of the MR fluid when no magnetic field is applied.

Thus, total damping torque developed in the rotary MR damper, shown in Figure 4-6, can be expressed as:

$$T_d \ = T_{d_1} + T_{d_2} = \frac{4}{3}\pi\tau_y R_d^3 + \frac{\pi\eta\omega}{d} R_d^4 + \ 2\pi R_d^2 b_d \left(\tau_{yo} + \eta_o \frac{\omega R_d}{d_0}\right) \tag{4-8}$$

Applying Newton's second law, the dynamics of the system with a rotary MR damper can be mathematically expressed as follows:

$$J_s\ddot{\psi}_s + T_d + k_s\psi_s = T_e \tag{4-9}$$

$$J_d\ddot{\phi}_d = T_d \tag{4-10}$$

such that, the shaft spins through an angle ψ_s with torsional stiffness k_s and inertia J_s. The rotating disk with inertia J_d spins through an angle ϕ_d. The shaft system is driven by an external harmonic torque T_e, and T_d is the total damping torque generated in MR damper as expressed in Eq. (4-8).

4.2.3 MR magnetostatic modeling

In order to calculate the damping torque, it is necessary to obtain the yield stress of the MR fluid. As can be seen from Eq. (4-2), the MR fluid yield stress in the active areas, at which the magnetic flux crosses MR fluid depends on applied magnetic field intensity, *H*, which can be subsequently obtained by solving the magnetic circuit of the damper.

The electromagnetic coil of the magnetic circuit in the MR damper is the main generating source for the magnetic flux through the damper. The magnetic circuit can be analytically expressed by using Ampere's law, in which the relationship between the current (*I*) and the magnetic field strength (*A/m*) could be formulated as:

$$\oint H \cdot dl = N \cdot I \tag{4-11}$$

where H is the magnetic field intensity, l is the length of the conductor enclosing the current and I is the applied current flowing through the coil wire. In addition, the magnetic flux can be written in terms of the magnetic flux density following the rule of magnetic flux conservation in the given circuit as:

$$\Phi = \oint \vec{B} \cdot dA \tag{4-12}$$

where Φ is the magnetic flux of the circuit, A and B are the cross sectional area and the magnetic flux density, respectively. Magnetic flux density and magnetic field intensity are also related by the following relation:

$$B = \mu_o \cdot \mu_r \cdot H \tag{4-13}$$

where μ_o is the magnetic permeability of vacuum ($4\pi 10^{-7}$ $T.m/A$) and μ_r is the relative permeability of materials. From Eqs. (4-12) and (4-13), it is clear that the magnetic flux depends on cross sectional area, magnetic field intensity and the core material.

As the magnetic field becomes large, saturation state of the material can be reached, and hence the material becomes magnetically saturated. Typically, different materials have different saturation levels; the nonlinear magnetization B-H curve shows the magnetic property of a material.

The B-H behavior of the structural steel used for damper housing and the rotating disk, also that of the MR fluid (MRF-132DG) are shown in Figure 4-7 and Figure 4-8, respectively.

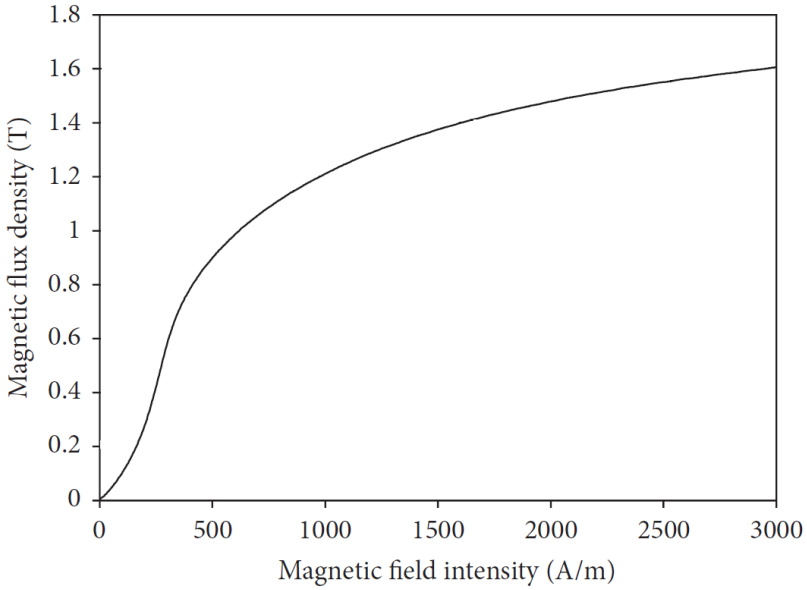

Figure 4-7 B-H curve of ferromagnetic material SS 400

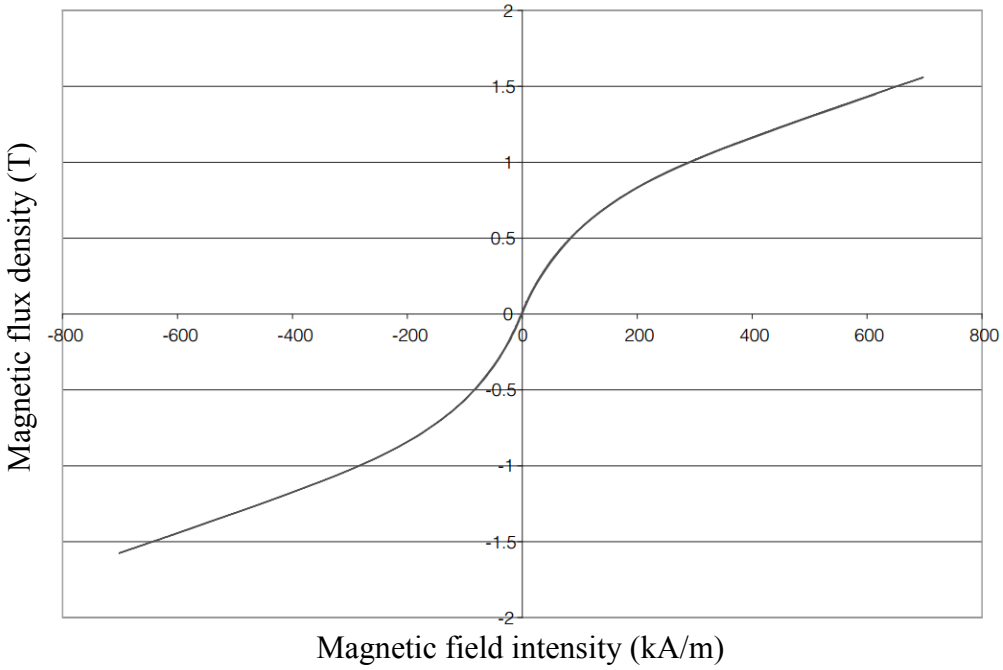

Figure 4-8 B-H curve of MRF 132 DG [89]

Since it is very difficult and complicated to find the exact analytical solution for the magnetic field intensity, H, generated in the magnetic circuit, typically simplified assumptions are made to find approximate solution for H [90]. Figure 4-9 shows the approximate magnetic circuit and flux lines in the typical rotary MR damper.

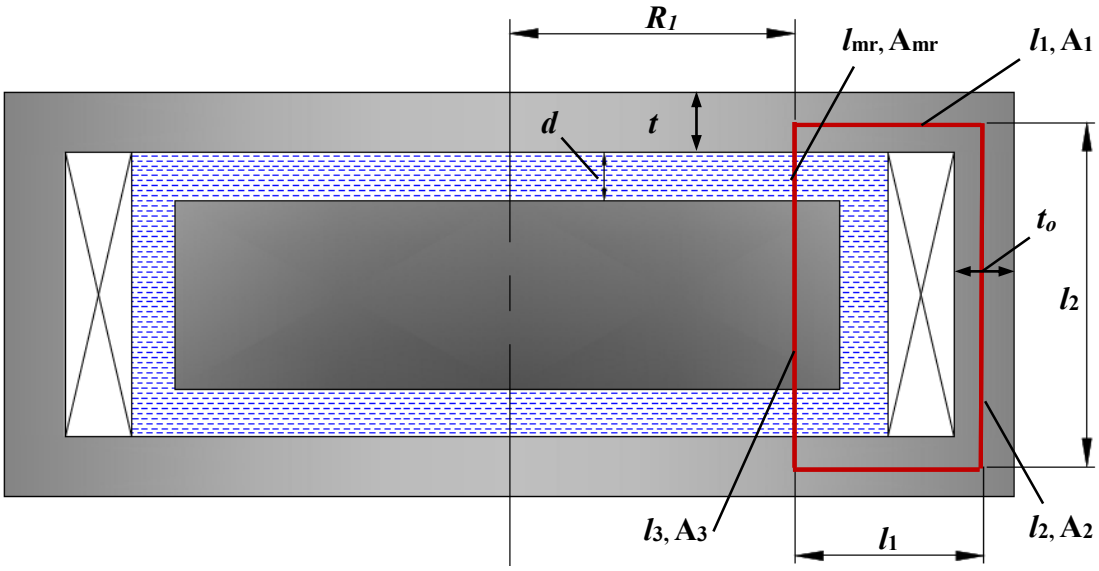

Figure 4-9 Approximate magnetic circuit of MR damper

Thus, the integration in Eq. (4-11) can be approximated by the summation along the approximated magnetic flux lines shown in Figure 4-9 as:

$$\sum_{i=1}^{4} H_i l_i = N \cdot I \tag{4-14}$$

while the magnetic flux is given by

$$\Phi = B_i \cdot A_i \; ; \qquad i = 1 \text{ to } 4. \tag{4-15}$$

Now assuming that there is no magnetic flux leakage, Eqs. (4-14) and (4-15) may be expanded as:

$$2H_1 l_1 + H_2 l_2 + H_3 l_3 + H_{mr} l_{mr} = N \cdot I \tag{4-16}$$

$$\Phi = B_1 A_1 = B_2 A_2 = B_3 A_3 = B_{mr} A_{mr} \tag{4-17}$$

where H_{mr} and B_{mr} are the effective magnetic field intensity and the magnetic flux density in the MR fluid region where the magnetic field crosses the MR fluid, respectively. Furthermore, A_{mr} and l_{mr} are the effective cross sectional area and the length of the MR fluid link, respectively, and are given by

$$l_{mr} = 2\,d \tag{4-18}$$

$$A_{mr} = \pi R_1^2 \tag{4-19}$$

$$A_1 = 2\pi(R_1 + l_1/2)\,t \tag{4-20}$$

$$A_2 = 2\pi(R_1 + l_1)\,t_o \tag{4-21}$$

$$A_3 = \pi R_1^2 \tag{4-22}$$

Therefore, by substituting Eqs. (4-18), (4-19), (4-20), (4-21) and (4-22) into Eqs. (4-16) and (4-17), and using the B-H curves of the MR fluid and damper structure material, the magnetic circuit can be solved to find magnetic field intensity in the MR fluids gap area. In general, for common magnetic materials, the magnetic flux density shows a nonlinear relationship with the applied magnetic induction. At low magnetic field, this relationship behaves linearly, i.e. below the saturation state of the magnetic material. Consequently, at low magnetic field, the approximated magnetic field intensity over the MR fluid link can be expressed as

$$H_{mr} = \frac{N\,I}{2\,d + \frac{2l_1\mu_{mr}A_{mr}}{\mu A_1} + \frac{l_2\mu_{mr}A_{mr}}{\mu A_2} + \frac{l_3\mu_{mr}A_{mr}}{\mu A_3}} \tag{4-23}$$

where μ_{mr} and μ are the relative permeability of the MR fluid and the damper structure material, respectively. The permeability can be calculated from the slopes of the B-H curves for the MR fluid and structural Steel materials. Therefore, magnetic saturation characteristics of the MR fluid and the structure material should be taken into consideration in the design and analysis of the MR damper.

4.2.4 Finite element analysis

In order to ensure efficient design of the proposed damper and to improve the accuracy of the magnetic circuit solution, a finite element (FE) model of the rotary MR damper has also been developed. Considering the intensity and the required nonmagnetic characteristic of the damper components, aluminum has been selected as the material for the bobbin. All the other components of the damper are made of steel, which is rigid enough to support the whole structure of the damper and can be magnetized as well. Since MR damper consists of several parts with different material properties, ferromagnetic and paramagnetic materials, the magnetic field distribution has to be calculated within the MR damper in order to evaluate the generated yield stress in MR fluids for analysis and design purposes. A FE model of MR damper is developed using commercial ANSYS software in order to obtain an accurate estimation of the magnetic field distribution within MR damper. The FE model is a quasi-static model, which investigates the relation between the magnetic field density in the MR fluid gap and the input current of the electromagnetic coil within the defined MR damper geometry.

First, a three-dimension model of the proposed damper is developed using Solidworks software and then imported into ANSYS workbench environment for FE analysis. Due to

the symmetrical structure of the rotary damper, a 2D axisymmetric model can be effectively used to reduce computational cost for the magnetostatic analysis. In this study, the PLANE13 element is used which has 2-D magnetic, thermal, electrical, piezoelectric, and structural field capabilities. The element is defined by four nodes having four degrees of freedom per node. For the finite element used in this study, the total number of elements is 60090 and number of nodes is 226621. The FE model showing the simulation results for the magnetic field distribution is shown in Figure 4-10. The characteristic B-H curve for the MR fluid is obtained from Lord Corporation [89] as shown in Figure 4-8, while that for steel assigned for housing and disc material is available in ANSYS material library as shown in Figure 4-7.

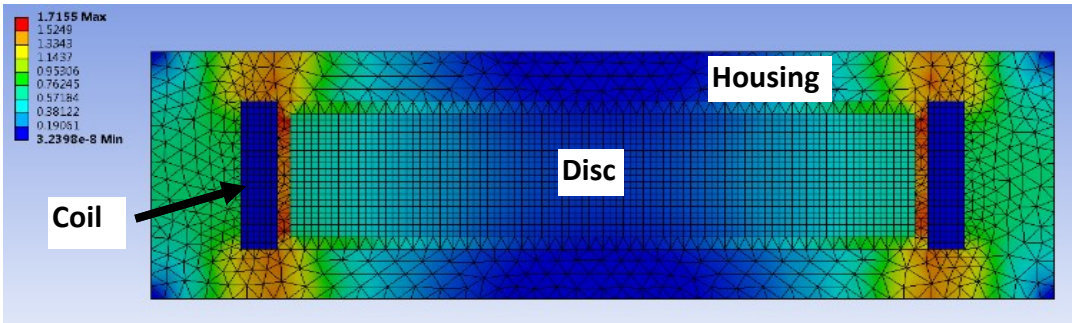

Figure 4-10 FE model of the rotary MR damper

After material properties were defined, an external air region surrounding the entire geometry of MR damper is created, and following that a suitable mesh is generated. It is obvious that the finer the mesh size, the more accurate solution can be obtained. However, small mesh size results in high computation time. Thus, the number of elements used in the analysis provides a fine mesh size at which the solution converges in reasonable computational time.

Using the FE model, the magnetic field distribution within the entire geometry is obtained. Figure 4-10 shows the magnetic flux density and distribution of magnetic field within MR damper. The magnetic field has been generated in the FE model based on 400 coil turns and an applied current of 1.6 A. The magnetostatic finite element analysis shows that the magnetic flux density value is around 1.33 - 1.52 T, near the electromagnetic coil which is an optimal desired value since it is lower than the saturation limit (~1.6T) of the chosen structural steel (SS-400) for the housing and disk of the MR damper [91]. Hence, the obtained results show a considerable agreement in the initial design phase of the rotary MR damper with a specified maximum applied current and unsaturated magnetic flux density.

4.3 Design optimization of rotary MR damper

In this section, a design optimization methodology is proposed to identify the optimum geometric dimensions of the MR damper. An optimization process is carried out with the main objective to maximize the generated damping torque subject to size and volume (or weight) constraints. The rotary MR damper is constrained in a specific volume considering an appropriate space and allowable weight for the MR damper.

A hybrid optimization technique has been used in this research, which combines the Genetic Algorithm (GA) with a Sequential Quadratic Programming (SQP) technique. GA algorithm is considered as a popular stochastic based optimization algorithm capable of locating the near global optimum point. Here GA is initially used to determine the near global optimum solution. The optimal results from GA are then used as initial values for the SQP technique to accurately capture the true global optimum point.

It is noted that SQP is a powerful gradient-based nonlinear programming technique capable of capturing the local optimum point accurately.

4.3.1 Optimization problem formulation

The optimization problem is to find the optimal value of significant geometrical dimensions of the rotary MR damper with the objective to maximizing the generated damping torque for a given volume. The MR damper has been constrained in a specific volume through axial and radial constrained dimensions. Basic configuration of MR damper is shown in Figure 4-11. The effective design parameters that significantly affect the performance of MR damper are considered as design variables and they are identified as follows:

a- The outer radius of the disc (R_d)

b- The bore radius (R_b)

c- The width of the disc (b_d)

The considered design variables contribute to both radial and axial dimensions of the MR damper subjected to geometry, inertia and torque constraints, where the geometry constraints are the spatial limits in radial and axial directions. The inertia constraints are the ratio of moments of inertia of the disc to that of the shaft system.

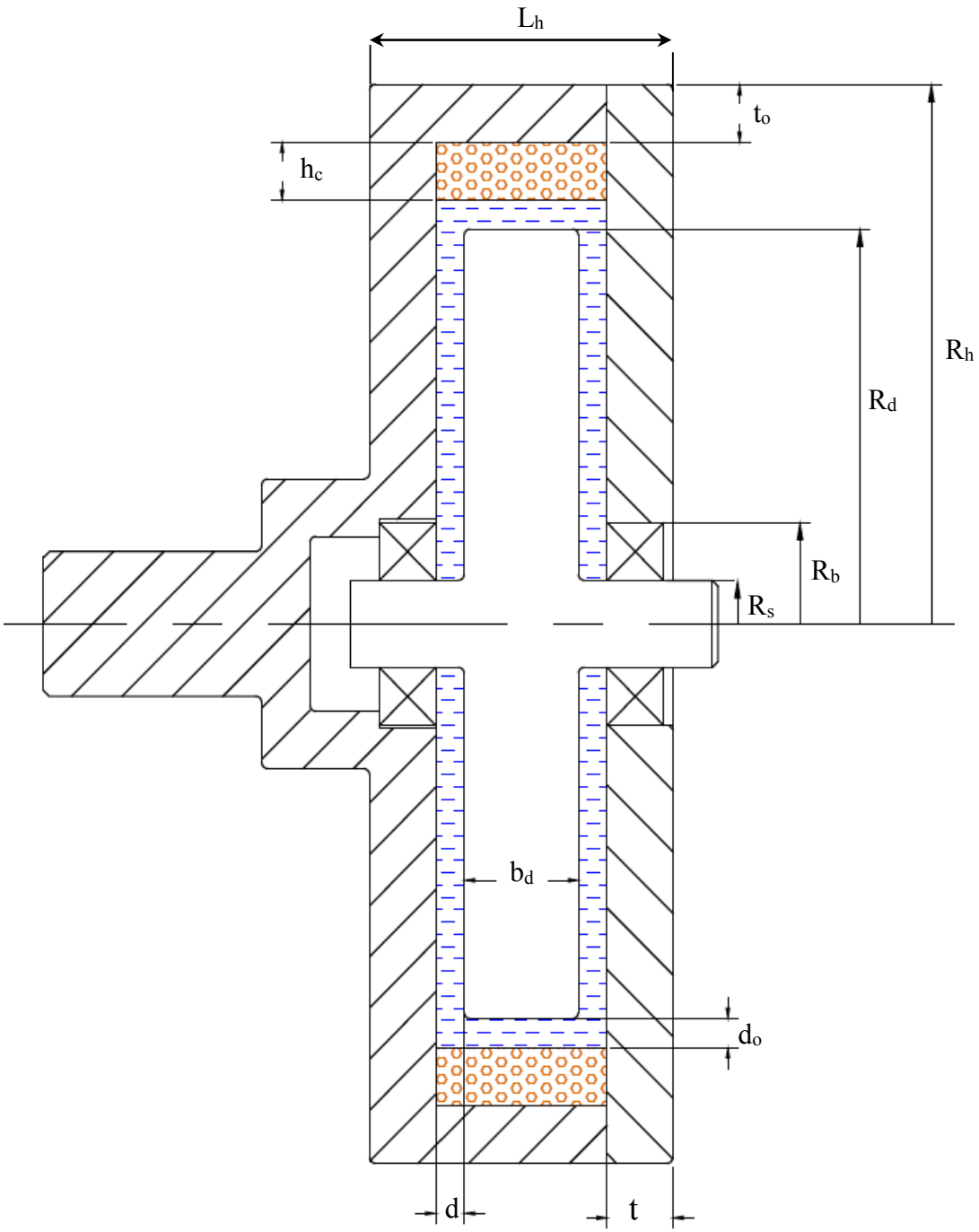

Figure 4-11 MR Brake basic configuration

It has been shown that in the design of the vibration dampers, the typical range of the value of this inertia ratio is from 0.25 to 0.5 [69]. In addition, it is recommended for fabrication convenience that the gap size of the MR fluid duct, d and d_o to be designed for 1 mm.

It should be noted that the smaller the size of the MR fluid gap, the greater is the generated damping torque. However, small gap size results in large zero-field damping torque that reduces the damper performance since it causes high-dissipated energy, overheating and smaller dynamic range of the damper [87].

The dynamic range of the MR damper is defined as the ratio of the peak torque with maximum current input and the zero-field torque at zero current input, as expressed in Eq. (4-24). Moreover, it is noteworthy that the dynamic range of the damper is a significant parameter in evaluating the overall performance of the damper, whereas a large value of the dynamic range is capable of providing a wide control range of the MR damper.

$$\lambda = \frac{T_{d\,max}}{T_{do}} \tag{4-24}$$

where $\boldsymbol{T_{d\,max}}$ represents the maximum generated torque at maximum applied current, while $\boldsymbol{T_{do}}$ represents the zero-field damping torque at zero current input.

Therefore, in order to provide large dynamic range for the designed MR damper, the torque ratio should be large enough. Thus, taking into account the recommended value of considerable dynamic range, the torque ratio is constrained to be greater than 50 [87]. The constraints of the optimization problem can be categorized into three types: geometric constraints, inertia constraint and torque ratio constraint. Considering above the optimization problem has been formally formulated as:

Find design variables R_d , R_b and b_d to:

Maximize the Generated damping torque T_d subject to the following constraints

Geometric constraints

$$R_d + d_o + h_c + t_o \leq R_h$$

$$R_s \leq R_b \leq R_d$$

$$b_d + 2\,t + 2d \leq L_h$$

Inertia constraint $$\mu_L \leq \mu_J = \frac{J_d}{J_h} \leq \mu_U$$

where J_d is the inertia of the disc while J_h is the inertia of the housing of the MR brake.

Torque ratio constraint

$$\lambda = \frac{T_{d\,max}}{T_{do}} \geq \lambda_d \tag{4-25}$$

where λ is the torque ratio of the MR damper and λ_d is the critical value of the torque ratio.

4.3.2 Optimization techniques

The solution of an optimization problem depends on the proper definition and the formulation of the problem, which takes about 50 percent of the total effort needed to solve it [92]. Some other factors affecting the successful closure to the optimum solution are the proper selection of the most suitable optimization technique that is best fit with the defined objective function and a good understanding of the given system. In this research, a hybrid optimization technique that combines stochastic based GA with gradient based SQP has been used to accomplish the optimization problem. GA is one of the popular non-gradient based optimization method that is capable of catching near global optimal solution [93, 94].

As the GA is mainly based on function evaluations not their gradients, the continuity or differentiability of the problem functions are not required which make it ideal for optimization problems with discrete design variables. On the other hand, SQP algorithm is a powerful robust gradient-based optimization algorithm, which can solve nonlinear mathematical problems with great accuracy. The main drawback of SQP similar to other gradient-based optimization algorithms is that it can only capture one of the local optimum point based on the selected initial value [95, 96].

Here both algorithms have been combined in order to accurately capture the true global optimum solution. First, the GA has been used to obtain the near global optimum point. Then optimum results obtained from GA has been used as initial values for the SQP algorithm to accurately capture the global optimum solution.

4.3.3 Genetic Algorithm

The name Genetic originates from the analogy between the complex structure of a given system that is represented by means of vector of zeroes and ones, and the idea, familiar to biologists, of the gene structure of a chromosome [97]. Charles Darwin, the famous naturalist, stated the theory of evolution in the origin of species. Among several generations, individuals evolve based on the principle of natural selection, known as "survival of the fittest" [98]. As a result, the genes of those individuals become adapted and then transmitted to their descendants with new and better characteristics. Later on, John H. Holland developed a technique known as reproductive plans that allowed computer program to imitate the natural algorithm of the evolution entirely [99]. Further, GA is considered as a powerful tool for solving search and optimization problems.

GA is a parallel mathematical algorithm, starts with a set of designs, randomly generated within the allowable design space. Each design is assigned a fitness value, which is used to estimate the sample quality with regard to the rest of the population [100]. The higher the estimated quality value, the higher is the probability of survival. Consequently, this leads to the reproduction operation with the generation of new designs, such that the good designs have more copies than bad ones [101]. A describing flowchart of the general procedures used for GA, is outlined in Figure 4-12.

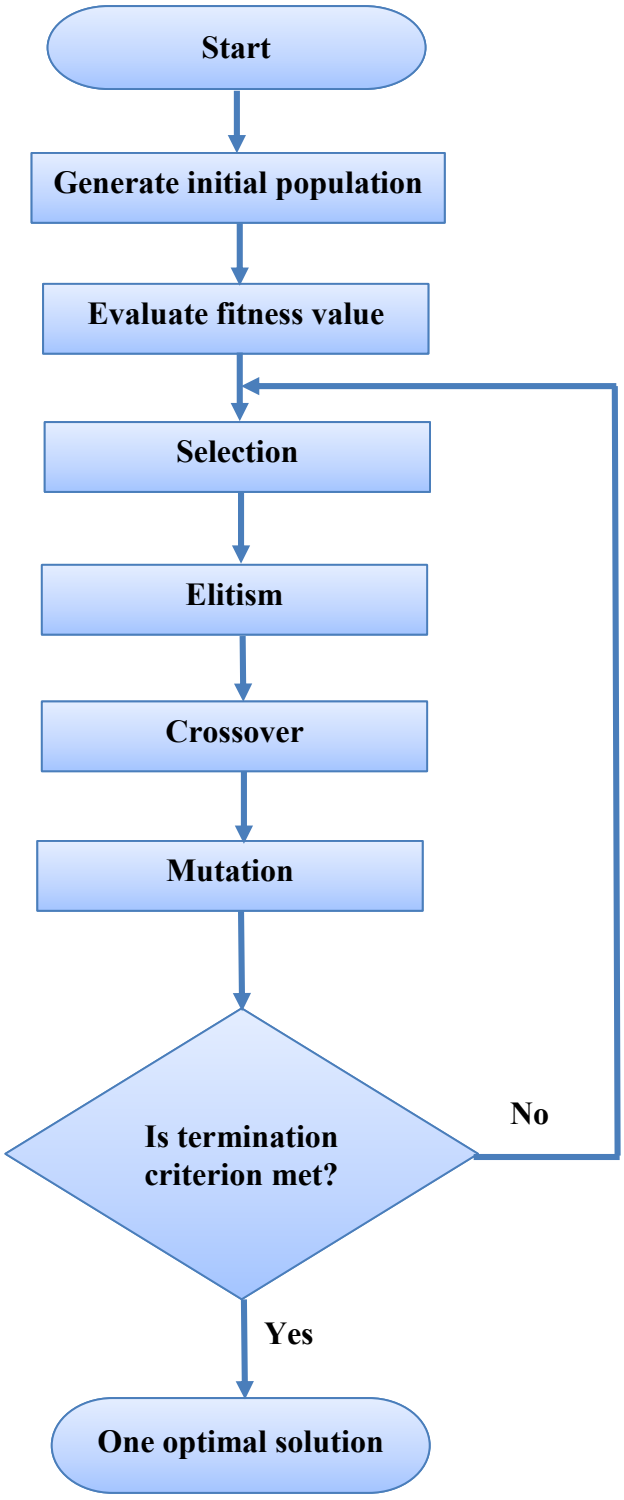

Figure 4-12 Flowchart illustrating GA operation

There are three main reproduction operations to create a new population (offspring):

Elite individual: some individuals in the current population with higher fitness value have chosen to survive and they are automatically transferred to the next generation. This operation is called *reproduction*.

Crossover: in this operation, the reproduced offspring are randomly mated together by combining two different designs (chromosomes) into the population, as shown in Figure 4-13. Usually the crossover is applied with high probability that represents what percentage of chromosomes cross over.

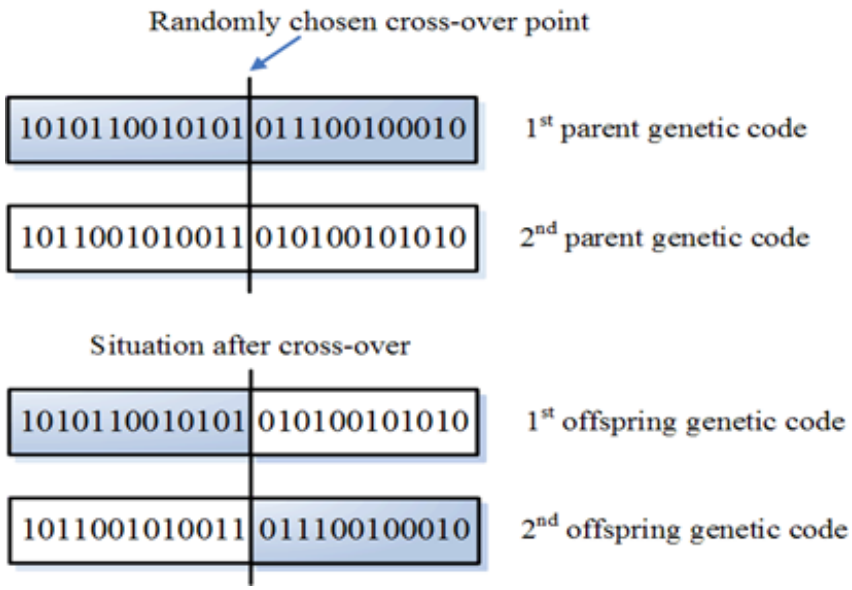

Figure 4-13 Crossover operation scheme [102]

Mutation: this operation is performed by applying changes to a gene of a single individual (chromosome) in the population. Usually mutation is applied with low probability. The algorithm replaces the current population with the new individuals to form the new generation.

As a result, this leads to reproduction of several generations with better fitness value. Each generation is evaluated and tested according to stopping criteria. Once the cumulative change in the fitness function value is less than 'function tolerance', the iterative process stops, otherwise, the population is iteratively processed until the termination criterion is reached [103].

4.3.4 Sequential Quadratic Programing (SQP) algorithm

SQP is a powerful gradient-based algorithm that is an extremely effective method in finding a local stationary point near the initial starting point. SQP has been effectively used for the solution of constrained nonlinear optimization problems. The method is based on sequence of quadratic programming (QP) sub problems in which a quadratic approximation is made to the Lagrangian and linear approximations are made to the nonlinear constraints [104].

The reason for using the SQP method is that it converges faster and can obtain optimum solution with higher accuracy compared to stochastic approaches in searching for local minima of a function [105]. However, the gradient-based methods often rely on the initial starting point. As a result, it is better to provide a good starting point for these methods to execute successfully.

To overcome the drawbacks of the gradient-based methods such as the SQP method in the optimization problem, good starting points near global optimum have been obtained from GA algorithm and transferred as initial points to the SQP technique to fine-tune the results of GA and in order to evaluate an accurate global optimum solution.

4.3.5 Optimization results

As discussed in section 4.3.1, the objective function is to maximize the damping torque generated in rotary MR damper subject to geometrical and torque ratio constraints. Using Eq. (4-8), we can write the following relations for damping torque in the presence and absence of the applied magnetic field considering Figure 4-11:

$$T_d = \frac{4}{3}\pi\tau_y\Delta R^3 + \frac{\pi\eta\omega}{d}\Delta R^4 + 2\pi R_d^2 b_d\left[\tau_{yo} + \eta_0\left(\frac{\omega R_d}{d_0}\right)\right] \tag{4-26}$$

$$T_{do} = \frac{4}{3}\pi\tau_{yo}\Delta R^3 + \frac{\pi\eta_o\omega}{d}\Delta R^4 + 2\pi R_d^2 b_d\left[\tau_{yo} + \eta_0\left(\frac{\omega R_d}{d_0}\right)\right] \tag{4-27}$$

$$\Delta R = R_d - R_i \tag{4-28}$$

where τ_y is the induced yield stress controlled by the applied magnetic field H, η is the post yield viscosity of the MR fluid, R_d and b_d are the radius and thickness of the disk, respectively. R_i is the inner radius of the active area of the MR fluid which in this case is equal to R_s. d and d_o are the gap at end faces of the disk and the gap of annular duct , filled with MR fluid respectively and τ_{yo} and η_o are, respectively, the yield stress and post yield viscosity of MR fluid. Further, ω is the angular velocity of the disk. It is noted that under maximum current T_d will be $T_{d\,max}$, which is required for the torque ratio constraint.

The parameters R_d, R_b and b_d are considered as the design variables and their lower and upper bounds are provided in Table 4-1.

Table 4-1 Allowable values for the design variables

Design variables	Allowable values [mm]
R_d	30 - 75
R_b	10 - 20
b_d	3 - 30

Other input parameters required to define objective and constraint functions are provided in Table 4-2.

Table 4-2 Values of fixed input parameters [68]

Parameters	Reference value	Units
η	3.8	Pa.s
η_o	0.1	Pa.s
τ_y	40000	Pa
τ_{yo}	15	Pa
ω	45	rad/s
d	1.0	mm
d_o	1.0	mm

For solving the optimization problem in this study, Matlab optimization toolbox is utilized for both GA and SQP optimization techniques. As mentioned before, the GA optimization problem is run first, and then the obtained results are used as initial values for SQP optimization problem in order to fine-tune the global optimum solution.

The optimum values of the design variables obtained by GA algorithm are presented in Table 4-3.

Table 4-3 Optimum values obtained from GA algorithm

Design variables	Optimum values [mm]
R_d	60
R_b	12
b_d	10

Figure 4-14 illustrates the convergence of the fitness function (objective function) with the number of generations. Note that the GA stops when the terminating criterion (function tolerance) is met.

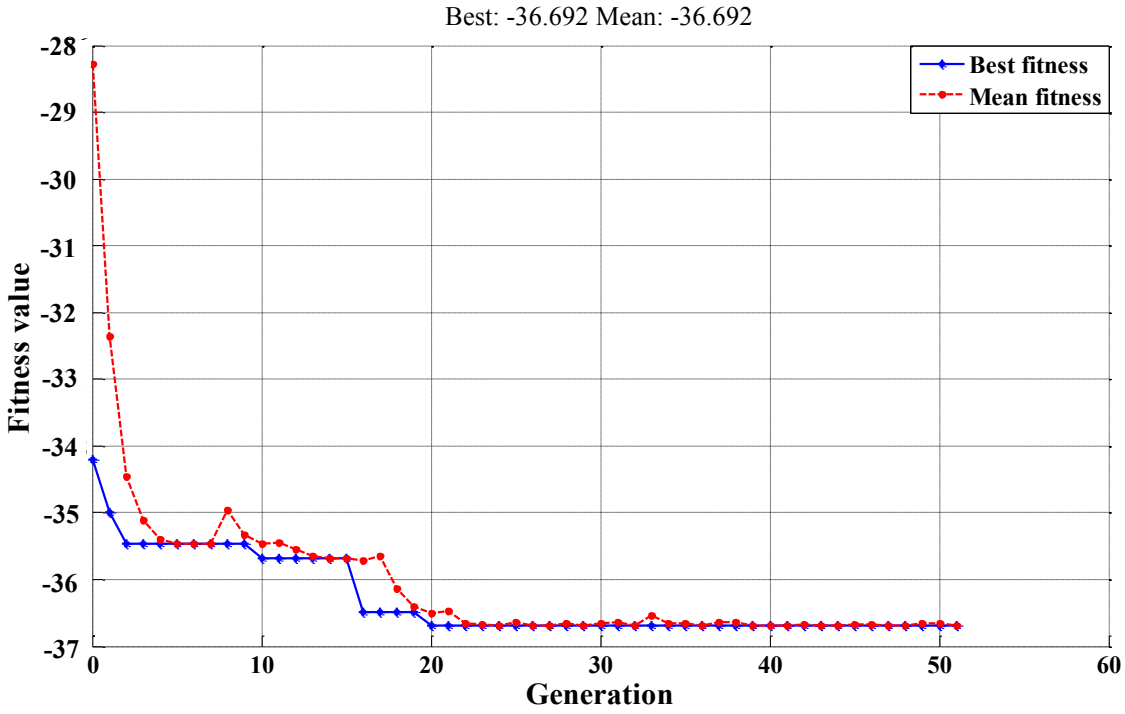

Figure 4-14 GA Variation of fitness value with number of generations

The optimum values of the design variables obtained by SQP algorithm are presented in Table 4-4.

Table 4-4 Optimum values obtained from SQP algorithm

Design variables	Optimum values [mm]
R_d	62
R_b	11
b_d	12

Figure 4-15 shows the historical values of the objective function versus number of iterations for the optimal value problem using SQP algorithm.

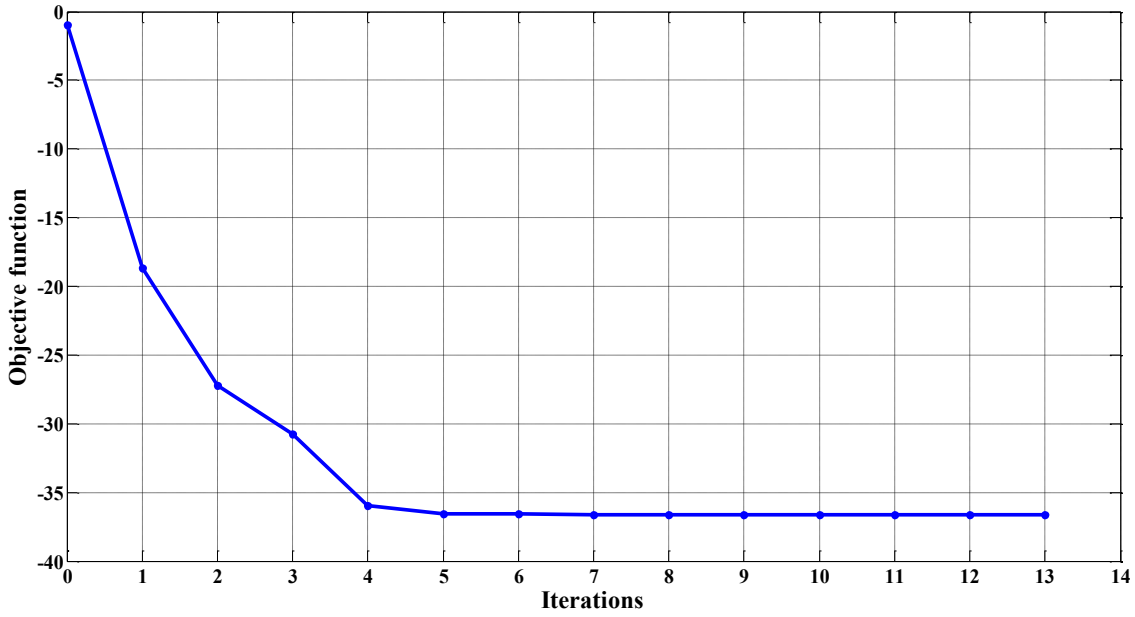

Figure 4-15 SQP number of iterations to optimum value

4.4 Fabrication of the rotary MR damper

In previous sections, analysis and optimum design of the rotary MR damper have been accomplished, and the optimal design parameters have been identified so as to maximize the damping torque subject to the size and volume or weight constraints.

A prototype of the proposed MR damper is manufactured according to the optimal dimensions obtained from design optimization analysis. A three-dimensional model of rotary MR damper is generated using Solidworks software package as shown in Figure 4-16. In addition, a detailed drawing for each part is created as well as assembly drawing for the whole damper as illustrated in Appendix A [106]. There are several significant issues considered during fabricating and assembly processes of the designed MR damper. All these design issues are listed in the following subsections.

4.4.1 Assembly overview

There are seven main parts that make up the damper assembly, that are illustrated in Appendix A. For assembly purposes, the housing is made of two halves that are bolted together after all components of the damper have been assembled inside the housing. The male housing represents the input side of the damper while the female housing represents the output side that was designed with a central hole to allow the output shaft of the disc to protrude. The rotating disc is located inside the housing with a small clearance on each side filled with MR fluid. The disc is fixed to the rotor shaft that is supported on a pair of roller-element bearings such that the disc can freely rotate independent to the housing. These bearings are lightly press-fitted to the shaft and the housing, making it possible for the damper to be disassembled for maintenance.

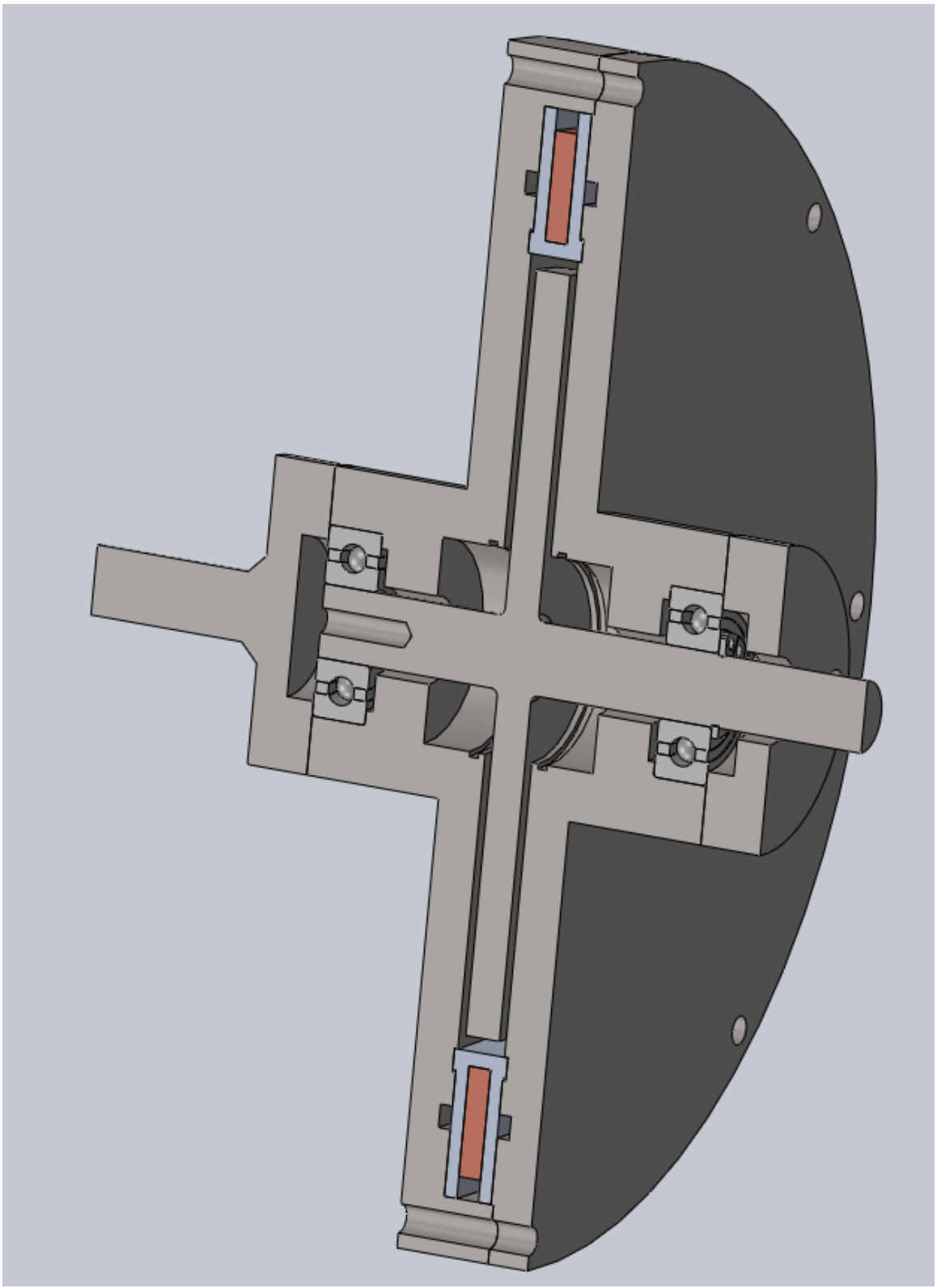

Figure 4-16 Three Dimensional MR damper CAD model

The outer race of the bearing on the side of output shaft is supported by a small cap fitted to the female housing, while a retaining ring ensures that the inner race is supported. However, a proper fixture is fitted on the input side of the damper so that the damper can be directly connected to the excitation source through a standard chuck. This fixture also acts as a support for the outer race of the bearing. A pair of dynamic seals have been chosen carefully such that they are fitted properly to either side of the disk to ensure that the MR fluid does not leak out of its cavity. Considering the design parameters of the magnetic circuit configuration, an aluminum bobbin is considered as a core element of the electromagnet. A coil coated with enamel is wrapped around the bobbin in which the magnetic flux is generated perpendicular to the disk's surface when current is applied. A pair of O-ring is added on either side of the bobbin, thus constraining the MR fluid in its cavity. To better visualize the involved components, an illustrative exploded assembly has been created using Solidworks and is shown in Figure 4-17.

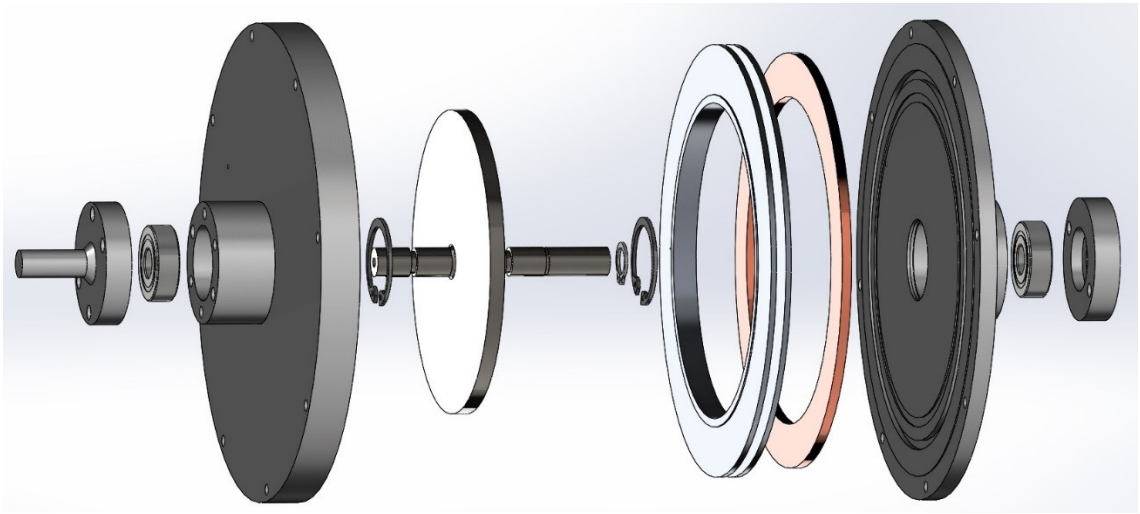

Figure 4-17 Exploded assembly view for the designed MR damper

4.4.2 Rotating disk

The disk (Appendix A, part #1) is designed to leave the longer shaft side to come out of the female housing for either capturing the angular velocity measurement of the disk inside the housing or driving the disk with an input torque, depending on the way in which the damper is used.

The machining process of the disk is performed on a conventional lathe. Concentricity and perpendicularity are two main design issues that have been considered during fabricating processes in order to ensure accurate design of the rotary disc. In order to ensure that the disk is always kept properly aligned within the housings with a clearance of 1 mm on either side, two important features were machined on the shaft of the disk.

First is the groove on the long shaft side to mate an external retaining ring which prevents the bearing from moving along the shaft. The specifications of this retaining ring are presented in Appendix B. On the other side, a tapered hole was machined on the end of the shaft to embed a screw and a washer. Since the bearing is flush with the end of the shaft, the washer supports the inner race of the bearing and prevents it from sliding on the shaft much like the retaining ring does on the other side. The shaft diameter is machined perfectly on the long shaft side up to the retaining groove in order to facilitate the bearing installation. The dimensions of the disk itself are determined using optimal values obtained in section 4.3.

4.4.3 Damper housing

The housing is the heaviest part of the damper. Its weight represents 77% of total weight of the damper. Its grooves and features make it the most expensive produced part in terms of machining time plus material cost. The housing is designed in two mating parts: male housing and female housing as shown in Figure 4-18. The two housing parts are presented in Appendix A part #2 and #4.

The bearing bore tolerance are specified to obtain a transitional fit with the bearings. This way, the bearing assembly can be done by lightly tapping the bearing in its bore and it allows the damper to be easily disassembled. A small shoulder is designed to support the outer race of the bearing internally. A bore with standard diameter is machined on the inner face of both housing parts to fit the lip seals. Furthermore, a tiny groove is machined inside the housing hub to embed an internal retaining ring, ensuring the seals will stay in place and avoid contact with the disk during operation. The specifications of these retaining rings are presented in Appendix C.

Two grooves are machined on the inner faces of the housing for proper sealing of the bobbin and are further discussed in section 4.4.6. There are eight holes drilled on the circumference of the housing and eight bolts and nuts are used to mount the two housing parts together, as shown in Figure 4-18.

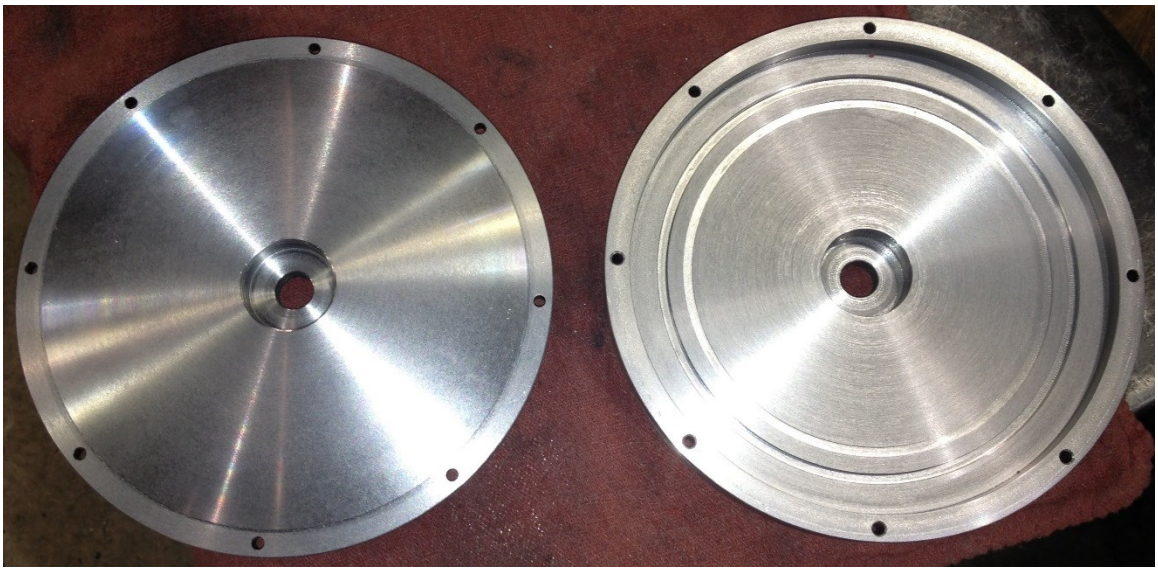

Figure 4-18 Male and Female housing

The two external shoulders mating the two parts together are designed for the male housing to be slotted in the female housing in order to constrain the axial motion, as illustrated in Figure 4-19.

On the female housing, two tapered holes are drilled to fix a cap covering the bearing and also supporting its outer race as illustrated in Appendix A. On the male housing, four tapered holes are drilled on the same diameter circle to screw the fixture part. Both housings have one hole drilled in order to fill the magneto-rheological fluid after the assembly, prior to operation.

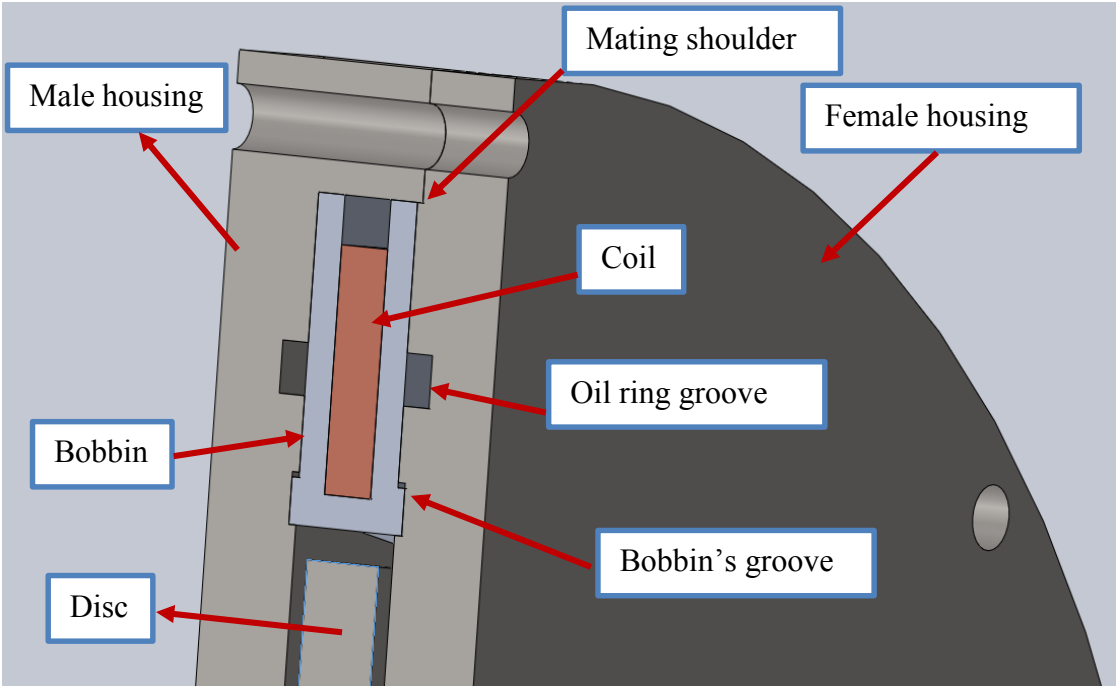

Figure 4-19 Grooves at the bobbin location

The fluid filling process and design is further described in section 4.4.7. While assembling, it is important to make sure that these two holes are aligned to facilitate filling operations.

4.4.4 Mounting fixture

To connect the damper with the input driving shaft, a mounting fixture is designed to link the input excitation from the shaker to the damper assembly, as illustrated in Appendix A. The mounting fixture is a single piece, base and shaft, which can be bolted to the damper's male housing through its axis via screws. The shaft is designed with appropriate diameter such that it can fit with a standard size chuck. The inner diameter of the base, facing the damper's housing, is created in such a way as to support the outer race of the bearing preventing the disk and bearing from drifting, which would violate the 1mm fluid gap condition.

4.4.5 Bobbin design

The bobbin is the only part of the damper made of aluminum. The bobbin can be viewed in Appendix A part # 3. Aluminum is chosen because a non-magnetic material is needed for an optimal magnetic field generation; in addition, it is easy to be machined. All machining operations are performed on a conventional lathe. There was a slight difficulty in fabricating the slot hosting the copper wire, since it is only 13 mm thick with 13 mm depth. Another important feature is the side shoulders that are designed to mate with the housing grooves in order to provide a complete sealing of the oil chamber.

On the other hand, the coil winding is also performed on a lathe by clamping the bobbin on the lathe chuck and precisely placing the first few turns. After wiring is done, the resistance of the wire is tested to make sure that no current shorting happened during wiring due to wire damage. Before assembling the prototype, the bobbin is tested under a current source to investigate the heat generation, and it is found that the heat generated within the specified standard range corresponding to the allowable temperature the coil can bear.

4.4.6 Sealing

Sealing is one of the critical features in the design considerations of the MR damper prototype, since MR fluid has to be sealed properly against leakage which otherwise will cause loss of damping and subsequently decrease the damper's efficiency. For this prototype, two locations are identified where the fluid might escape: the bearings and the junction where the bobbin and the housing mate.

Double sealed bearings are chosen for this design. The specifications of these bearings are presented in Appendix D. They are found to be slightly leaking during testing. That is why the initial design is composed of lip seals located before the bearings to reduce their exposure to MR fluid. However, during assembly, it was found that the torque due to friction between the seals and the disk's shaft were higher than expected. Since the torque ratio is critical in torsional vibration dampers, these seals were removed to decrease the torque due to friction. In future designs, a polished shaft could mitigate the problem.

On the other hand, in order to seal the bobbin and avoid the fluid escaping from the oil chamber and infiltrating the coil wire, two grooves are machined in the housing. The first groove is to mate the bobbin shoulder and the second groove is to host a static O-ring, as can be seen in Figure 4-20.

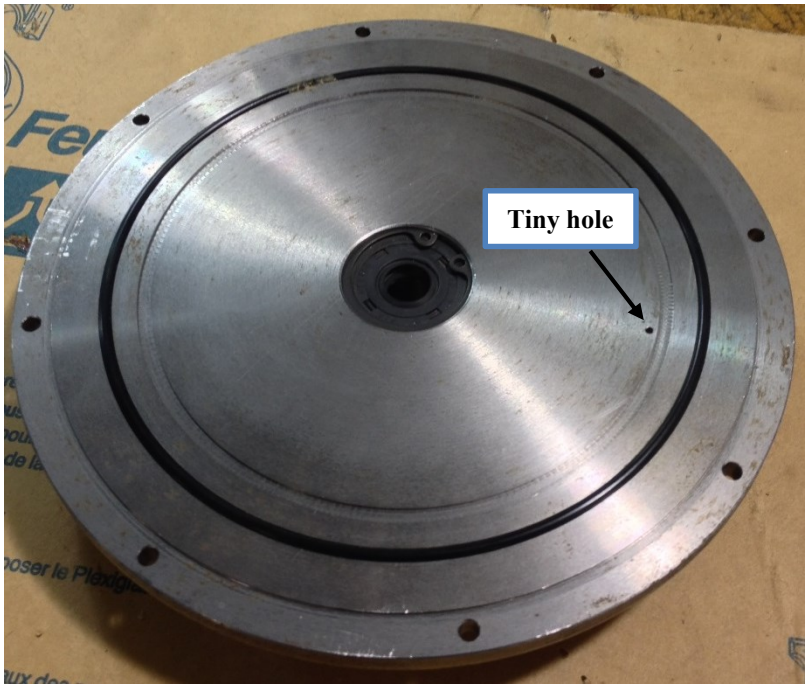

Figure 4-20 Dynamic seal and static O-ring

The groove size of the O-ring was determined in order to insure optimal sealing. This combination proved to be very effective since no leakage was observed at this location.

4.4.7 MR fluid injection

The filling of the MR fluid damper is an issue that was considered in the initial design but only decided in the final stages of fabrication and assembly. Since the MR fluid exhibits high viscosity due to the colloidal mixture of silicon oil and iron particles, filling the MR fluid into narrow cavity of the assembled damper is difficult. Two tiny holes are made on either side of the housing located just below the wall of the bobbin, at smaller radius than the inner radius of the bobbin. This hole can be seen in Figure 4-20.

Gravity filling of the fluid might result in non-uniform distribution of the fluid and unfilled volume. The aim is to inject the fluid from one side and allow the displaced air to exit from the other hole so that the MR fluid fills the cavity completely. After the cavity is completely filled both the holes are sealed.

In order to fill the damper, it was carefully clamped in a vice grip and fluid injected using special syringe with a modified tip to fit into the intake hole. Before injection, the volume of the cavity is calculated in order to estimate the number of times the syringe needs to be filled and emptied into the cavity. When injection began, a problem was encountered during injection process, in which the fluid started coming out of the hole where it was being injected. In order to solve this issue, the output shaft of the inner disk was turned while fluid was injected, which moved it downwards into the cavity.

4.5 Experimental work

As described in previous section, a prototype rotary MR Damper was fabricated that can be used as a variable friction damper. In order to validate the proposed MR damper model, the damping torque generated from MR damper should be measured. To do so, an experimental test rig was designed to link the input rotating shaft from the shaker directly to the housing of the MR damper and the whole test setup is illustrated in Figure 4-21.

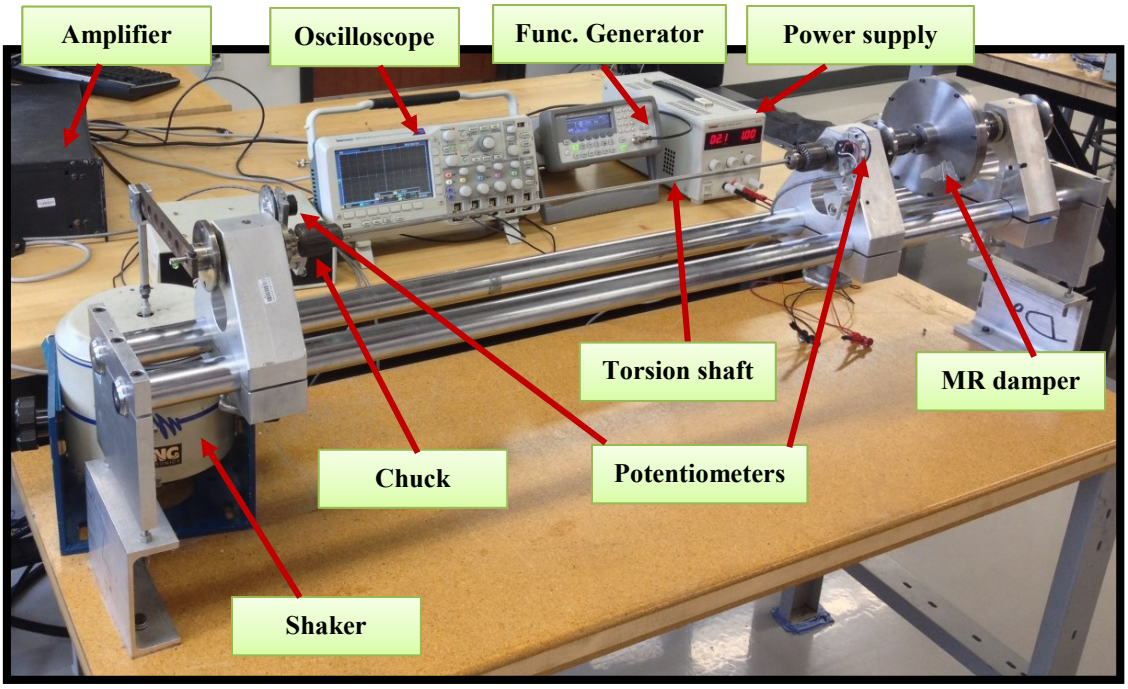

Figure 4-21 Test rig setup to measure the generated damping torque

4.5.1 Test rig setup

As can be seen from Figure 4-21 the test rig consists of the following devices, a torsional vibration apparatus, a function generator, an amplifier, a shaker (vibration exciter), two potentiometers, an oscilloscope, and a PC machine.

The torsional vibration apparatus includes a 70 cm mild steel torsion shaft of ¼-inch (6.35mm) diameter clamped in between two bearing housings provided with chucks for clamping the torsion shaft that are mounted on a base frame. A potentiometer is provided at the two ends of the shaft to measure the relative angular displacement as well as relative angular velocity across the shaft ends. These potentiometers are spring loaded to avoid slipping between the potentiometer and the flange of the rotor. The electromagnetic shaker is used for generation of oscillatory excitation. Thus, the translational motion from the shaker is converted into rotational motion through a linkage mechanism as illustrated in Figure 4-21. The shaker is driven by a function generator and a power amplifier by which the type and amplitude of excitation are selected through the function generator. The function generator and oscilloscope are set prior to the experiment.

In order to calculate the damping torque as a function of the applied current, tests were carried out at different currents from 0 – 2 Amps with increment 0.5 Amps. In each case, readings from both angular displacement potentiometers at the two ends of the input shaft were recorded, in order to calculate the difference in shaft twist angle for each case.
A steel shaft of diameter 6.35 mm (d_1), 0.7 m length (L_1) and modulus of rigidity (G) 80 GPa has been used in this experiment.

Two different methods have been utilized for calculation of the generated damping torque. The logarithmic decrement method is used for torque calculation when the damping ratio is less than 0.5. Another convenient method has been used for calculating the generated torque when the damping ratio exceeds 0.5, which is the half power bandwidth method.

4.5.2 Logarithmic decrement method

This method is commonly used for determining the amount of damping present in a system by measuring the rate of decay of free oscillations [107]. A free damped vibration response is shown in Figure 4-22.

The ratio of the amplitude of successive peaks is given by

$$\frac{\theta_{n+2}}{\theta_n} = e^{-\left(\frac{2\pi\zeta}{\sqrt{1-\zeta^2}}\right)} \tag{4-29}$$

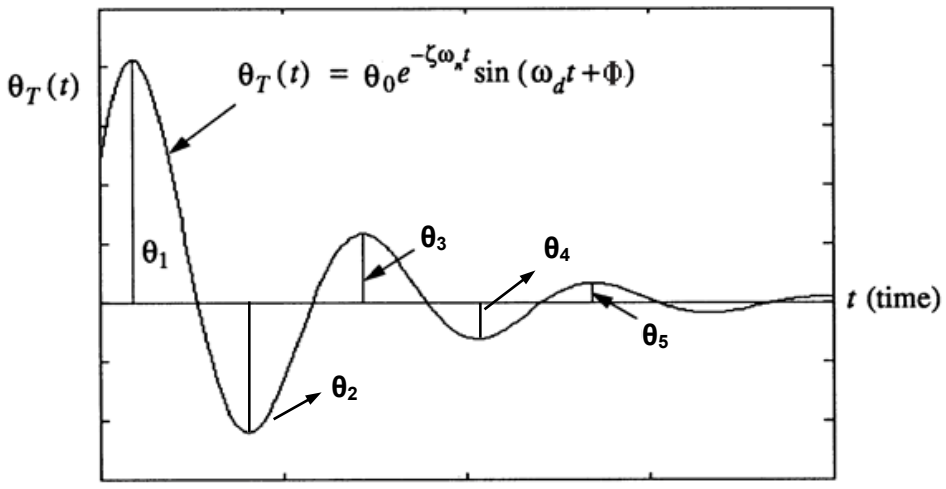

Figure 4-22 Damped oscillation

Thus, the amplitude ratio of successive peaks is a constant for a given damping ratio ζ. The expression for the logarithmic decrement (δ) is then given by:

$$\delta = \ln\frac{\theta_{n+2}}{\theta_n} = \ln\frac{\theta_3}{\theta_1} = -\frac{2\pi\zeta}{\sqrt{1-\zeta^2}} \tag{4-30}$$

Thus, by measuring the ratio between two successive amplitudes, one can find the damping ratio from the following equation:

$$\zeta = \frac{\delta}{\sqrt{4\pi^2 + \delta^2}} \tag{4-31}$$

However, the relationship between the size of first overshoot θ_1 and the second θ_2 is useful for cases where the number of oscillations is small ($\zeta > 0.3$). In this case

$$\frac{\theta_2}{\theta_1} = e^{-\left(\frac{\pi\zeta}{\sqrt{1-\zeta^2}}\right)} \tag{4-32}$$

Once the damping ratio ζ is obtained for each case, assuming constant velocity and linear shear rate in the MR fluid gaps, the damping torque can easily be calculated, since

$$C_{MR} = \zeta\, C_{Cr} = 2\zeta\sqrt{k\,J} \tag{4-33}$$

By analyzing the captured free damped response signals via oscilloscope, the calculated damping ratios based on this method are presented in Table 4-5 and 4-6.

Table 4-5 Calculated data using logarithmic decrement approach for $\zeta < 0.3$

No.	I	θ_1	θ_3	δ	ζ	C_{MR}
1	0.00	-220	-84	-0.9628	0.1515	0.1344
2	0.25	-195	-29	-1.9057	0.2902	0.2576

Table 4-6 Calculated data using logarithmic decrement approach for $\zeta \geq 0.3$

No.	I	θ_1	θ_2	δ	ζ	C_{MR}
3	0.50	-151	-34	-1.4909	0.4287	0.3804

4.5.3 Half power bandwidth method

As the logarithmic decrement approach is difficult to apply when the damping ratio is greater than 0.5, half-power bandwidth is more conveniently used for determining the damping ratio ζ under current above 0.5. This method makes use of the width of the peak value of the frequency response function of the structure, as illustrated in Figure 4-23.

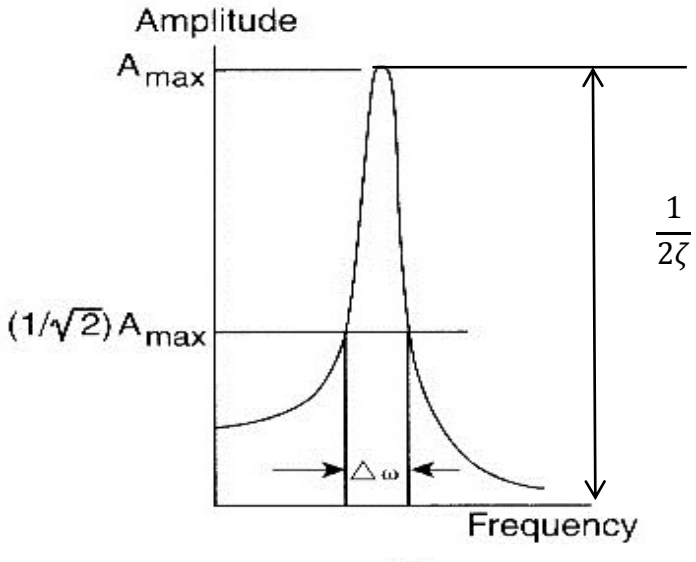

Figure 4-23 Half power bandwidth

Let us consider the two frequencies on either side of the resonance (sidebands) where amplitude, A *is* $1/\sqrt{2}\, A_{max}$. These points are typically known as the half-power points and the distance between them is referred to as half-power bandwidth as shown in Figure 4-23.

These frequencies are related to the damping and natural frequency of the system according to the following relations:

$$\frac{f_2^2 - f_1^2}{f_n^2} = 4\,\zeta \qquad or \qquad \frac{f_2 - f_1}{f_n} = 2\,\zeta \tag{4-34}$$

Thus, the damping ratio can be easily obtained by evaluating bandwidth points and natural frequency of the system. Thus, the generated damping torque can be described as:

$$T_d \;=\; C_{MR}\,(\omega_{shaft} \;-\; \omega_{disk}) \tag{4-35}$$

4.5.4 Experimental procedure and test results

The rotary MR damper is installed into the experimental setup as shown in Figure 4-21. The logarithmic decrement method is used to obtain the damping of the system at low current values (0.0, 0.25 and 0.5 A). An initial angular displacement is given to the damper and the free damped oscillations are captured by oscilloscope via angular transducer, and the damping ratio is calculated. For higher values of the applied current, the damping in the system is increased, and the half power bandwidth method will be more convenient for determining the damping in the system. The function generator is adjusted for a suitable sweep excitation frequency in the range 1 Hz to 20 Hz. Since the function generator capacity is relatively low, an amplifier is used for an appropriate gain that is to be fed to electromagnetic shaker. The electromagnetic shaker is connected to one end of the torsional shaft through a lever mechanism while the damper is fixed at the other end. In addition, two angular transducers installed at both ends of the torsional shaft near the chucks to measure the angular displacement at each end. The MR damper is connected to the power supply to provide the required current value.

For calculating the damping of the system at higher current values (1.0, 1.5 and 2.0 A), half power bandwidth approach has been applied. The response amplitude versus the excitation frequency have been measured at different current values and the damping ratio is calculated for each case. Figure 4-24 shows the response amplitude against the excitation frequency at I = 1.0 A, from which the damping ratio is calculated.

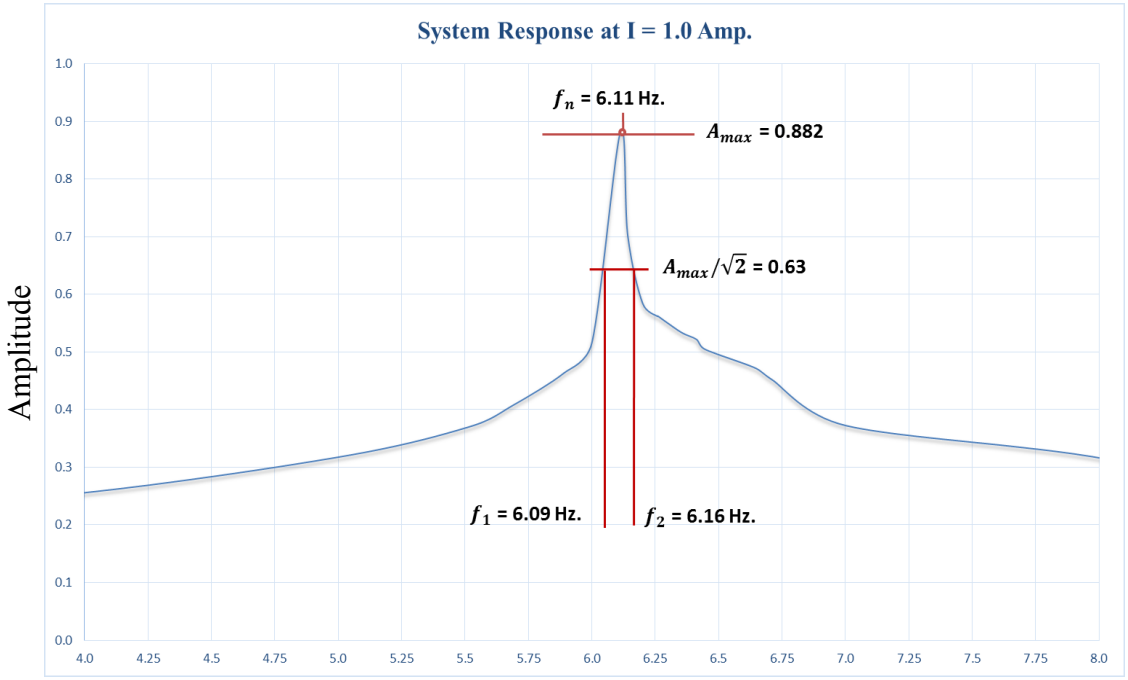

Figure 4-24 Response amplitude versus excitation frequency at I=1.0 A.

Evaluating the half-power points from Figure 4-24 and then substituting in Eq. (4-34), the damping ratio can be calculated as follows:

$$\frac{f_2^2 - f_1^2}{f_n^2} = 4\,\zeta \qquad \text{or} \qquad \frac{f_2 - f_1}{f_n} = 2\zeta$$

$$\frac{(6.16)^2 - (6.09)^2}{(6.11)^2} = 4\zeta \qquad \text{Therefore} \qquad \zeta = 0.57$$

The damping ratio is calculated at different current values and it is presented in Table 4-7

Table 4-7 Damping ratios at different current values

I	1.0	1.5	2.0
ξ	0.57	0.7485	0.8685

Further investigations are carried out for the damping torque at different operating speeds and different current values. First, the generated torque is measured at different operating speeds when there is no magnetic field applied, i.e. at zero current value. After that, the experiment is repeated at different applied current values. The results are provided in Table 4-8.

Table 4-8 Corresponding torque values at different applied current and rotation speeds

Applied Current (A)	Generated damping torque (N.m)			
	ω = 10 rad/s	ω = 20 rad/s	ω = 30 rad/s	ω = 40 rad/s
0.00	1.344	2.688	4.032	5.376
0.50	3.802	7.603	11.405	15.207
1.00	5.030	10.059	15.089	20.119
1.50	6.642	13.284	19.926	26.568
2.00	7.707	15.414	23.121	30.827

Figure 4-25 and Figure 4-26 also show the variation of damping torque versus rotation velocity at different applied current and also versus applied current at different rotation velocity, respectively.

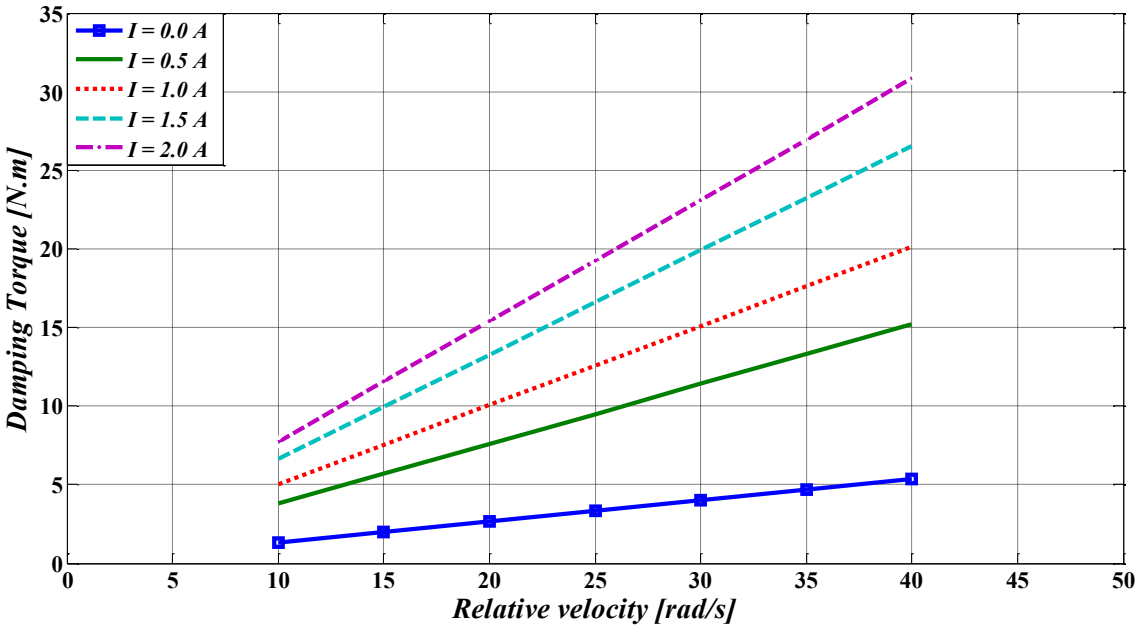

Figure 4-25 Measured damping torque vs velocity at different applied current

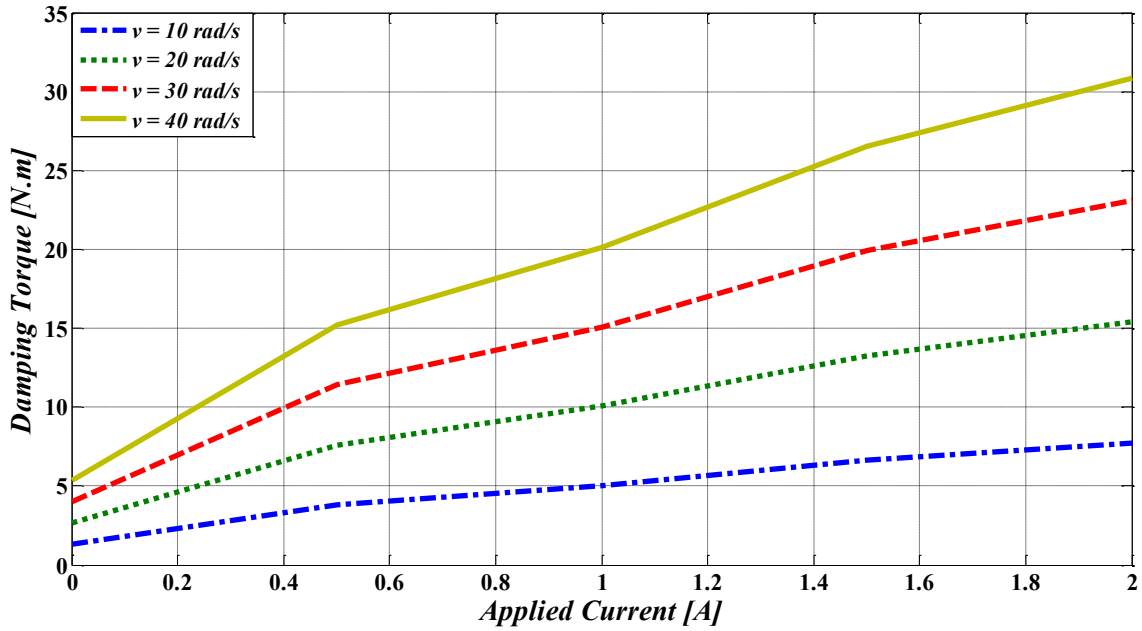

Figure 4-26 Measured damping torque vs applied current at different speeds

Examination of results reveal that the rate of increase in damping torque versus rotation velocity is higher for higher applied current as shown in Figure 4-25. Also for the given rotation velocity, the rate of increase in damping torque decreases as the applied current increases reaching to the saturation at high applied current as shown in Figure 4-26.

4.5.5 Validation of the MR damper

In order to validate the MR damper model, a comparison between the simulation model and the experimental results is carried out. Figure 4-27 shows the damping torque as a function of the applied current at rotation speed of 20 rad/s obtained from experiment and model.

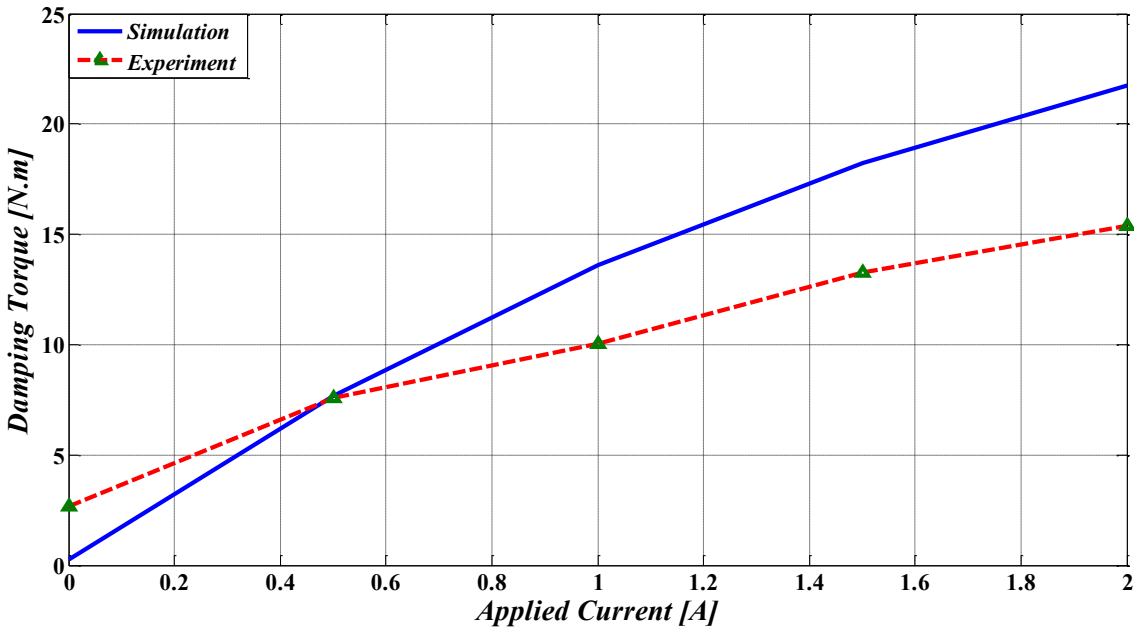

Figure 4-27 Damping torque values versus applied current at ω=20 rad/s

In addition, Figure 4-28 shows the damping torque as a function of the applied current at speed of 30 rad/s. Figure 4-29 illustrates the values of the damping torque corresponding to specified values of applied current at average operating speed of 30 rad/s.

Generally, good agreement exists between the experimental and simulation results, although some deviation exists.

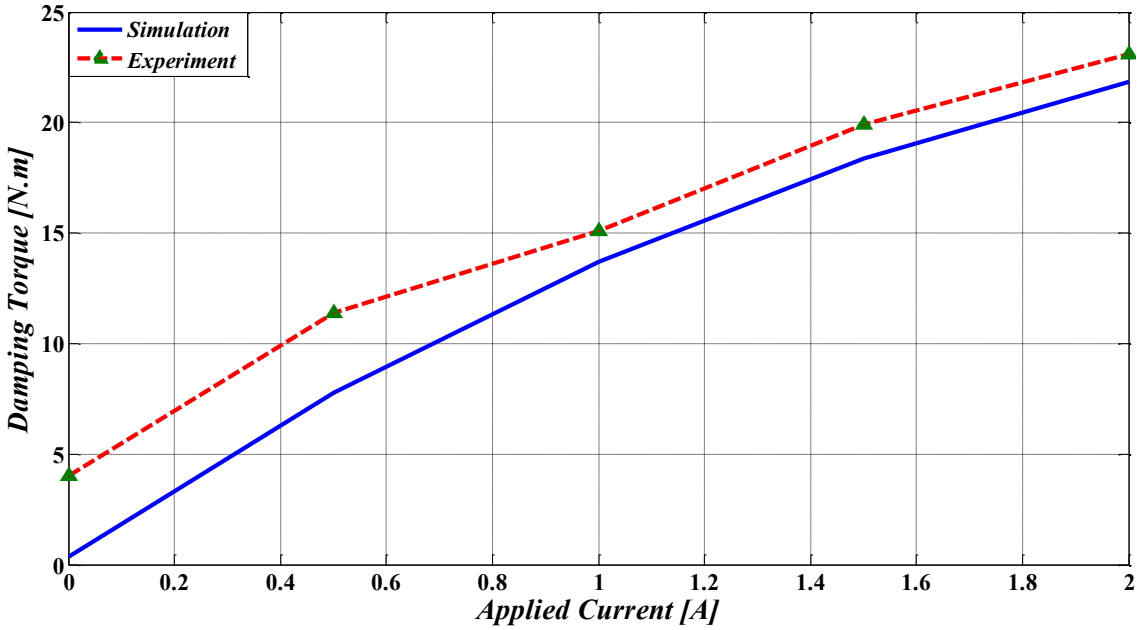

Figure 4-28 Damping torque values versus applied current at ω=30 rad/s

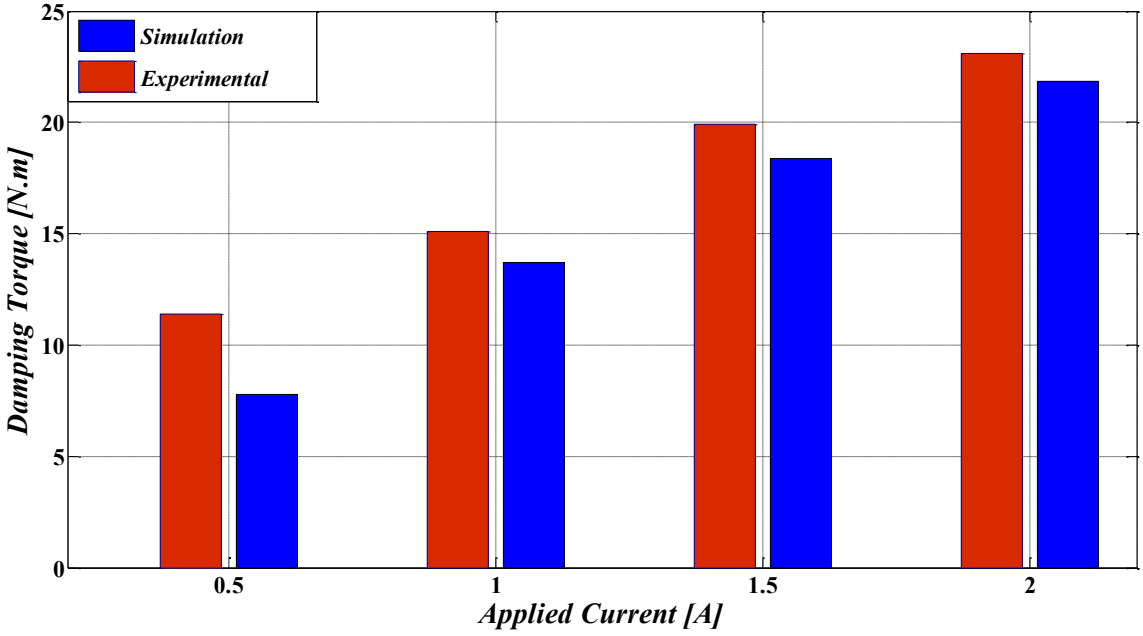

Figure 4-29 Simulation and experimental damping torque at different applied current

The reason for this deviation might be due to the following considerations:

a. The non-homogenous distribution of the magnetic field through MR fluid gap. Since the winding coil has been assembled manually, as a result, the magnetic flux path might not be uniformly distributed as assumed in the FE model. Since the FE simulation model is generated assuming a uniform distribution of the magnetic flux density as well as magnetic field intensity, naturally any deviation from this condition in the experimental model will affect the generated damping torque.

b. Heating of the prototype during experimental measurements. Heating generated due to the friction was not taken into account in the FE model. High temperature has an effect on both the magnetic field density and the MR fluid viscosity. It has been observed that, during experiment between every two consecutive readings, the temperature of the MR fluid and the MR damper has increased due to applied current and shear friction generation in the MR damper. This may be avoided in future study, by incorporating proper coolant to avoid temperature rise.

c. Leakage of MR fluid. Possible leakage might also affect the experimental measurements. Due to low surface finish quality of the sealing surface, the sealing generates large torque due to friction, which might affect the measured damping torque. Although a double sealed bearing is used, there still exists a small leakage amount of MR fluid during the experiment, which in turn might affect the magnetic field density through MR fluid due to lack of sufficient amount of MR fluid in the cavity.

4.6 Summary

This chapter initially introduced constitutive Bingham modeling approach for a rotary type MR damper along with a classification of rotary MR damper. The characteristic equation for the proposed MR damper model was derived and the magnetostatic analysis for the magnetic circuit of the rotary MR damper has been carried out. The FE model of the MR damper is developed using finite element software package in order to simulate the magnetic field distribution through the MR fluid and test the effectiveness of the proposed design configuration as well as the selected material for the MR damper components.

In addition, an optimization problem formulation was carried out to obtain the optimal dimensions for the designed MR damper. Two optimization techniques have been used for accurate optimum solution. Moreover, the fabricating procedures of the MR damper regarding the assembly overview and design consideration of each component have been presented.

Finally, the chapter ends with the experimental procedure for calculation of the generated damping torque and a brief description for the methods used, and then an experimental validation for the experimental results with the simulation model has been presented.

The next chapter will present the hybrid damper that includes CPVA with a MR damper and the corresponding control considerations.

Chapter 5
Modeling and Control of Hybrid Torsional MR Damper

5.1 Introduction

In chapter three, a mathematical model for pendulum absorber has been presented. It has been shown that CPVAs are considered as tuned absorbers with their natural frequencies directly proportional to the rotational speed of the shaft and therefore they are effective over a continuous range of rotating speeds. While CPVAs are expected to be efficient absorbers under steady state conditions, the MR damper would be efficient under essentially unpredictable operating conditions. Over the past few decades, there have been several investigations on MR dampers as well as CPVAs; however, there has been no study reported on integrating the two systems for attenuating torsional vibration. In this chapter, the dynamic model of a novel hybrid torsional vibration damper has been developed. The proposed hybrid rotary damper combines the conventional CPVA with the MR rotary damper in which the conventional centrifugal pendulum is attached to the cylindrical housing of the MR damper. The performance of the proposed hybrid rotary damper in open-loop passive on, *constant current*, and off, *zero current*, modes is then investigated and compared with that of CPVA and MR rotary damper alone. Furthermore, a Skyhook control algorithm has been employed to evaluate the performance of the proposed hybrid damper in the closed-loop control system and its capability to reduce torsional vibration of the shaft system.

5.2 Modelling of hybrid torsional damper

The proposed hybrid rotary damper consists of a driving shaft that is directly connected to the damper housing and they are rotating together, while the disc inside the housing is free to rotate relative to the housing. The centrifugal pendulum with length l is attached to the cylindrical housing of the MR rotary damper by a guided pin that is free to rotate in a plane perpendicular to the axis of rotation. Figure 5-1 shows the schematic drawing of the proposed hybrid torsional damper. The shaft system is driven by an excitation torque T_e. The mass moment of inertia and the torsional stiffness of the shaft system are represented by J_s and k_s, respectively.

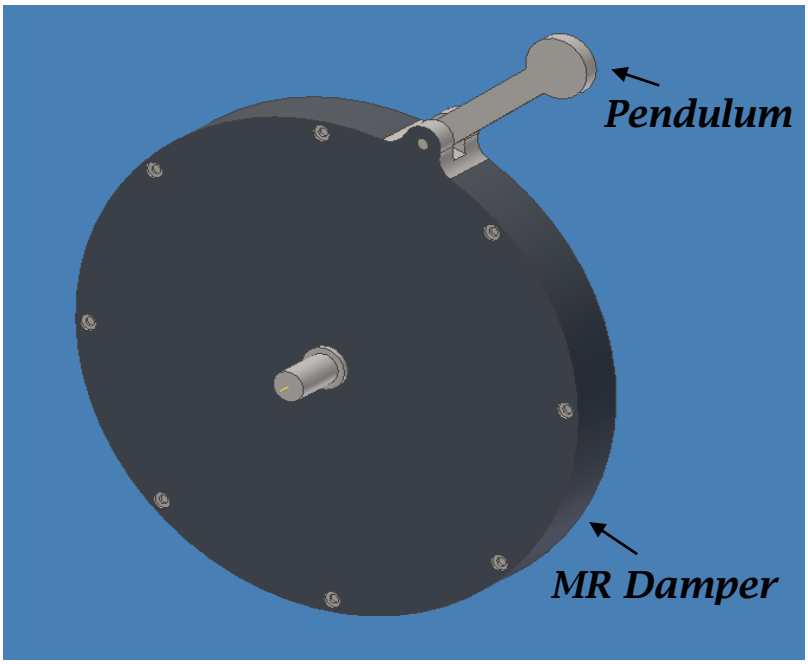

Figure 5-1 Schematic of hybrid torsional damper

Proper selection of pendulum effective length provides an optimum reduction in torsional vibration amplitude as discussed in Chapter 3. Mathematical modeling of the whole system has been accomplished using Lagrange's principle, resulting in three coupled nonlinear

differential equations of motion. First, the kinetic and potential energies for the whole system are determined, and then Lagrangian formulation has been carried out. By referring to Eqs. (3-1) and (3-5), and considering the inertia of the rotating disc, the kinetic energy expression for the hybrid rotary can be written as:

$$T = \frac{1}{2} m\, v_m^2 + \frac{1}{2} J\, (\Omega + \dot{\psi})^2 + \frac{1}{2} J_d \dot{\phi}_d^2 \tag{5-1}$$

Substituting the expression for $\boldsymbol{v_m}$ from Eq. (3-3) into Eq. (5-1) yields:

$$T = \frac{1}{2} m\big[2l(R\cos\phi + l)(\Omega + \dot{\psi})\dot{\phi} + (R^2 + l^2 + 2Rl\cos\phi)(\Omega + \dot{\psi})^2 + l^2\dot{\phi}^2\big] + \frac{1}{2} J(\Omega + \dot{\psi})^2 + \frac{1}{2} J_d \dot{\phi}_d^2 \tag{5-2}$$

where J_d and ϕ_d represent the mass moment of inertia and the angular displacement of the rotating disc inside the MR damper.

Referring to Eqs. (3-2) and (3-5) the potential energy of the system can be expressed as:

$$V = mg\,[R\sin(\Omega t + \psi) + l\sin(\Omega t + \psi + \phi)] + \frac{1}{2} k\psi^2 \tag{5-3}$$

Therefore, the Lagrangian ($L = T - V$) can be written in terms of the three independent generalized coordinates ψ, ϕ and ϕ_d as follows:

$$L = \tfrac{1}{2} J\big(\Omega + \dot{\psi}\big)^2 + \tfrac{1}{2} m\Big[2l(R\cos\phi + l)\big(\Omega + \dot{\psi}\big)\dot{\phi} + (R^2 + l^2 + 2Rl\cos\phi)\big(\Omega + \dot{\psi}\big)^2 + l^2\dot{\phi}^2\Big] + \tfrac{1}{2} J_d \dot{\phi}_d^2 - mg\,[R\sin(\Omega t + \psi) + l\sin(\Omega t + \psi + \phi)] - \tfrac{1}{2} k\psi^2 \tag{5-4}$$

The Lagrangian equations of motion are given by

$$\frac{d}{dt}\left(\frac{\partial L}{\partial \dot{\psi}}\right) - \frac{\partial L}{\partial \psi} = T_e - T_d - c_r\dot{\psi} \tag{5-5}$$

$$\frac{d}{dt}\left(\frac{\partial L}{\partial \dot{\phi}}\right) - \frac{\partial L}{\partial \phi} = - c_a\dot{\phi} \tag{5-6}$$

$$\frac{d}{dt}\left(\frac{\partial L}{\partial \dot{\phi}_d}\right) - \frac{\partial L}{\partial \phi_d} = T_d \tag{5-7}$$

where T_d is the total damping torque generated in MR rotary damper where its value is given by Eq. (4-8) in Chapter 4.

Now, substituting Eq. (5-4) into Eqs. (5-5), (5-6) and (5-7) results in the final governing equations of motion of the proposed hybrid rotary damper as follows:

$$\begin{aligned}(J + ml^2 + mR^2 + 2mRl\cos\phi)\ddot{\psi} + (ml^2 + mRl\cos\phi)\ddot{\phi} - (2mRlsin\phi)\left(\dot{\psi} + \Omega\right)\dot{\phi} \\ -(mRl\sin\phi)\dot{\phi}^2 + mg[Rcos\,(\psi + \Omega t) + l\cos(\psi + \Omega t + \phi)] + k\psi \\ = T_e - T_d - C_r\dot{\psi}\end{aligned} \tag{5-8}$$

$$\begin{aligned}(ml^2 + mRl\cos\phi)\ddot{\psi} + ml^2\ddot{\phi} + mRl\sin\phi\,(\dot{\psi} + \Omega)^2 \\ + mgl\cos(\psi + \Omega t + \phi) = -C_a\dot{\phi}\end{aligned} \tag{5-9}$$

$$J_a\ddot{\phi}_d = T_d \tag{5-10}$$

5.3 Semi-active control of hybrid torsional damper

In order to evaluate the effectiveness of the proposed hybrid torsional damper in attenuation of torsional vibrations adaptively, a semi-active control algorithm has been implemented. In addition, the dynamic performance of the semi-active control system with the hybrid torsional damper is investigated and presented in the subsequent sections.

The schematic of the proposed semi-active control system is illustrated in Figure 5-2. As it can be seen, the MR based semi-active control system consists of two nested controllers: system controller and damper controller.

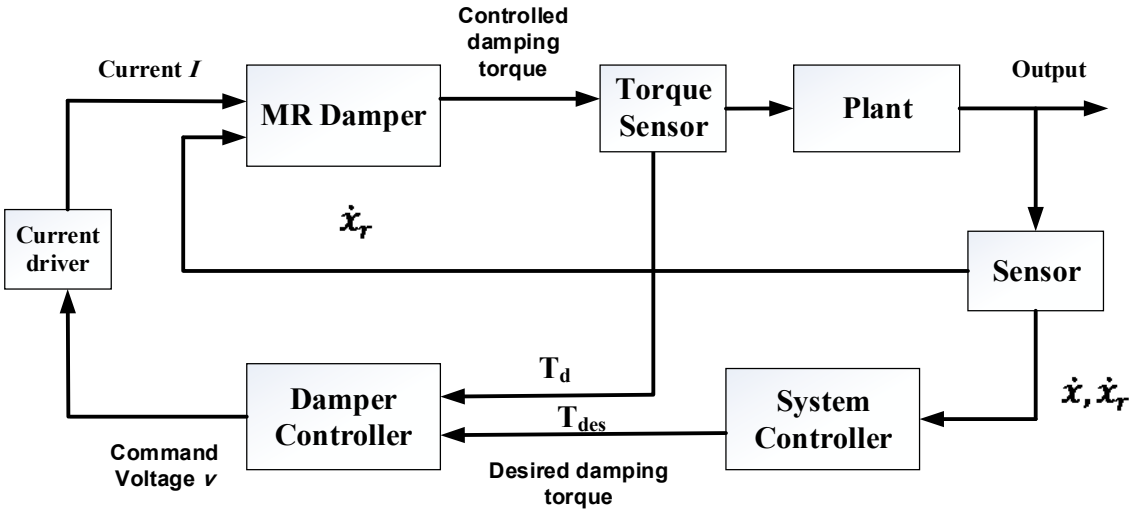

Figure 5-2 Schematic of the semi-active control system [41]

The system controller generates the desired damping torque according to the measured dynamic response of the system. However, the damper controller is used to regulate the command voltage to the current driver to track the desired damping torque, determined by the system controller, based on the desired and the actual damping torque. The system controller used in this study is the Skyhook controller while the damper controller is represented by the Heaviside step function.

5.3.1 Skyhook controller

As mentioned in Chapter 2, although various system controller policies have been proposed in the last two decades, the most widely used semi-active control policy is the Skyhook control [49]. Here in this study the Skyhook controller has been employed. The Skyhook control algorithm can be simply described as:

$$\begin{cases} (\dot{\psi} - \dot{\phi}_d)\dot{\psi} \geq 0 & T_{des} = T_{max} \\ (\dot{\psi} - \dot{\phi}_d)\dot{\psi} < 0 & T_{des} = 0 \end{cases} \tag{5-11}$$

where T_{des} is the desired semi-active torque. The basic Skyhook semi-active control logic can be described as follows. The controller should generate a damping torque only when the sign of the relative velocity $(\dot{\psi} - \dot{\phi}_d)$ and the absolute velocity $\dot{\psi}$ is the same. This combination can be better understood by considering the situation when the sign of $\dot{\psi}$ is positive. In this case, if sign $(\dot{\psi} - \dot{\phi}_d)$ is also positive, then the disc is either rotating in positive direction with smaller velocity than the shaft system torsional velocity or the disc is rotating with negative velocity. In either case, the effect of increasing the damping torque will decelerate the torsional vibration of the shaft system.

In the alternate case, the sign of $(\dot{\psi} - \dot{\phi}_d)$ is negative. This indicates that the disc is rotating in positive direction with a faster velocity than the shaft system and thus applying further damping torque will accelerate the shaft system. Similar results would be obtained when considering the case that the sign of absolute velocity $\dot{\psi}$ is negative. Eq. (5-11) can be represented by Simulink model as shown in Figure 5-3.

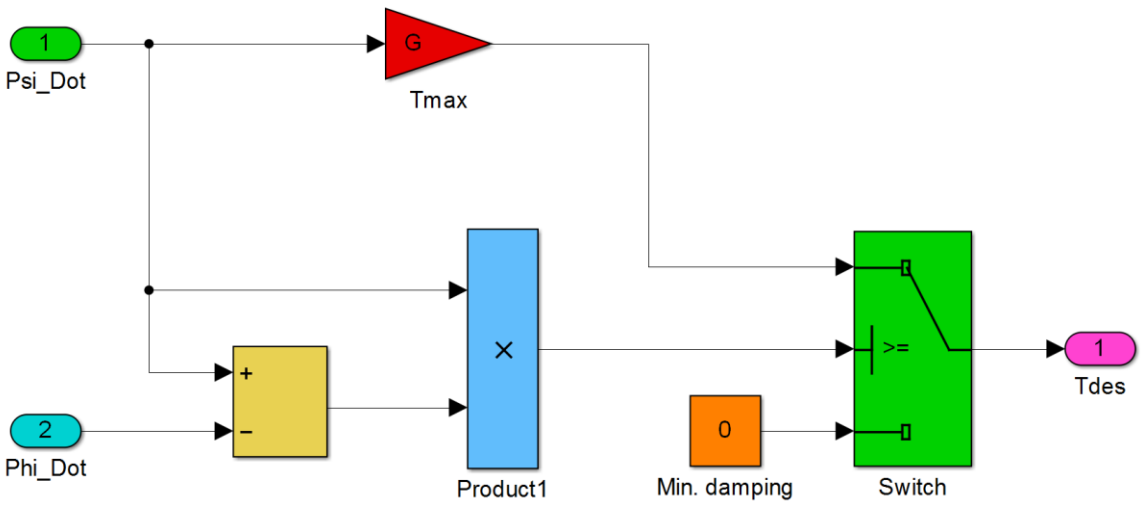

Figure 5-3 Simulink model of Skyhook logic

5.3.2 Damper controller

The Heaviside Step Function (HSF) damper controller is presented in this part. The applied voltage to MR damper is either turned on (Maximum voltage) or turned off (no applied voltage); and no intermediate voltage value will be applied. The Heaviside control algorithm can be simply described as [38]:

$$v = v_{max}\, H\,[(T_{des} - T_d).T_d\,] \tag{5-12}$$

where v_{max} is the maximum voltage applied to the current driver of the MR damper while H (.) is the Heaviside Step Function.

When the torque generated by the MR damper is similar to the desired torque, then the voltage applied to the MR damper should remain at the same level. If the magnitude of the

torque generated by the MR damper is smaller than that of the desired torque and the two torques have the same sign, the voltage applied to the current driver is increased to the maximum level to increase the torque generated by the damper to match the desired control torque. Otherwise, the applied voltage is set to zero. Eq. (5-12) can be represented by Simulink model as shown in Figure 5-4.

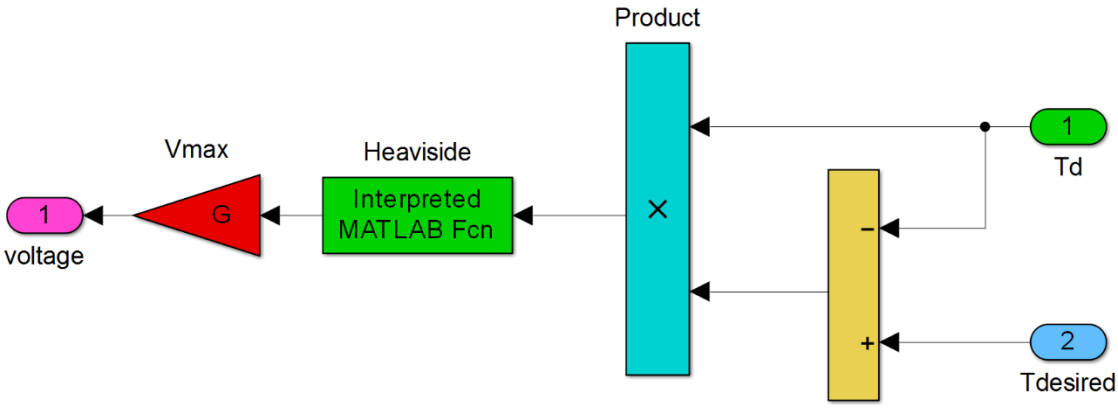

Figure 5-4 Simulink model of Heaviside Function

5.4 Test rig Simulink model

In order to evaluate the closed loop system response of the hybrid torsional vibration damper integrated with proposed system and damper controllers, a simulation model employing the whole components of the system is developed in Matlab/Simulink environment.

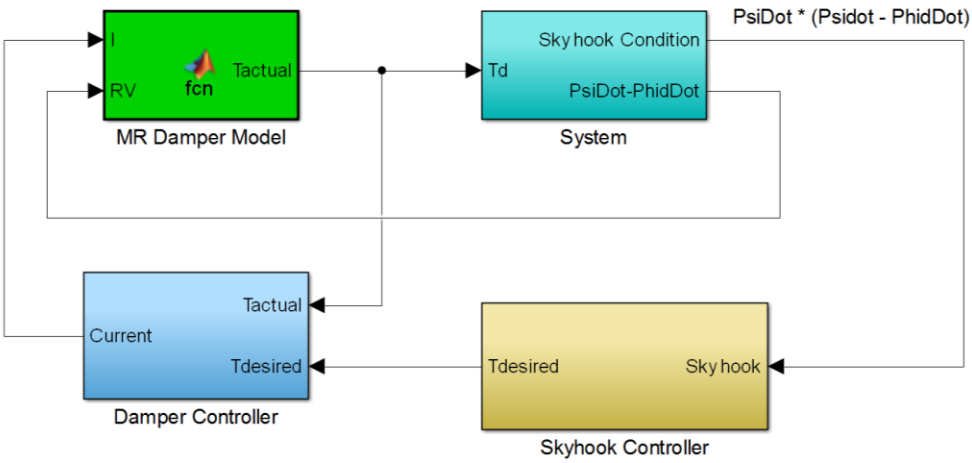

Figure 5-5 The proposed semi-active control system Simulink model

The Simulink model has been developed based on governing differential equations stated in Section 5.2. Required parameters used in the simulation are provided in Table 5-1.

Table 5-1 Specific values used in the analysis

Name	Unit	Value
Housing outer radius	*mm*	*80*
Housing inner radius	*mm*	*74*
Disc radius	*mm*	*60*
Disc width	*mm*	*10*
Shaft radius	*mm*	*17.5*
Coil width	*mm*	*13*
Coil height	*mm*	*13*
MR fluid film thickness at end-faces of disc	*mm*	*1.0*
Width of the annular duct of MR fluid	*mm*	*1.0*
Pendulum length	*mm*	*80*
Pendulum mass	*kg*	*1.0*
Torsional stiffness of the shaft	*kN.m/rad*	*23.57*

5.5 Summary

In this chapter, mathematical modelling of the new hybrid torsional vibration damper has been developed. The governing coupled nonlinear equations of motion have been derived based on Lagrange's principle. In addition, an appropriate semi-active control algorithm has been adopted for controlling the MR damper. The scheme for the complete semi-active control system has been shown in illustrative block diagram. The commonly used Skyhook control was employed for the system controller and its control logic has been described. The Heaviside Step Function is assigned for the damper controller and the function's logic has been described as well. A Simulink model for the shaft system with the hybrid torsional damper has been developed. In the next chapter, different cases for the system with different types of absorbers that are attached to the system will be investigated. Results obtained for each case will be illustrated and discussed.

Chapter 6
Results and Discussion

6.1 Introduction

In this chapter, results obtained from six different cases have been presented in order to evaluate the performance of proposed passive and the semi-active hybrid torsional dampers. In case 1, the rotor system without any dampers has been investigated at resonance condition. In case 2, the rotor system torsional response is illustrated when it is attached to only CPVA at the same condition. In case 3, response of the shaft system attached with only MR damper has been investigated at resonance condition under maximum applied current (passive mode on). In case 4, the proposed hybrid torsional damper is attached to the shaft system with zero current applied to the electromagnetic coil and the system torsional response is studied in the absence of the magnetic field (Passive mode off). In case 5, is similar to the case 4, except the system response has been studied under maximum applied current (passive mode on). Finally, the torsional vibration response of the system integrated with the semi-active hybrid torsional vibration damper has been investigated in the case 6.

6.2 Case 1- Rotor system without absorber

In this section, results obtained from numerical simulation of the rotor system without absorber has been illustrated. Figure 6-1 shows the system torsional response when it is operating without absorber, which can be obtained by solving Eq. (3-19) numerically with design parameters provided in Table 5-1.

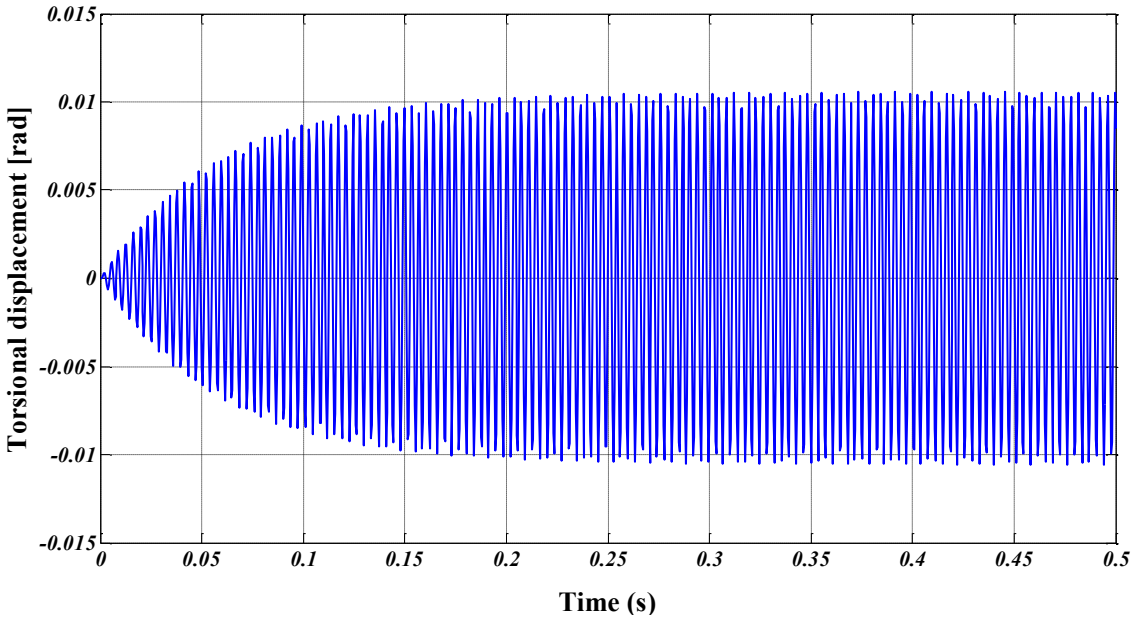

Figure 6-1 System torsional response when it is operating without absorber

As it can be realized, the torsional response of the rotor system operating without absorber is considerably high (0.01 rad) when the system is operating at its resonant frequency.

6.3 Case 2– Rotor system attached with CPVA

In this section, the centrifugal pendulum absorber is attached to the rotor system and the system torsional response is investigated. The system is modeled as a rotating shaft-disc system with CPVA attached to the disc and subjected to an external harmonic torque. Specific values used in the analysis are provided in Table 5-1. In order to achieve the best effective inertia of the pendulum absorber, the pendulum length is selected based on the resonance tuning condition. Solving the two coupled nonlinear differential Eqs. (3-11) and (3-12) numerically in Matlab environment using ode45 solver based on Runge-Kutta method, the rotor system torsional response is obtained as shown in Figure 6-2.

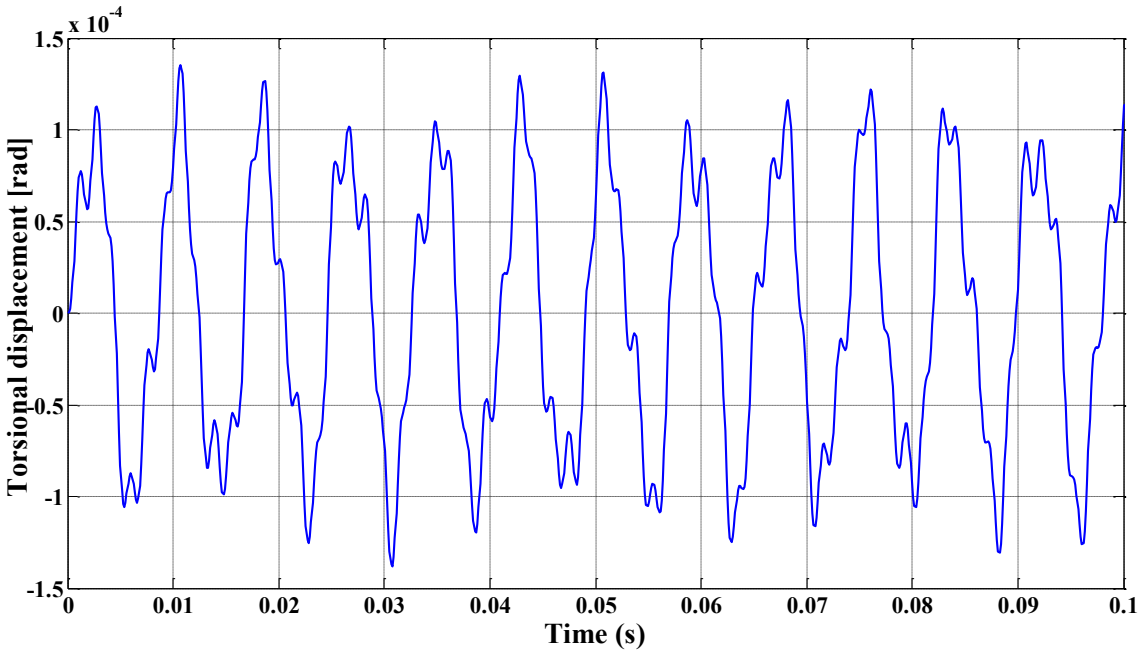

Figure 6-2 System torsional response when it is operating with CPVA

It is observed from Figure 6-2 that the amplitude of the torsional response of the rotor system operating with tuned CPVA is limited to around 1.2×10^{-4} rad, which is considerably lower than that of the system without absorber.

6.4 Case 3– Rotor system with MR damper

Here the rotor system with MR damper has been investigated. The system shown in Figure 4-6 consists of a shaft that is connected to the housing of the MR damper such that they are rotating together with the same rotational speed. All design parameters used in the developed model are illustrated in Table 5-1. The response of the rotor system integrated with MR damper is investigated at critical resonance condition in which excitation frequency coincides with natural frequency of the system under maximum applied current of 1.6 A (passive mode on).

Solving Eqs. (4-9) and (4-10) numerically, the torsional response of the system can be obtained. The results are shown in Figure 6-3.

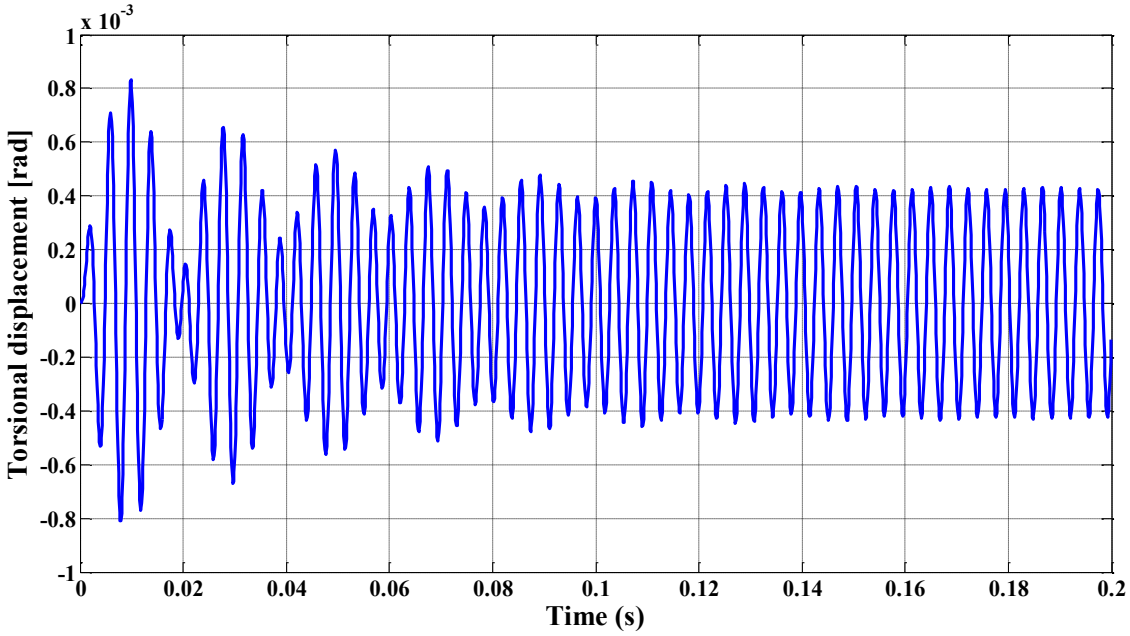

Figure 6-3 System torsional response when it is operating with MR damper

It is observed from Figure 6-3, that the steady state torsional response amplitude of the shaft system when it is operating with MR damper is reduced to a value of 4×10^{-4} rad, which is again considerably lower than that of the system without absorber (1×10^{-2} rad). As discussed before, the vibration energy of the shaft system can be effectively absorbed by the inertia disc inside the MR damper through the friction damping torque of the MR damper.

6.5 Rotor system with hybrid damper

In order to evaluate the performance of the proposed hybrid torsional damper, the developed model of the hybrid damper comprising the CPVA integrated with MR damper is investigated. First, the rotor system with the hybrid torsional damper is investigated when no current (zero current) is applied to the electromagnetic coil inside the damper (passive mode off). In this case, the generated damping torque is mainly due to the viscous effect as well as pendulum absorber. Second, a constant current value is applied to the damper coil in order to evaluate the passive mode on of the damper. Finally, the shaft system with semi-active control algorithm is investigated and results obtained in each case compared against one another. The torsional response of the shaft system for each case have been presented and discussed.

6.5.1 Case 4- Hybrid torsional damper with no current applied (passive mode off)

The rotor system with hybrid torsional damper is now investigated when no current is applied to the electromagnetic coil of the damper under resonance condition. Thus, by solving Eqs. (5-8), (5-9) and (5-10) numerically, the system output response for the three generalized coordinates related to angular displacement of shaft, pendulum and disk can be obtained. The results are shown in Figure 6-4. In addition, the amplitude of angular velocities for the shaft, disc and pendulum are presented in Figure 6-5, Figure 6-6 and Figure 6-7, respectively.

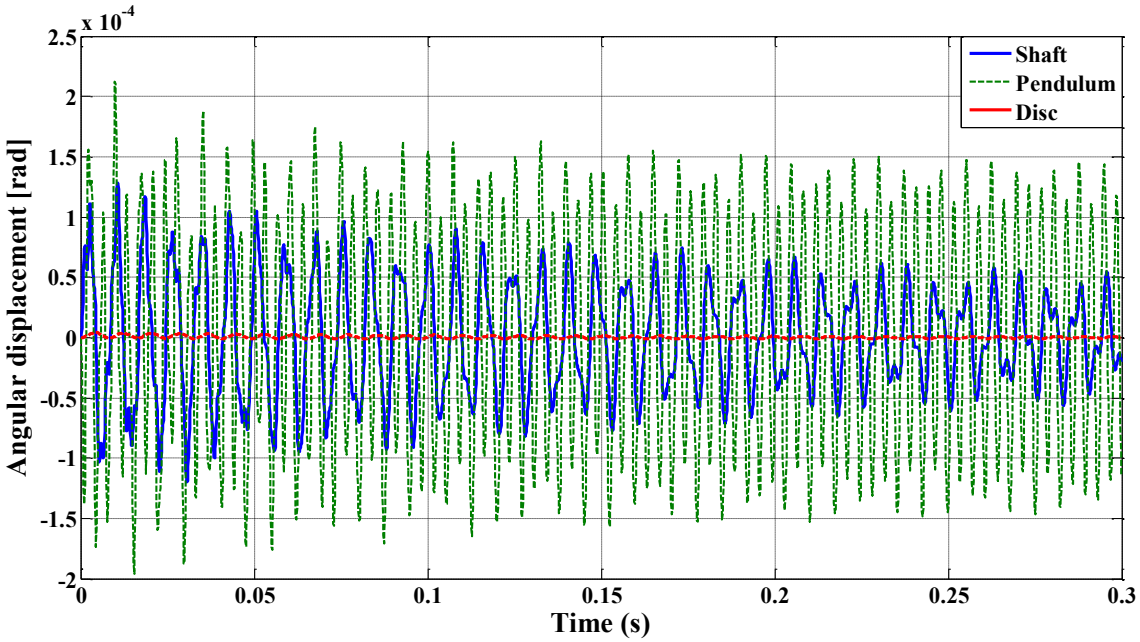

Figure 6-4 Shaft system response at zero current

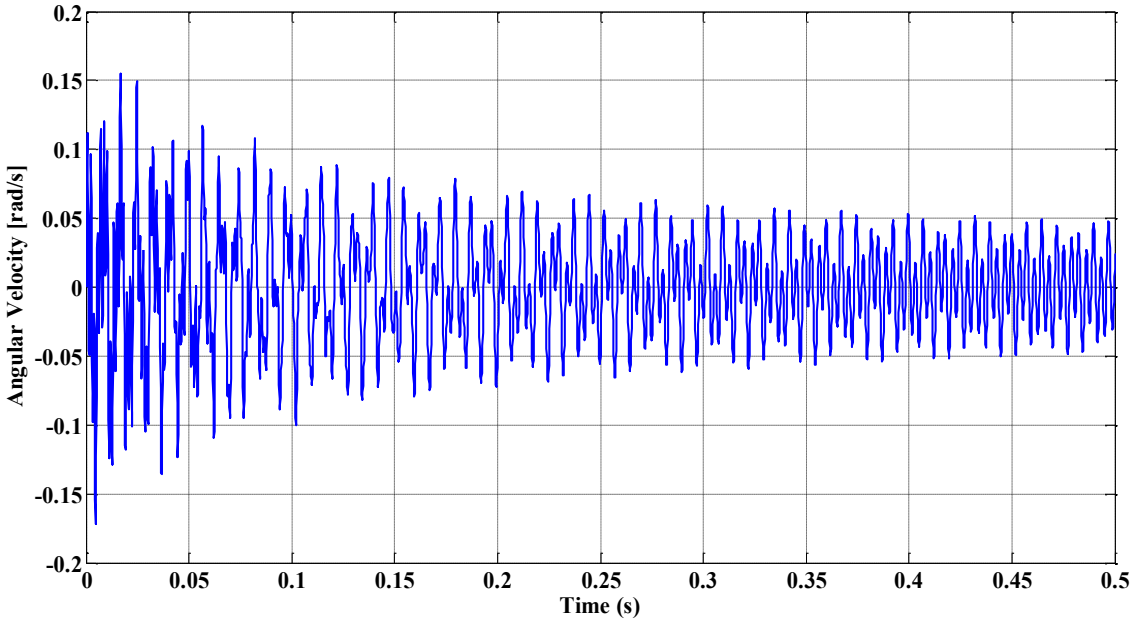

Figure 6-5 Angular velocity of the shaft torsional oscillation at zero current

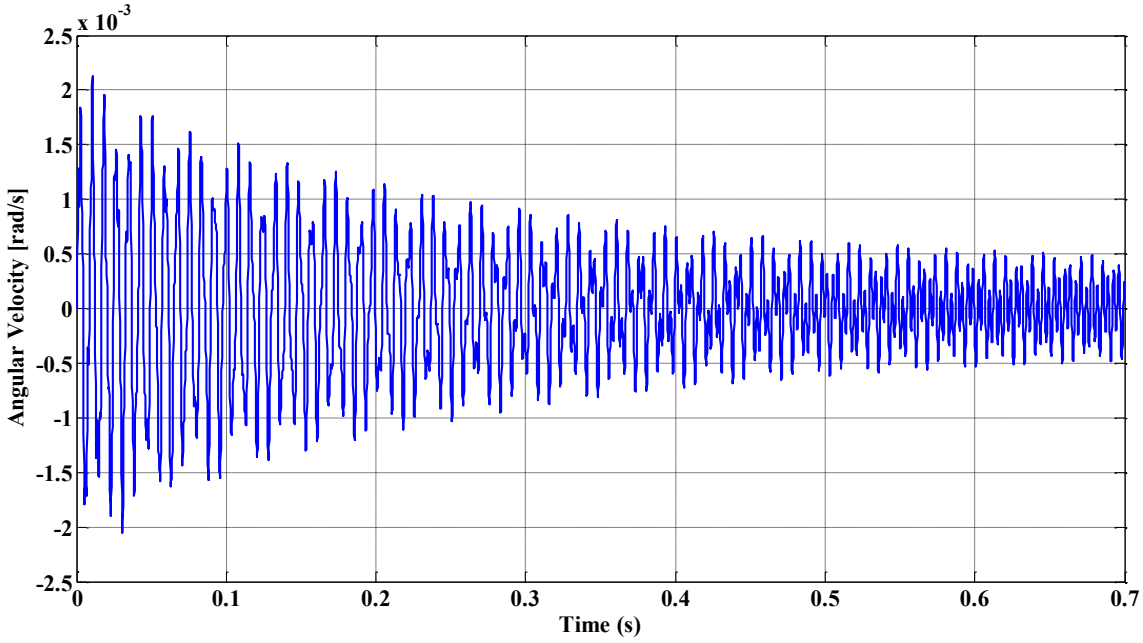

Figure 6-6 Angular velocity of the rotating disc at zero current

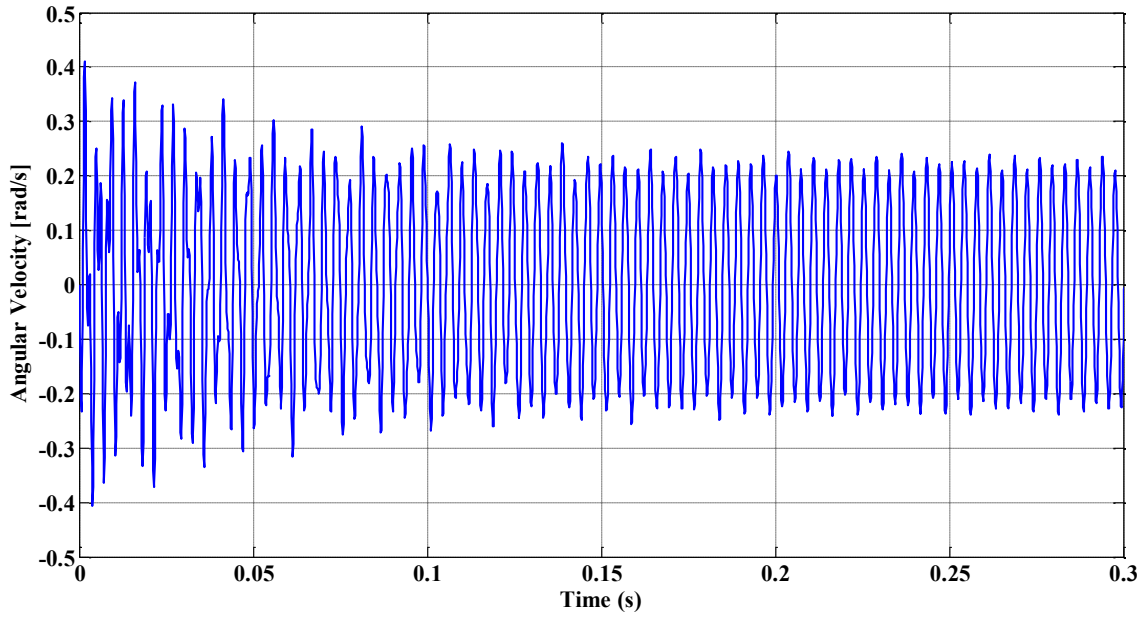

Figure 6-7 Pendulum angular velocity at zero current

6.5.2 Case 5- Hybrid torsional damper with applied constant current (passive mode on)

Here in this case, a constant current value of 1.6 Ampere (maximum value) is applied to the electromagnetic coil of the proposed hybrid torsional damper. The system output response for this case is illustrated in Figure 6-8.

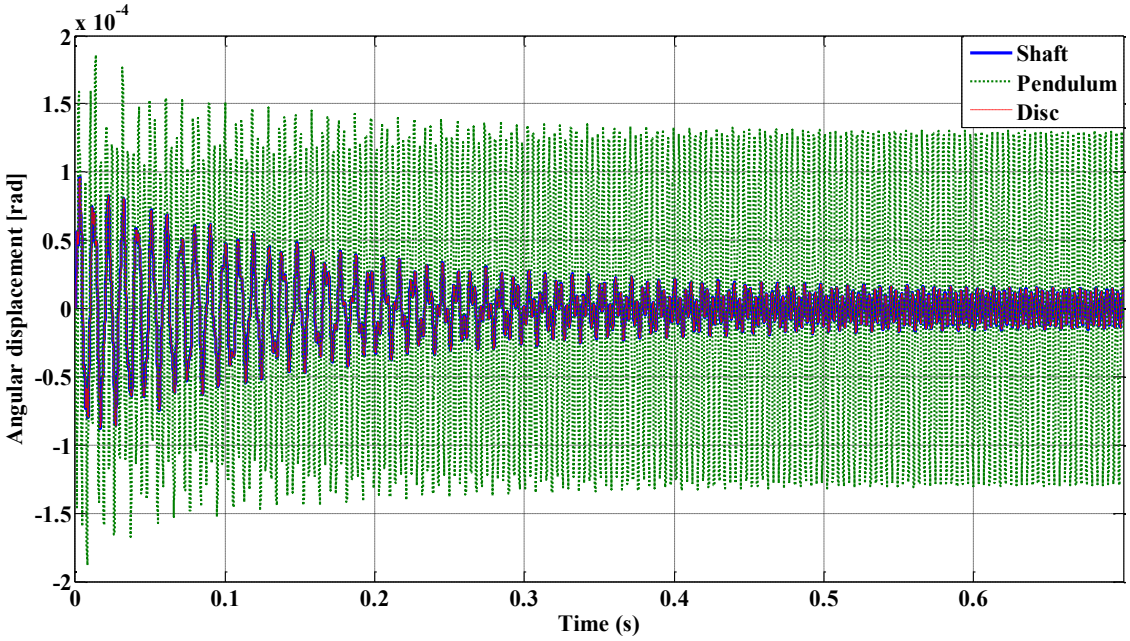

Figure 6-8 Shaft system response at maximum current

Moreover, the amplitude of angular velocities for the shaft, disc and pendulum for this case are also presented in Figure 6-9, Figure 6-10 and Figure 6-11, respectively. As can be observed from Figure 6-8, after applying maximum current value, the shaft torsional response and the rotating disc coincide with each other. In addition, it can be seen from Figure 6-9 and Figure 6-10 that the angular velocities for both shaft torsional response and the rotating disc are almost the same. That can be attributed to the generated friction torque due to the applied magnetic field and the induced shear stress through the MR fluid in the gaps causing the relative motion between the rotating disc and the damper's housing to be reduced.

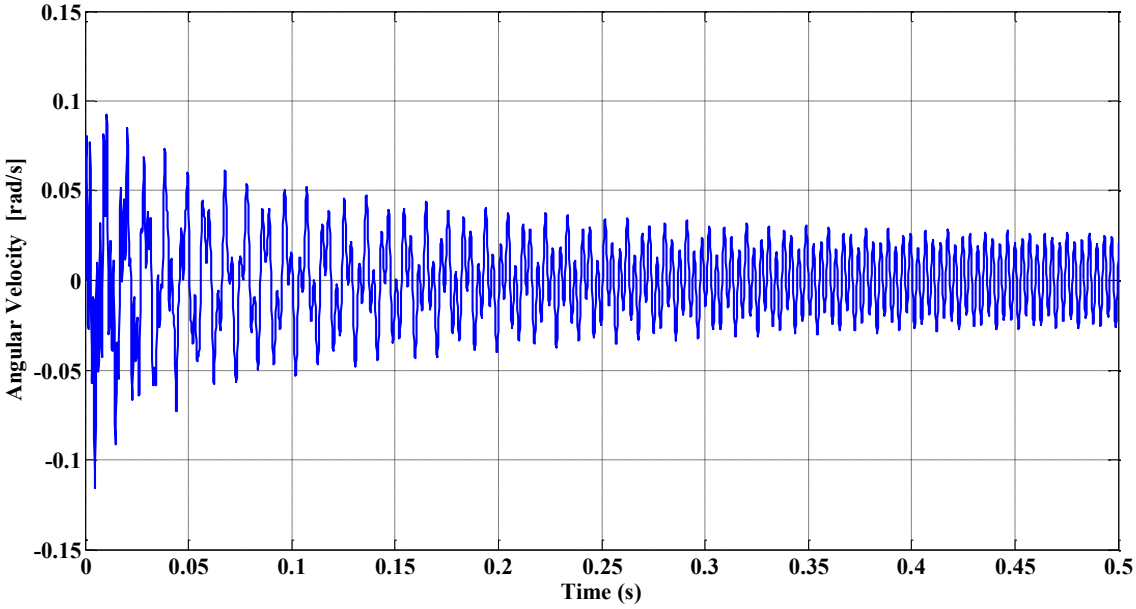

Figure 6-9 Angular velocity of the shaft torsional oscillation at maximum current

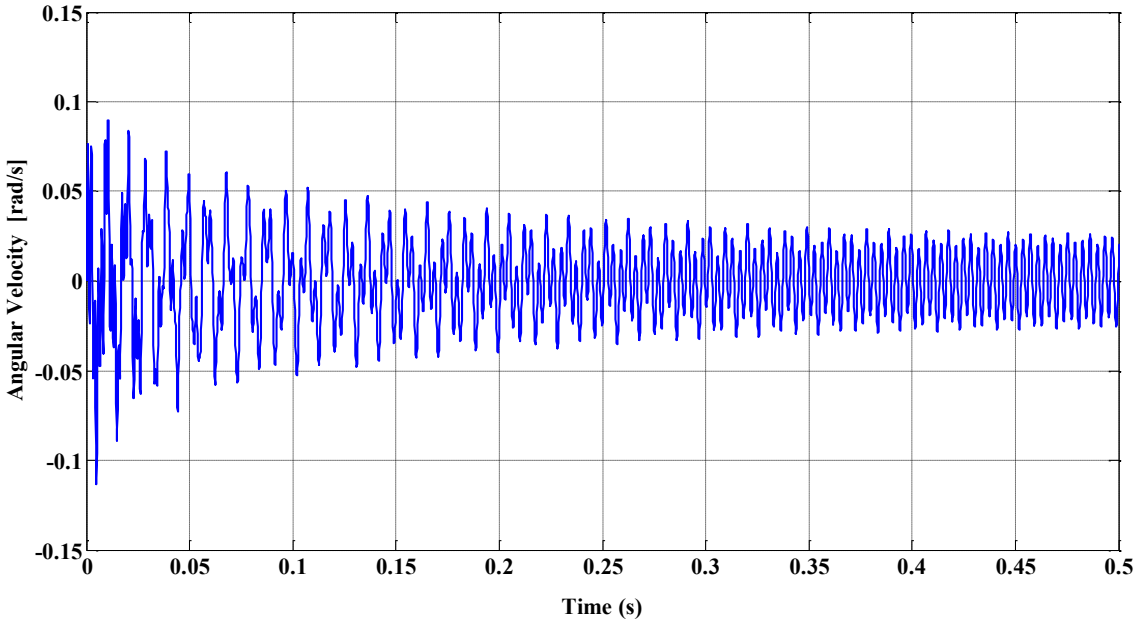

Figure 6-10 Angular velocity of the rotating disc at maximum current

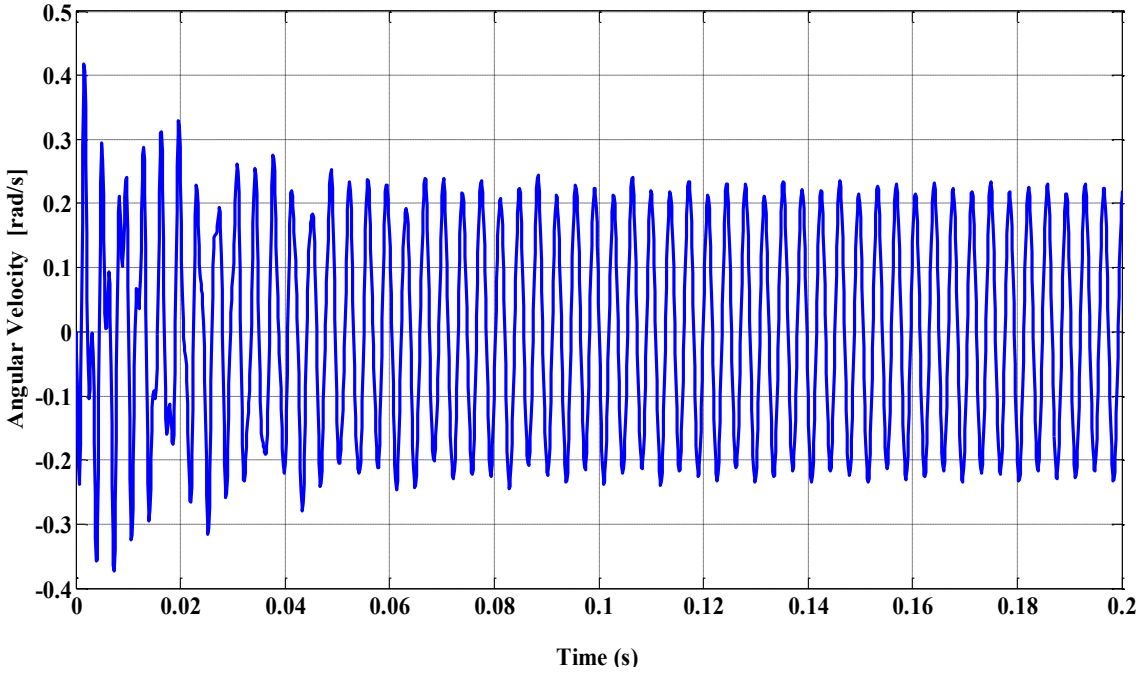

Figure 6-11 Pendulum angular velocity at maximum current

To better compare results for the cases with passive off and on modes (Cases 4 and 5), the steady state angular displacements and angular velocities of the system for both cases are presented in Table 6-1 and Table 6-2, respectively.

Table 6-1 Angular displacements of the shaft system [rad]

	Zero current	Maximum current
Shaft torsional response "$\|\psi\|$"	2×10^{-5}	1.25×10^{-5}
Disc angular displacement "$\|\phi_d\|$"	1.5×10^{-7}	1.25×10^{-5}
Pendulum angular displacement "$\|\phi\|$"	1.3×10^{-4}	1.25×10^{-4}

It can be observed that the amplitude of the shaft torsional response is reduced by 37 % when the maximum current is applied. That is because of the effect of the generated damping torque when the magnetic field is activated.

In contrast, the disc angular displacement is increased when the maximum current is applied, since the activation of the magnetic field causes generation of the friction torque that helps in contribution of the disc's inertia in the vibration energy dissipation; hence the disc vibration amplitude has been increased.

Table 6-2 Angular velocities of the shaft system

	Zero current	Maximum current
Angular velocity of the shaft torsional response "$\|\dot{\psi}\|$"	0.035	0.023
Disc angular velocity "$\|\dot{\phi}_d\|$"	0.0003	0.023
Pendulum angular velocity "$\|\dot{\phi}\|$"	0.22	0.22

Examination of results in Table 6-2 also reveals that the angular velocity of the shaft is significantly decreased when the maximum current is applied while the disc angular velocity is increased. However, the pendulum angular velocities are almost the same in both cases.

6.6 Case 6- Hybrid damper with semi-active control system

In this section, the developed model of the hybrid torsional damper comprising the CPVA integrated with MR damper is investigated at resonant frequency. The semi-active control algorithm as discussed in chapter 5 is applied. The hybrid torsional damper is attached to the driving shaft, which is under external excitation torque. Results of angular displacements for the shaft, disc and pendulum are illustrated in Figure 6-12, Figure 6-13 and Figure 6-14, respectively. Similar results for angular velocities are shown in Figure 6-15, Figure 6-16 and Figure 6-17.

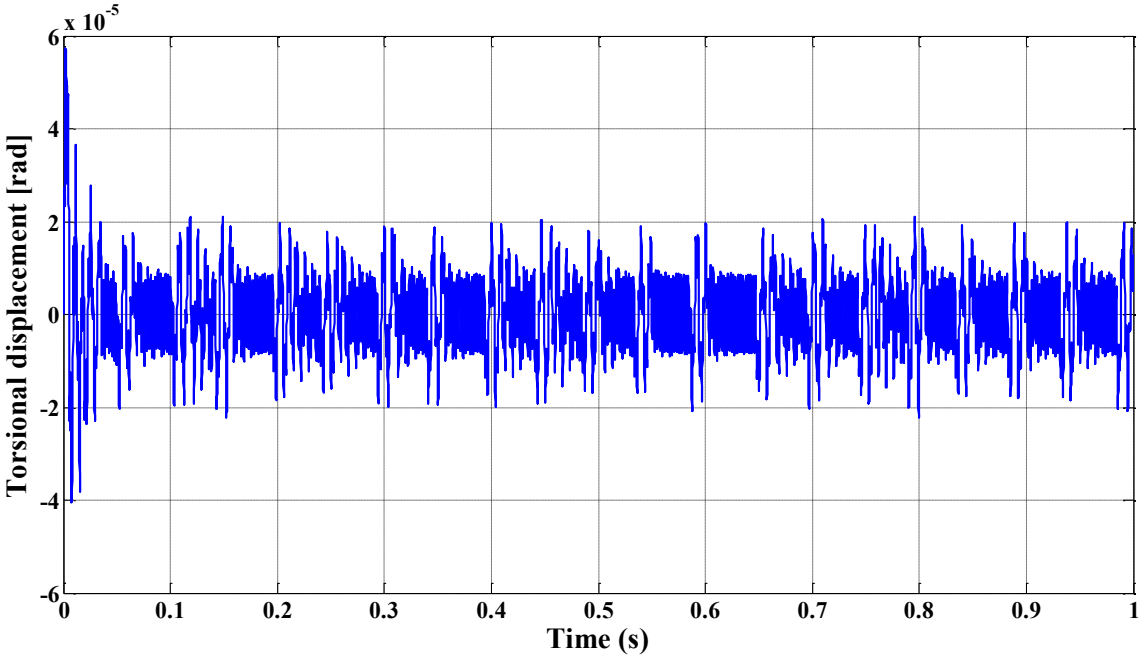

Figure 6-12 Shaft torsional response with semi-active control system

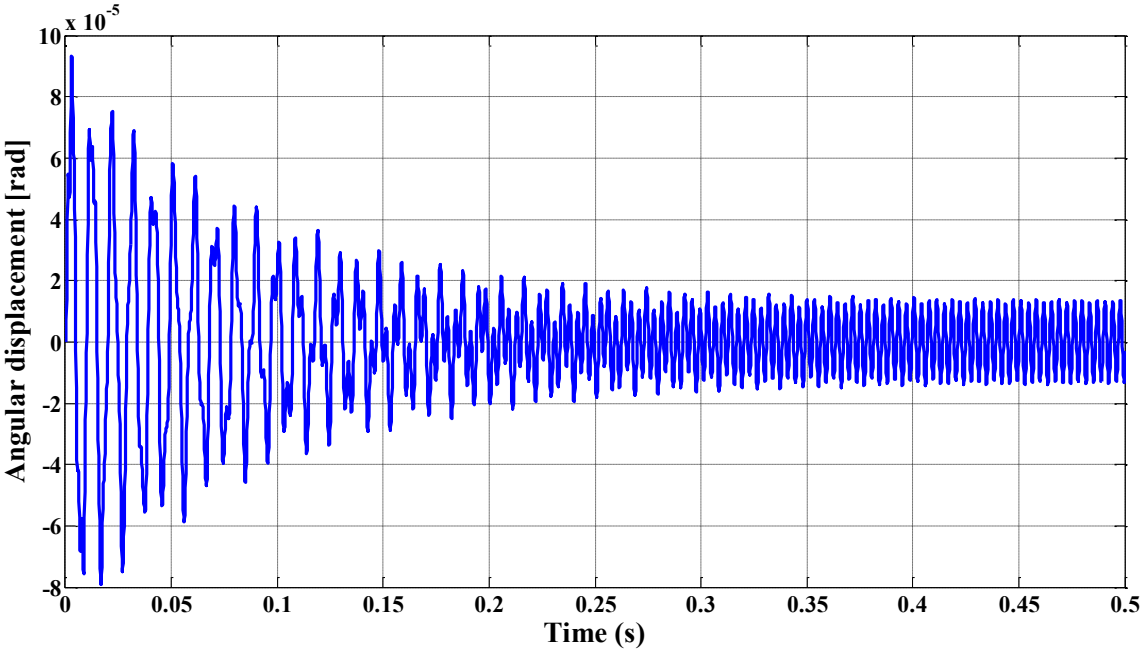

Figure 6-13 Disc angular displacement with semi-active control system

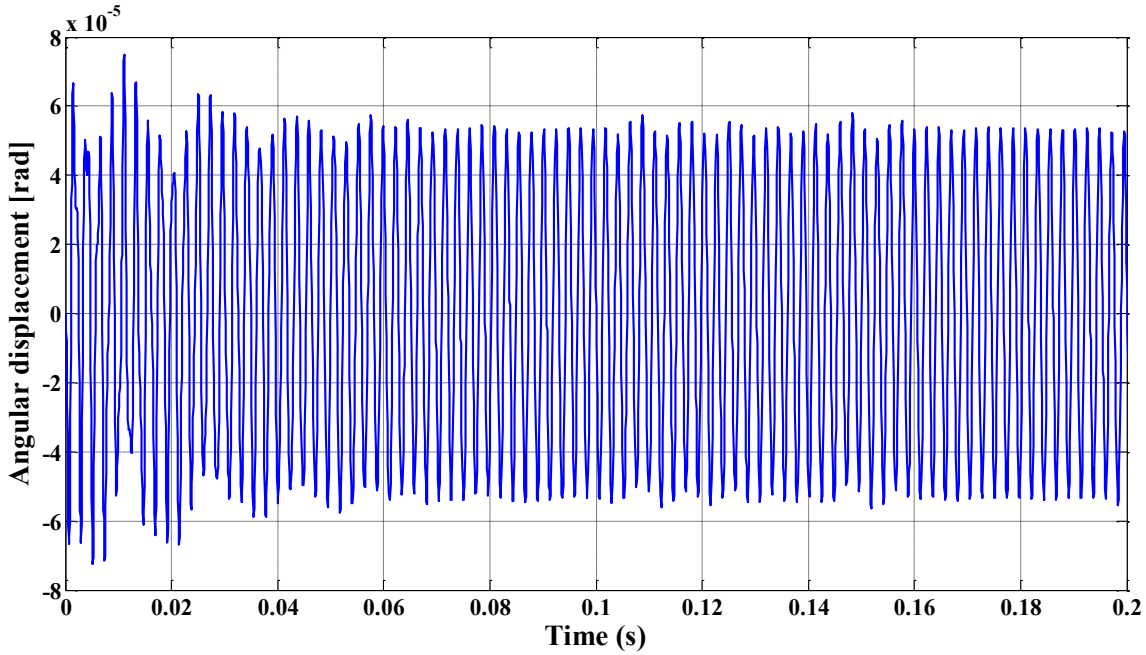

Figure 6-14 Pendulum angular displacement with semi-active control system

As discussed before, the Skyhook controller continuously specifies the desired damping torque based on the control logic strategy. As a result, the damper controller specifies the MR power supply to adjust the output current to the MR damper. Thus, the damper generates a damping torque that closely tracks the desired torque. It can be seen from Figure 6-12 that the torsional amplitude of the shaft system is reduced to a better value ($\approx 1\times10^{-5}$ rad) as compared with those of passive modes in Table 6-1. The angular velocities of the shaft, disc and pendulum as shown in Figure 6-15, Figure 6-16 and Figure 6-17, respectively, are also reduced, since the semi-active control system adjusts the desired damping torque required for better performance of the MR damper. Hence, as the damping is increased, the angular velocities decreased.

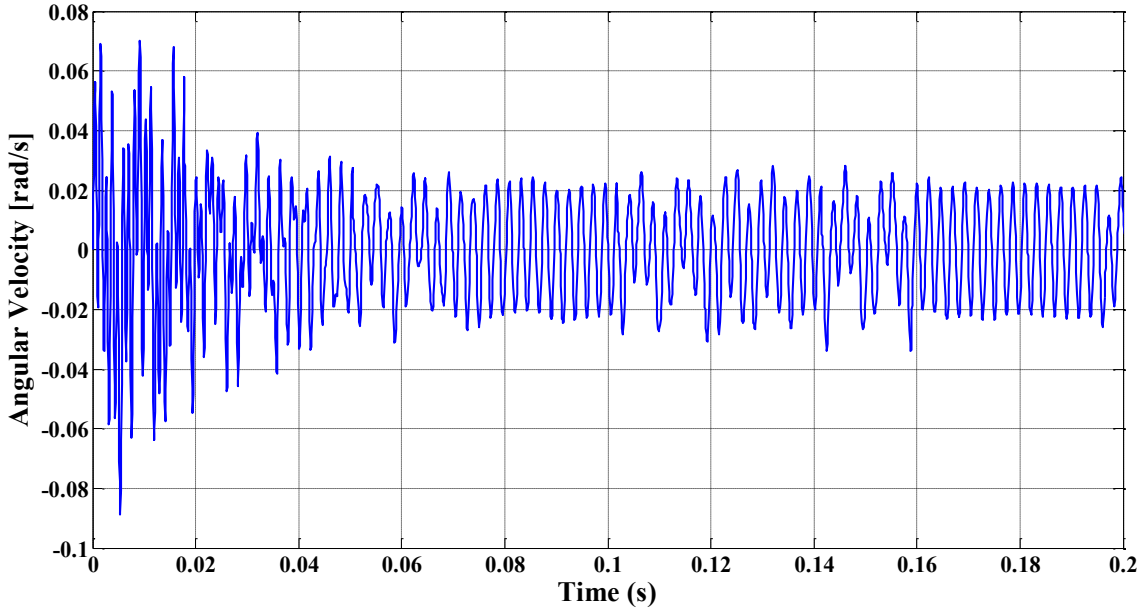

Figure 6-15 Angular velocity of the shaft torsional response with semi-active control system

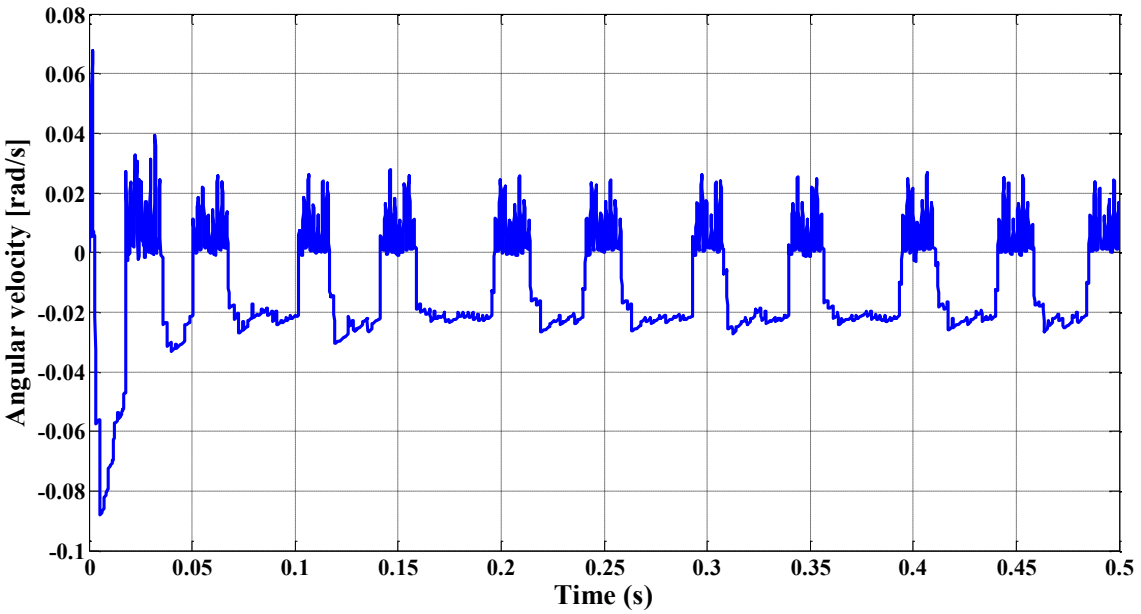

Figure 6-16 Disc angular velocity with semi-active control system

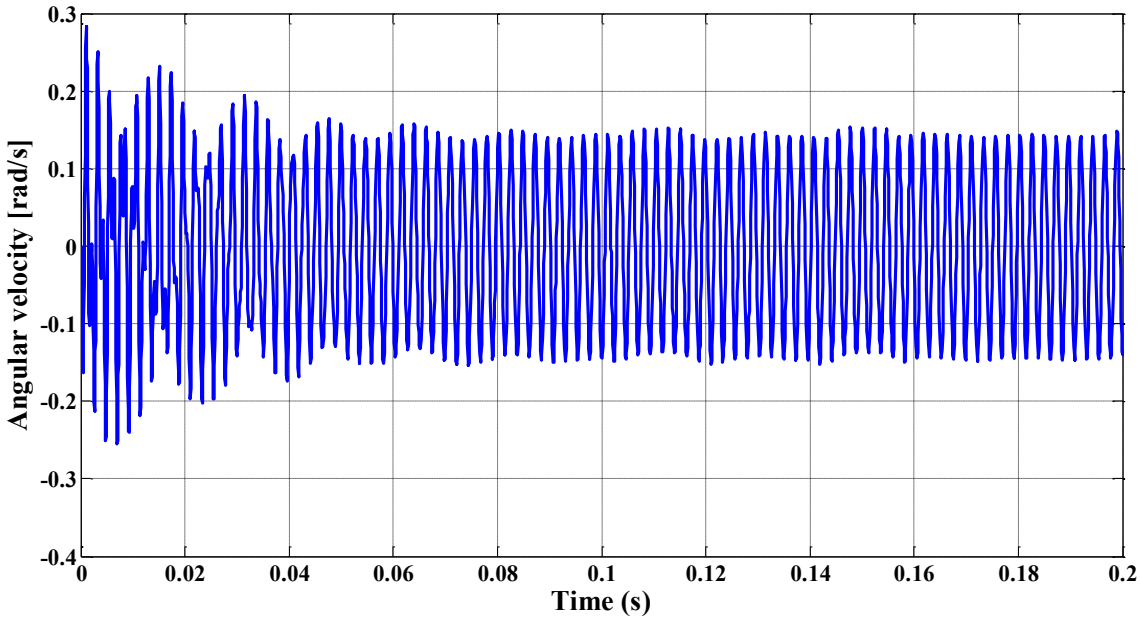

Figure 6-17 Pendulum angular velocity with semi-active control system

The time histories of the controlled damping torque and its corresponding applied current are also shown in Figure 6-18 and Figure 6-19, respectively. It is shown in Figure 6-19 that the applied current varies from zero to maximum value that is 1.6 Ampere.

As can be seen from Figure 6-19, the current applied to the MR damper varies between zero and 1.6 A according to the sign of the product of the two velocities (the absolute and the relative velocities). When their product is positive, the controller generates maximum torque and consequently the damper controller increases the current to the MR damper to increase the damper torque that closely matches the controller torque. Otherwise, the current is set to zero thus generating minimum damping torque.

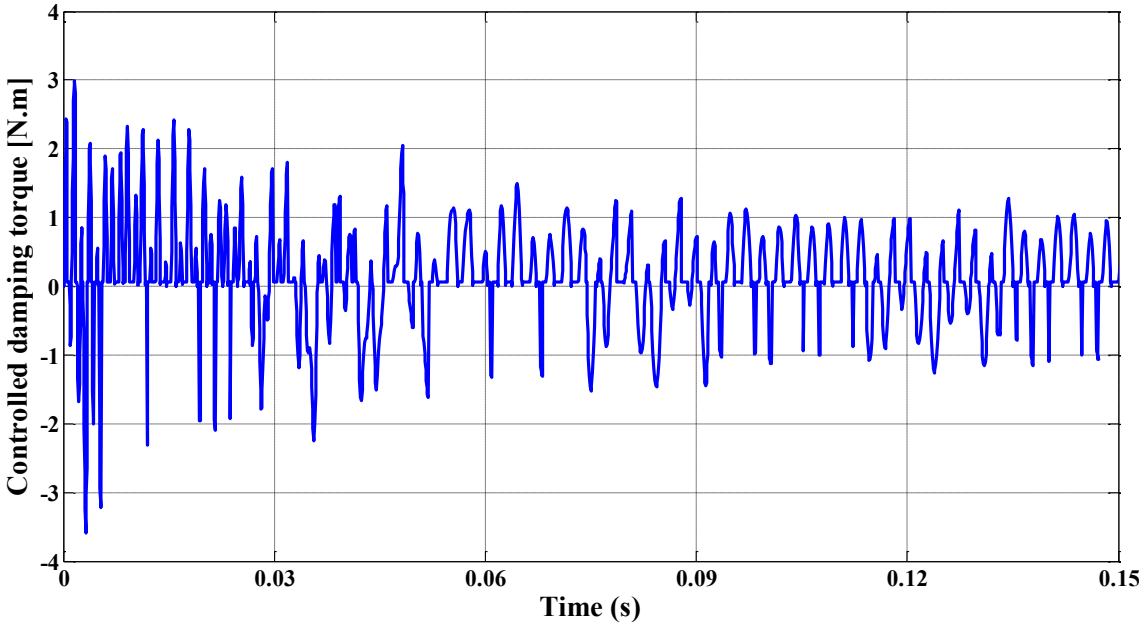

Figure 6-18 Time history of the controlled damping torque

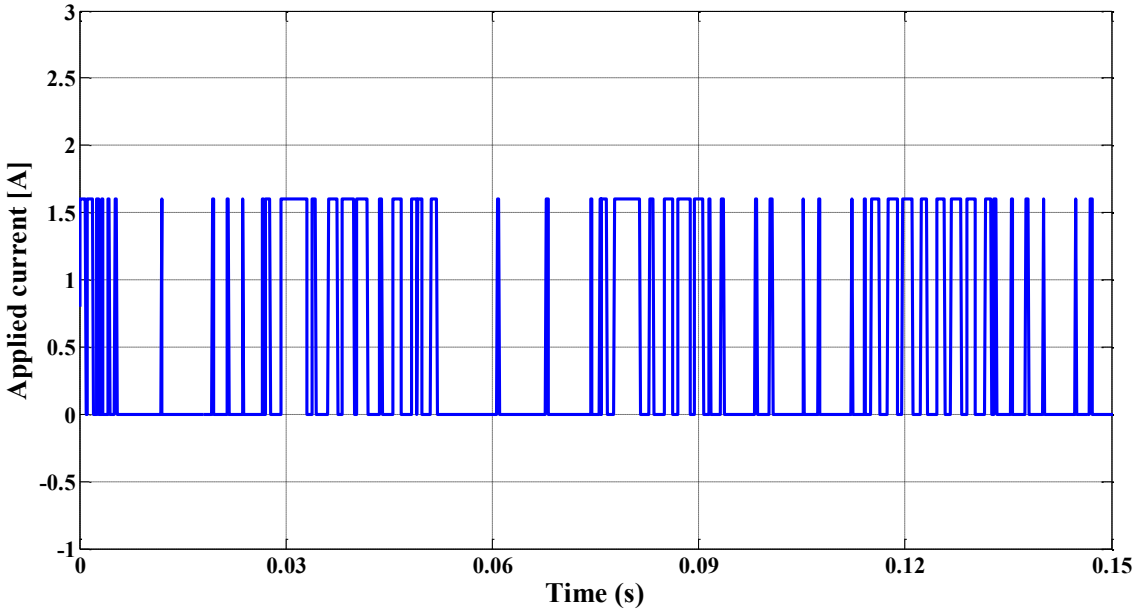

Figure 6-19 Time history of the applied current from the current driver

Moreover, it should be noted that the controlled system requires much less power, compared with the system with constant current applied to the MR damper. That particularly demonstrates the advantage of the semi-active system such that less power is needed while achieving better performance for vibration suppression. Furthermore, the semi-active controlled system generates less heat within the MR fluid as compared with passive mode with constant applied current.

6.7 Summary

In this chapter, torsional vibration response of the shaft system has been investigated for different cases. First, the response of the rotor system is investigated without any absorber and with then attached CPVA. This is followed by analysis of the rotor system integrated with only rotary MR. Subsequently, the rotor system with the proposed hybrid torsional vibration damper, which incorporates both CPVA, and rotary MR damper has been investigated. The dynamic performance of the hybrid torsional vibration damper has been evaluated for three control strategies. First, the performance of the system under passive control strategies in which the applied current is set to minimum (zero) and constant maximum values are investigated. Then, the semi-active Skyhook control strategy with variable applied current is considered. The semi-active control method offers an effective and reliable way to increase the system performance and to decrease the torsional vibration amplitude of the shaft system.

Chapter 7
Conclusion, Contributions and Future Recommendation

7.1 Conclusions

Attenuation of torsional vibrations in many mechanical systems with rotating components have become very challenging in recent years. Centrifugal Pendulum Vibration Absorber (CPVA) is a simple and reliable passive vibration absorber that has been widely used in rotary system to attenuate torsional vibration. Past research has focused mainly on the analysis of CPVAs operating in horizontal plane in which the effect of gravity has not been considered. In this study, the rotor system integrated with the pendulum absorber has been investigated in both vertical and horizontal planes in order to assess the effect of gravity.

It was determined that it is important to consider the effects of gravity at low operating speed where the torsional response amplitude of the shaft system is found to be considerably larger than that obtained when the absorber is operating in horizontal plane at which no gravity effect acted on the entire system. In automotive applications, the obtained results could serve as important guidelines in design stage since at low operating speed, torsional vibrations transmitted from cylinders to the crank at every power stroke could be quite high which may affect fatigue life of the crankshaft and system performance if not controlled properly. Consequently, it is important to take into account the gravity effect especially when the rotor system is operating at low speeds.

Also, it has been shown that there is no change in pendulum angular displacement amplitude when the absorber is operating either in vertical or horizontal plane. Moreover, the softening nonlinear behavior of CPVA is investigated over the operating speed range and it has been shown that the natural frequency of the pendulum decreases when the rotor speed increases. Hence, absorbers with circular paths exhibit softening nonlinear behavior in which their frequency decreases as the amplitude increases. To overcome this shortcoming in the circular path absorbers, a slight mistuning should be intentionally introduced to ensure stable and reliable operation of the CPVA.

Although CPVA is one of the effective passive devices used for reducing torsional vibrations, semi-active control systems are becoming more popular because they offer both the reliability of passive systems and the versatility and adaptability systems of active control systems without requiring high power demands. It has been found that Magnetorheological (MR) fluid dampers can be very effectively used for adaptive vibration damping under essentially unpredictable environmental conditions as in an internal combustion engine where the load, speed, acceleration, braking and road conditions are highly unpredictable.

This research presented the development of a novel hybrid torsional vibration damper combining conventional CPVA with the MR damper in which the conventional centrifugal pendulum is attached to the cylindrical housing of the MR damper. In order to develop an accurate model of hybrid torsional damper, the characteristic equations of the transmitted torque is derived to provide the theoretical basis for the design of the rotary MR damper using Bingham plastic model. Subsequently, the magnetostatic analysis for the magnetic circuit of the rotary MR damper has been carried out.

In addition, a FE model of the MR damper is developed in ANSYS in order to accurately simulate the magnetic field distribution through the MR fluid and test the effectiveness of the proposed design configuration as well as the selected material for the MR damper components.

Moreover, a design optimization methodology has been developed to identify the optimal dimensions of the designed rotary MR damper (disc radius, bore diameter and disc width) in order to maximize the generated damping torque under size and volume constraints. Genetic algorithm optimization technique has been used first to obtain approximately the near global optimum point. Then the obtained results from GA are used as initial values for SQP algorithm. It has been shown that GA and SQP can be effectively combined together to capture the global optimum solutions accurately than if they are used independently. Optimization results showed considerable improvement in the damper dynamic range as well as large amplitude of the generated torque.

A proof-of-concept of the optimally designed rotary MR damper has also been fabricated and experimentally tested to validate the simulation results. The experimental results showed that the damping torque increases when the applied current increases, reaching 20 N.m at 1.6 A, showing good agreement with the simulation predictions. Therefore it was concluded that the Bingham plastic model could satisfactory predict the operational torque range of the proposed damper.

Finally, a comprehensive evaluation of the dynamic performance of the proposed hybrid torsional vibration damper has been carried out. Both passive control and semi-active control based on Skyhook algorithm have been investigated. It has been shown that the semi-active control offers an effective and reliable approach that increases the system performance and decreases the torsional vibration amplitude in the shaft system.

Consequently, the proposed hybrid damper has proved to be one of the promising effective devices for semi-active control of torsional vibration due to the inherent fail-safe feature, low power requirement and capability to attenuate vibration under unpredictable environmental conditions.

7.2 Contributions

The major contributions of this dissertation research are summarized as follows:

a. Developing an accurate theoretical model of CPVA investigating the torsional vibration amplitude in both vertical and horizontal planes in order to assess the effect of gravity, using an appropriate term in the potential energy.
b. Investigating the torsional vibration amplitude of the rotor system at different operating speeds when the pendulum absorber is operating in both vertical and horizontal plane.
c. Developing an accurate model of the MR damper based on the Bingham constitutive plastic model to provide the theoretical basis in the design of the hybrid torsional damper.

d. Developing an efficient and accurate design optimization algorithm to improve the performance of the designed hybrid torsional damper as well as maximizing the generated damping torque.
e. Combining Genetic Algorithm (GA) and Sequential Quadratic Programming (SQP) optimization techniques to accurately capture the optimal geometric dimensions of the proposed hybrid damper.
f. Developing a FE model to conduct magnetostatic analysis for the magnetic circuit of the rotary MR damper; thus, a rotary MR damper is designed successfully with a specified damping torque capacity and unsaturated magnetic flux density.
g. Designing and fabricating a proof-of-concept rotary MR damper with the optimal dimensions.
h. Designing an experimental test rig set up to validate the experimental model.
i. Developing an effective control strategy that enhance the hybrid torsional damper dynamic behavior and minimizes the MR damper power requirements.
j. Investigating the passive control approach for the hybrid torsional damper.
k. Evaluating the semi-active Skyhook control algorithm with variable applied current applied to the system with hybrid torsional damper.

Furthermore, this research has advanced the state of the art in the semi-active torsional vibration control and nonlinear dynamics, since new contributions have been accomplished by introducing the new proposed hybrid torsional damper.

7.3 Publications

1. E. Abouobaia, R. Bhat and R. Sedaghati, "*Analytical Investigations of the Gravity Effect on the Dynamics and Performance of Centrifugal Pendulum Vibration Absorber*", proceedings of 16th int. Conf. on Applied Mechanics & Mechanical Engineering, Cairo, Egypt, May 2014.
2. E. Abouobaia, R. Bhat and R. Sedaghati, *"Hybrid Torsional Vibration Damper Incorporating Conventional Centrifugal Pendulum Absorber And Magnetorheological Damper*", Proceedings of the ASME 2014 Smart Materials, Adaptive Structures and Intelligent Systems SMASIS 2014, Newport, Rhode Island, USA , September 8-10, 2014.
3. E. Abouobaia, R. Bhat and R. Sedaghati, *"Semi-Active Control of Torsional Vibration Using a New Hybrid Torsional Damper*" Proceedings of the AIAA SciTech 2015, Gaylord Palms and Convention Center, Kissimmee, FL. Jan. 5-9, 2015.

7.4 Recommendations and future work

The present research was comprehensive enough in bringing out some useful conclusions; however, further interesting studies are needed in order to understand the advantages and effectiveness of the hybrid damper in practical applications. The following is a list of research studies that can enhance the understanding of the behavior of the hybrid damper:

1. Developing an experimental model of the proposed hybrid torsional damper.
2. Design and development of different models of pendulum absorbers such as cycloidal and epicycloidal path with hybrid damper and evaluation of the dynamic performance for each case.
3. Design and development of a drum type or T-shaped rotary MR damper and seek the torsional amplitude of the shaft system for each type.
4. Investigating of other advanced semi-active control algorithm for controlling the magnetic field in the MR damper.

Bibliography

[1] W. K. Wilson, *Pratical Solution of Torsional Vibration Problems: Devices for Controlling Vibration, Chapter III* vol. IV: Chapman & Hall, 1968.

[2] C. F. Taylor, *The Internal-combustion Engine in Theory and Practice: Combustion, fuels, materials, design* vol. 2: MIT press, 1985.

[3] T. Igusa and K. Xu, "Vibration control using multiple tuned mass dampers," *Journal of sound and vibration,* vol. 175, pp. 491-503, 1994.

[4] A. Joshi and R. Jangid, "Optimum parameters of multiple tuned mass dampers for base-excited damped systems," *Journal of sound and vibration,* vol. 202, pp. 657-667, 1997.

[5] A. H. Vonflotow, A. Beard, and D. Bailey, "Adaptive tuned vibration absorbers: tuning laws, tracking agility, sizing, and physical implementations," in *Proceedings of the National Conference on Noise Control Engineering*, pp. 437-454, 1994.

[6] R. Rana and T. Soong, "Parametric study and simplified design of tuned mass dampers," *Engineering structures,* vol. 20, pp. 193-204, 1998.

[7] A. Alsuwaiyan and S. W. Shaw, "Performance and dynamic stability of general-path centrifugal pendulum vibration absorbers," *Journal of Sound and Vibration,* vol. 252, pp. 791-815, 2002.

[8] J. den Hartog, "Mechanical vibrations, a general treatise on the vibrations of lumped and continuous physical systems," *New York, itd: McGraw-Hill,* 1956.

[9] W. Thomson, *Theory of vibration with applications*: CRC Press, 1996.

[10] M. Hamouda, H. Nabil, and G. A. Pierce, "Helicopter vibration suppression using simple pendulum absorbers on the rotor blade," *Journal of the American Helicopter Society,* vol. 29, pp. 19-29, 1984.

[11] V. Borowski, H. Denman, D. Cronin, S. Shaw, J. Hanisko, L. Brooks, D. Mikulec, W. Crum, and M. Anderson, "Reducing vibration of reciprocating engines with crankshaft pendulum vibration absorbers," SAE Technical Paper, 1991.

[12] T. M. Nester, A. G. Haddow, S. W. Shaw, J. E. Brevick, and V. J. Borowski, "Vibration reduction in a variable displacement engine using pendulum absorbers," SAE Technical Paper, 2003.

[13] A. G. Haddow and S. W. Shaw, "Centrifugal pendulum vibration absorbers: An experimental and theoretical investigation," *Nonlinear Dynamics,* vol. 34, pp. 293-307, 2003.

[14] H. Denman, "Tautochronic bifilar pendulum torsion absorbers for reciprocating engines," *Journal of Sound and Vibration,* vol. 159, pp. 251-277, 1992.

[15] C. T. Lee and S. W. Shaw, "Torsional vibration reduction in internal combustion engines using centrifugal pendulums," in *Proceedings of ASME Design Engineering Technical Conference*, pp. 487-492, 1995.

[16] M. J. Ryan and S. W. Shaw, "Nonlinear transient dynamics of pendulum torsional vibration absorbers—part I: theory," *Journal of Vibration and Acoustics,* vol. 135, pp. 1-10, 2013.

[17] Y. D. Chen, C. C. Fuh, and P. C. Tung, "Application of voice coil motors in active dynamic vibration absorbers," *Magnetics, IEEE Transactions on,* vol. 41, pp. 1149-1154, 2005.

[18] C. Liang and P. Tung, "Application of genetic algorithms to active vibration control of a centrifugal pendulum vibration absorber," *Proceedings of the Institution of Mechanical Engineers, Part I: Journal of Systems and Control Engineering,* vol. 224, pp. 329-338, 2010.

[19] A. Muhammad, X. L. Yao, and Z. L. Deng, "Review of magnetorheological (MR) fluids and its applications in vibration control," *Journal of Marine Science and Application,* vol. 5, pp. 17-29, 2006.

[20] J. Rabinow, "The magnetic fluid clutch," *American Institute of Electrical Engineers, Transactions of the,* vol. 67, pp. 1308-1315, 1948.

[21] J. Carlson, "Magnetorheological fluid actuators," *Adaptronics and Smart Structures. Basics, Materials, Design and Applications,* pp. 180-195, 1999.

[22] S. Abu-Ein, S. Fayyad, W. Momani, A. Al-Alawin, and M. Momani, "Experimental investigation of using MR fluids in automobiles suspension systems," *Research Journal of Applied Sciences, Engineering and Technology,* vol. 2, pp. 159-163, 2010.

[23] P. P. Phule, "Magnetorheological fluid," US Washington, DC Patent, 1999.

[24] A. Spaggiari, "Properties and applications of Magnetorheological fluids," *Fracture and Structural Integrity,* pp. 48-61, 2012.

[25] G. Yao, F. Yap, G. Chen, W. Li, and S. Yeo, "MR damper and its application for semi-active control of vehicle suspension system," *Mechatronics,* vol. 12, pp. 963-973, 2002.

[26] N. Wereley, J. Cho, Y. Choi, and S. Choi, "Magnetorheological dampers in shear mode," *Smart Materials and Structures,* vol. 17, pp. 1-11, 2008.

[27] K. J. Kim, C. W. Lee, and J. H. Koo, "Design and modeling of semi-active squeeze film dampers using magneto-rheological fluids," *Smart Materials and Structures,* vol. 17, pp. 1-12, 2008.

[28] W. Li, G. Chen, and S. Yeo, "Viscoelastic properties of MR fluids," *Smart Materials and Structures,* vol. 8, pp. 460-468, 1999.

[29] R. W. Phillips, "Engineering applications of fluids with a variable yield stress," University of California, Berkeley, 1969.

[30] X. Wang and F. Gordaninejad, "Flow analysis of field-controllable, electro-and magneto-rheological fluids using Herschel-Bulkley model," *Journal of Intelligent Material Systems and Structures,* vol. 10, pp. 601-608, 1999.

[31] D. Wang and W. Liao, "Magnetorheological fluid dampers: a review of parametric modelling," *Smart materials and structures,* vol. 20, pp. 1-34, 2011.

[32] B. Spencer, S. Dyke, M. Sain, and J. Carlson, "Phenomenological model for magnetorheological dampers," *Journal of engineering mechanics,* vol. 123, pp. 230-238, 1997.

[33] N. M. Wereley, L. Pang, and G. M. Kamath, "Idealized hysteresis modeling of electrorheological and magnetorheological dampers," *Journal of Intelligent Material Systems and Structures,* vol. 9, pp. 642-649, 1998.

[34] R. Stanway, J. Sproston, and A. El-Wahed, "Applications of electro-rheological fluids in vibration control: a survey," *Smart Materials and Structures,* vol. 5, pp. 464-482, 1996.

[35] A. W. Smyth, S. F. Masri, E. B. Kosmatopoulos, A. G. Chassiakos, and T. K. Caughey, "Development of adaptive modeling techniques for non-linear hysteretic

systems," *International Journal of Non-Linear Mechanics,* vol. 37, pp. 1435-1451, 2002.

[36] D. Q. Truong and K. K. Ahn, "MR fluid damper and its application to force sensorless damping control system," *Smart Actuation and Sensing Systems-Recent Advances and Future Challenges, Dr. Giovanni Berselli (Ed.),(book) Chap,* vol. 15, 2012.

[37] F. Imaduddin, S. A. Mazlan, and H. Zamzuri, "A design and modelling review of rotary magnetorheological damper," *Materials & Design,* vol. 51, pp. 575-591, 2013.

[38] C. Y. Lai and W. H. Liao, "Vibration control of a suspension system via a magnetorheological fluid damper," *Journal of Vibration and Control,* vol. 8, pp. 527-547, 2002.

[39] M. Zribi and M. Karkoub, "Robust control of a car suspension system using magnetorheological dampers," *Journal of Vibration and Control,* vol. 10, pp. 507-524, 2004.

[40] M. A. Karkoub and M. Zribi, "Active/semi-active suspension control using magnetorheological actuators," *International journal of systems science,* vol. 37, pp. 35-44, 2006.

[41] D. Wang and W. Liao, "Semiactive controllers for magnetorheological fluid dampers," *Journal of intelligent material systems and structures,* vol. 16, pp. 983-993, 2005.

[42] S. J. Dyke, B. F. Spencer Jr, M. K. Sain, and J. D. Carlson, "Modeling and control of magnetorheological dampers for seismic response reduction," *Smart Materials and Structures,* vol. 5, pp. 565-575, 1996.

[43] W. Liao and D. Wang, "Semiactive vibration control of train suspension systems via magnetorheological dampers," *Journal of Intelligent Material Systems and Structures,* vol. 14, pp. 161-172, 2003.

[44] N. Sims, R. Stanway, D. Peel, W. Bullough, and A. Johnson, "Controllable viscous damping: an experimental study of an electrorheological long-stroke damper under proportional feedback control," *Smart Materials and Structures,* vol. 8, pp. 601-615, 1999.

[45] A. H. F. Lam and W. H. Liao, "Semi-active control of automotive suspension systems with magneto-rheological dampers," *International Journal of Vehicle Design,* vol. 33, pp. 50-75, 2003.

[46] S. B. Choi, S. K. Lee, and Y. P. Park, "A hysteresis model for the field-dependent damping force of a magnetorheological damper," *Journal of Sound and Vibration,* vol. 245, pp. 375-383, 2001.

[47] C. C. Chang and L. Zhou, "Neural network emulation of inverse dynamics for a magnetorheological damper," *Journal of Structural Engineering,* vol. 128, pp. 231-239, 2002.

[48] D. Wang and W. Liao, "Modeling and control of magnetorheological fluid dampers using neural networks," *Smart Materials and Structures,* vol. 14, pp. 111-126, 2005.

[49] M. Ahmadian and C. A. Pare, "A quarter-car experimental analysis of alternative semiactive control methods," *Journal of Intelligent Material Systems and Structures,* vol. 11, pp. 604-612, 2000.

[50] H. S. Lee and S. B. Choi, "Control and response characteristics of a magneto-rheological fluid damper for passenger vehicles," *Journal of Intelligent Material Systems and Structures,* vol. 11, pp. 80-87, 2000.

[51] S. Ye and K. A. Williams, "Torsional vibration control with an MR fluid brake," *Smart Structures and Materials,* pp. 283-292, 2005.

[52] Y. Shen, M. Golnaraghi, and G. Heppler, "Semi-active vibration control schemes for suspension systems using magnetorheological dampers," *Journal of Vibration and Control,* vol. 12, pp. 3-24, 2006.

[53] F. Beltran-Carbajal, *Vibration Analysis and Control - New Trends and Developments*, 1st ed. Croatia: InTech, 2011.

[54] S. B. Choi, H. S. Lee, and Y. P. Park, "H∞ control performance of a full vehicle suspension featuring magnetorheological dampers," *Vehicle System Dynamics,* vol. 38, pp. 341-360, 2002.

[55] H. Du, K. Yim Sze, and J. Lam, "Semi-active H∞ control of vehicle suspension with magneto-rheological dampers," *Journal of Sound and Vibration,* vol. 283, pp. 981-996, 2005.

[56] L. H. Zong, X. L. Gong, S. H. Xuan, and C. Y. Guo, "Semi-active H∞ control of high-speed railway vehicle suspension with magnetorheological dampers," *Vehicle System Dynamics,* vol. 51, pp. 600-626, 2013.

[57] S. B. Choi, M. S. Seong, and S. H. Ha, "Vibration control of an MR vehicle suspension system considering both hysteretic behavior and parameter variation," *Smart Materials and Structures,* vol. 18, pp. 1-14, 2009.

[58] J. Wang, C. Dong, Y. Shen, and J. Wei, "Robust modelling and control of vehicle active suspension with MR damper," *Vehicle System Dynamics,* vol. 46, pp. 509-520, 2008.

[59] J. Lam, K. Sze, and H. Du, "Semi-active H-infinity control of vehicle suspension with magneto-rheological dampers," *Sound and Vibration,* vol. 283, pp. 981-996, 2005.

[60] G. Wenzhi and H. Zhiyong, "Active control and simulation test study on torsional vibration of large turbo-generator rotor shaft," *Mechanism and Machine Theory,* vol. 45, pp. 1326-1336, 2010.

[61] S. B. Choi, S. R. Hong, K. G. Sung, and J. W. Sohn, "Optimal control of structural vibrations using a mixed-mode magnetorheological fluid mount," *International Journal of Mechanical Sciences,* vol. 50, pp. 559-568, 2008.

[62] E. J. Park, D. Stoikov, L. Falcao da Luz, and A. Suleman, "A performance evaluation of an automotive magnetorheological brake design with a sliding mode controller," *Mechatronics,* vol. 16, pp. 405-416, 2006.

[63] Y. T. Choi and N. M. Wereley, "Vibration control of a landing gear system featuring electrorheological/magnetorheological fluids," *Journal of Aircraft,* vol. 40, pp. 432-439, 2003.

[64] J. Den Hartog and J. Ormondroyd, "Torsional vibration dampers," *Transactions of the American Society of Mechanical Engineers, Applied Mechanics Division,* pp. 133-152, 1929.

[65] S. Ye and K. A. Williams, "Torsional friction damper optimization," *Journal of sound and vibration,* vol. 294, pp. 529-546, 2006.

[66] S. Ye and K. A. Williams, "MR fluid brake for control of torsional vibration," SAE Technical Paper, 2005.

[67] K. A. Williams and Y. Shaochun, "Semi-active control of torsional vibrations using an MR fluid brake," in *SPIE proceedings series*, pp. 135-146, 2004.

[68] Q. H. Nguyen and S. B. Choi, "Optimal design of an automotive magnetorheological brake considering geometric dimensions and zero-field friction heat," *Smart Materials and Structures,* vol. 19, pp. 1-11, 2010.

[69] Q. H. Nguyen and S. B. Choi, "Optimal design of a magneto-rheological brake absorber for torsional vibration control," *Smart Materials and Structures,* vol. 21, pp. 1-9, 2012.

[70] G. Yang, B. F. Spencer Jr, J. D. Carlson, and M. K. Sain, "Large-scale MR fluid dampers: modeling and dynamic performance considerations," *Engineering structures,* vol. 24, pp. 309-323, 2002.

[71] S. J. Dyke, B. F. Spencer Jr, M. K. Sain, and J. D. Carlson, "An experimental study of MR dampers for seismic protection," *Smart materials and structures,* vol. 7, pp. 693-703, 1998.

[72] G. Yang, B. F. Spencer Jr, H. J. Jung, and J. D. Carlson, "Dynamic modeling of large-scale magnetorheological damper systems for civil engineering applications," *Journal of Engineering Mechanics,* vol. 130, pp. 1107-1114, 2004.

[73] J. D. Carlson, D. M. Catanzarite, and K. A. St. Clair, "Commercial magneto-rheological fluid devices," *International Journal of Modern Physics B,* vol. 10, pp. 2857-2865, 1996.

[74] X. Q. Ma, S. Rakheja, and C. Y. Su, "Development and relative assessments of models for characterizing the current dependent hysteresis properties of magnetorheological fluid dampers," *Journal of intelligent material systems and structures,* vol. 18, pp. 487-502, 2007.

[75] Y. Duan, Y. Ni, and J. Ko, "Cable vibration control using magnetorheological dampers," *Journal of intelligent material systems and structures,* vol. 17, pp. 321-325, 2006.

[76] W. Wei and X. Pinqi, "Adaptive control of helicopter ground resonance with magnetorheological damper," *Chinese Journal of Aeronautics,* vol. 20, pp. 501-510, 2007.

[77] M. D. Rao, "Recent applications of viscoelastic damping for noise control in automobiles and commercial airplanes," *Journal of Sound and Vibration,* vol. 262, pp. 457-474, 2003.

[78] A. Karamodin and H. Haji Kazemi, "Semi-active control of structures using neuro-predictive algorithm for MR dampers," *Structural Control and Health Monitoring,* vol. 278, pp. 1002-1020, 2008.

[79] F. Gordaninejad and S. P. Kelso, "Magneto-rheological fluid shock absorbers for HMMWV," in *SPIE's 7th Annual International Symposium on Smart Structures and Materials*, pp. 266-273, 2000.

[80] J. D. Carlson and M. R. Jolly, "MR fluid, foam and elastomer devices," *mechatronics,* vol. 10, pp. 555-569, 2000.

[81] Y. T. Choi, J. U. Cho, S. B. Choi, and N. M. Wereley, "Constitutive models of electrorheological and magnetorheological fluids using viscometers," *Smart materials and structures,* vol. 14, pp. 1025-1036, 2005.

[82] W. H. Li and H. Du, "Design and experimental evaluation of a magnetorheological brake," *The International Journal of Advanced Manufacturing Technology,* vol. 21, pp. 508-515, 2003.

[83] D. Senkal and H. Gurocak, "Compact MR-brake with serpentine flux path for haptics applications," in *EuroHaptics conference and Symposium on Haptic Interfaces for Virtual Environment and Teleoperator Systems. World Haptics. Third Joint*, pp. 91-96, 2009.

[84] J. Huang, J. Zhang, Y. Yang, and Y. Wei, "Analysis and design of a cylindrical magneto-rheological fluid brake," *Journal of Materials Processing Technology,* vol. 129, pp. 559-562, 2002.

[85] T. Kikuchi and K. Kobayashi, "Design and development of cylindrical MR fluid brake with multi-coil structure," *Journal of System Design and Dynamics,* vol. 5, pp. 1471-1484, 2011.

[86] Y. Shiao and Q. A. Nguyen, "Development of a multi-pole magnetorheological brake," *Smart Materials and Structures,* vol. 22, pp. 1-13, 2013.

[87] Q. H. Nguyen and S. B. Choi, "Selection of magnetorheological brake types via optimal design considering maximum torque and constrained volume," *Smart Materials and Structures,* vol. 21, pp. 1-12, 2012.

[88] W. Phillips, "Engineering applications of fluids with a variable yield stress," Ph.D. Thesis, Berkeley, California, 1969.

[89] *http://www.lord.com/products-and-solutions/magneto-rheological-(mr)/product.xml/1645*.

[90] Q. H. Nguyen and S. B. Choi, "Optimal design of a vehicle magnetorheological damper considering the damping force and dynamic range," *Smart Materials and Structures,* vol. 18, pp. 1-10, 2009.

[91] J. H. Lee, C. Han, D. Ahn, J. K. Lee, S. H. Park, and S. Park, "Design and performance evaluation of a rotary magnetorheological damper for unmanned vehicle suspension systems," *The Scientific World Journal,* vol. 2013, pp. 1-10, 2013.

[92] A. Jasbir, *Introduction to optimum design*, 3rd ed.: Elsevier, 2012.

[93] K. C. Tan, T. H. Lee, and E. F. Khor, "Evolutionary algorithms for multi-objective optimization: performance assessments and comparisons," *Artificial intelligence review,* vol. 17, pp. 251-290, 2002.

[94] A. Hadadian, R. Sedaghati, and E. Esmailzadeh, "Optimal Design of Magnetorheological Damper using Response Surface Method," in *53rd AIAA/ASME/ASCE/AHS/ASC Structures, Structural Dynamics and Materials Conference*, pp. 1-10, 2012.

[95] M. Eslami, H. Shareef, and M. Khajehzadeh, "Damping controller design for power system oscillations using hybrid GA-SQP," *International Review of Electrical Engineering (IREE),* vol. 6, pp. 888-896, 2011.

[96] K. Karakoc, "Design of a magnetorheological brake system based on magnetic circuit optimization," University of Victoria, 2007.

[97] C. R. Reeves, "A genetic algorithm for flowshop sequencing," *Computers & Operations Research,* vol. 22, pp. 5-13, 1995.

[98] D. Charles, *The origin of species*: John Murry, 1929.

[99] J. H. Holland, *Adaptation in natural and artificial systems: An introductory analysis with applications to biology, control, and artificial intelligence*: U Michigan Press, 1975.

[100] K.-F. Man, K. S. TANG, and S. Kwong, *Genetic Algorithms: Concepts and Designs, Avec disquette* vol. 1: Springer, 1999.

[101] Z. Michalewicz, G. Algorithms, and D. Structures, *Evolution Programs*, 3rd ed.: Springer, 1996.

[102] M. Gen and R. Cheng, *Genetic algorithms and engineering optimization* vol. 7: John Wiley & Sons, 2000.

[103] M. Sadeghifar, M. Bagheri, and A. Jafari, "Multiobjective optimization of orthogonally stiffened cylindrical shells for minimum weight and maximum axial buckling load," *Thin-Walled Structures,* vol. 48, pp. 979-988, 2010.

[104] P. E. Gill and E. Wong, "Sequential quadratic programming methods," in *Mixed integer nonlinear programming*, 1st ed: Springer, pp. 147-224, 2012.

[105] M. Fesanghary, M. Mahdavi, M. Minary-Jolandan, and Y. Alizadeh, "Hybridizing harmony search algorithm with sequential quadratic programming for engineering optimization problems," *Computer methods in applied mechanics and engineering,* vol. 197, pp. 3080-3091, 2008.

[106] C. Guillaume, D. Laurent, F. Yao, H. Dominik, S. Kevin, E. Abouobaia, R. Sedaghati, and R. Bhat, "Design and manufacturing of a magnetorheological torsional vibration damper," Concordia, Montreal, QC, CA. Project Report, 2014.

[107] S. S. Rao and F. F. Yap, *Mechanical vibrations*, 5th ed.: Addison-Wesley New York, 2011.

Appendix A

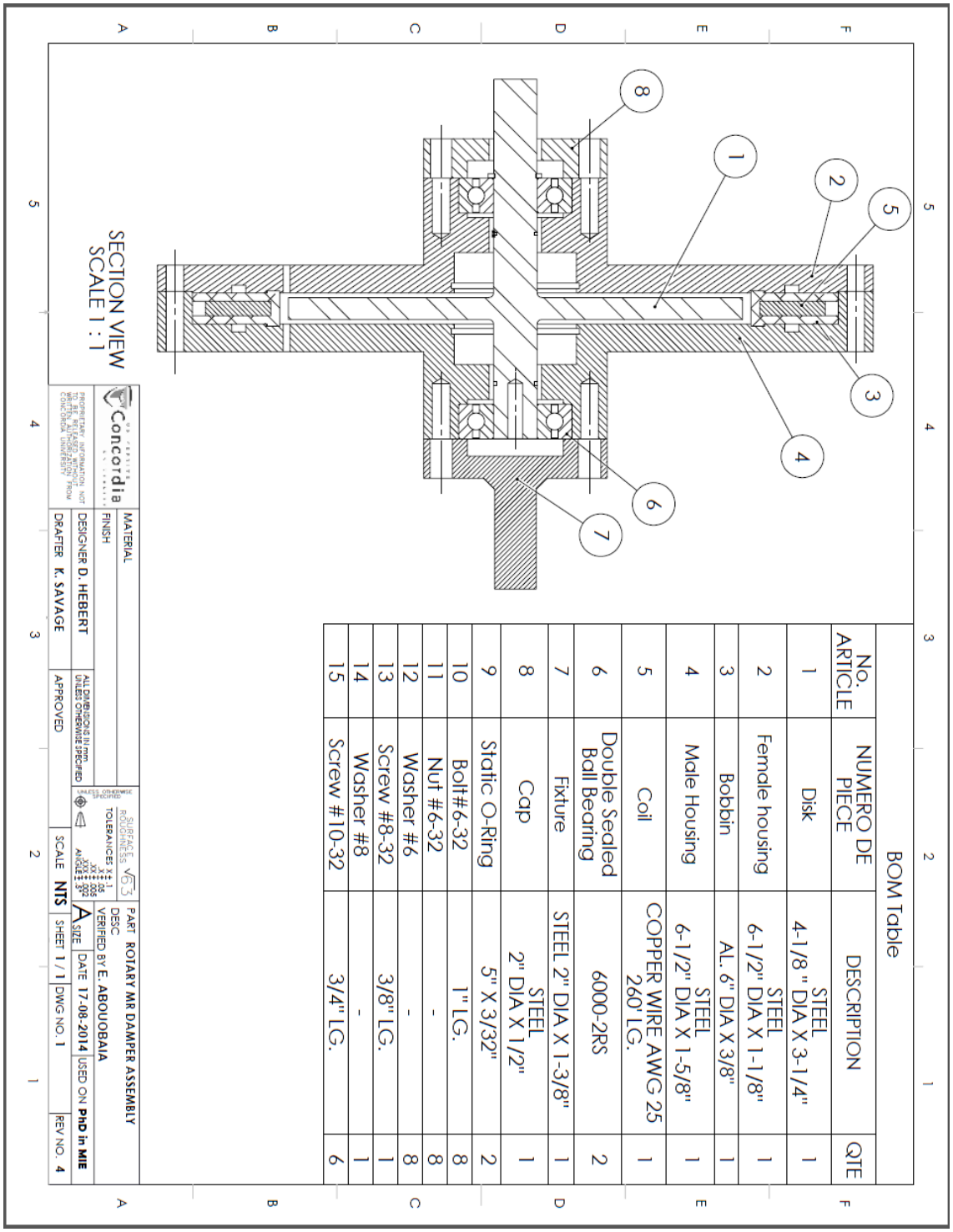
SECTION VIEW
SCALE 1 : 1
BOM Table
No. ARTICLE
NUMERO DE PIECE
DESCRIPTION
QTE
1 Disk STEEL 4-1/8 " DIA X 3-1/4" 1
2 Female housing STEEL 6-1/2" DIA X 1-1/8" 1
3 Bobbin AL. 6" DIA X 3/8" 1
4 Male Housing STEEL 6-1/2" DIA X 1-5/8" 1
5 Coil COPPER WIRE AWG 25 260' LG. 1
6 Double Sealed Ball Bearing 6000-2RS 2
7 Fixture STEEL 2" DIA X 1-3/8" 1
8 Cap STEEL 2" DIA X 1/2" 1
9 Static O-Ring 5" X 3/32" 2
10 Bolt#6-32 1" LG. 8
11 Nut #6-32 - 8
12 Washer #6 - 8
13 Screw #8-32 3/8" LG. 1
14 Washer #8 - 1
15 Screw #10-32 3/4" LG. 6
Concordia
MATERIAL
FINISH
DESIGNER D. HEBERT
DRAFTER K. SAVAGE
APPROVED
ALL DIMENSIONS IN mm UNLESS OTHERWISE SPECIFIED
SURFACE ROUGHNESS √63 UNLESS OTHERWISE SPECIFIED
TOLERANCES X ± 1 XX ± .05 XXX ± .025 ANGLE ± 30'
SCALE NTS
SIZE A
SHEET 1 / 1
DWG NO. 1
REV NO. 4
PART DESC ROTARY MR DAMPER ASSEMBLY
VERIFIED BY E. ABOUOBAIA
DATE 17-08-2014
USED ON PhD in MIE
PROPRIETARY INFORMATION. NOT TO BE RELEASED WITHOUT CONSENT FROM CONCORDIA UNIVERSITY

Appendix B

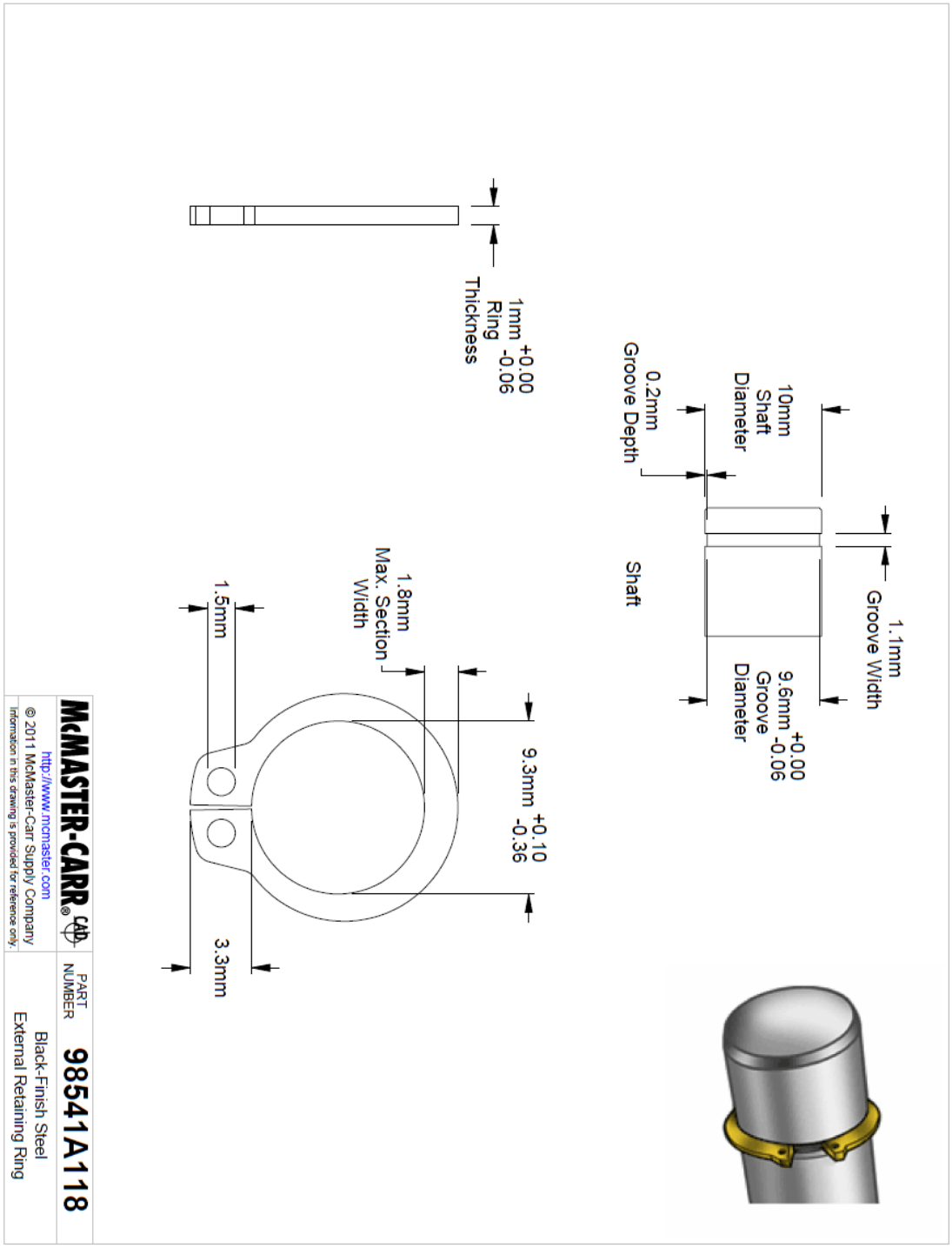
1.1mm
Groove Width
10mm
Shaft
Diameter
0.2mm
Groove Depth
9.6mm +0.00 -0.06
Groove
Diameter
Shaft
1mm +0.00 -0.06
Ring
Thickness
1.8mm
Max. Section
Width
9.3mm +0.10 -0.36
1.5mm
3.3mm
McMASTER-CARR
http://www.mcmaster.com
© 2011 McMaster-Carr Supply Company
Information in this drawing is provided for reference only.
PART NUMBER
98541A118
Black-Finish Steel
External Retaining Ring

Appendix C

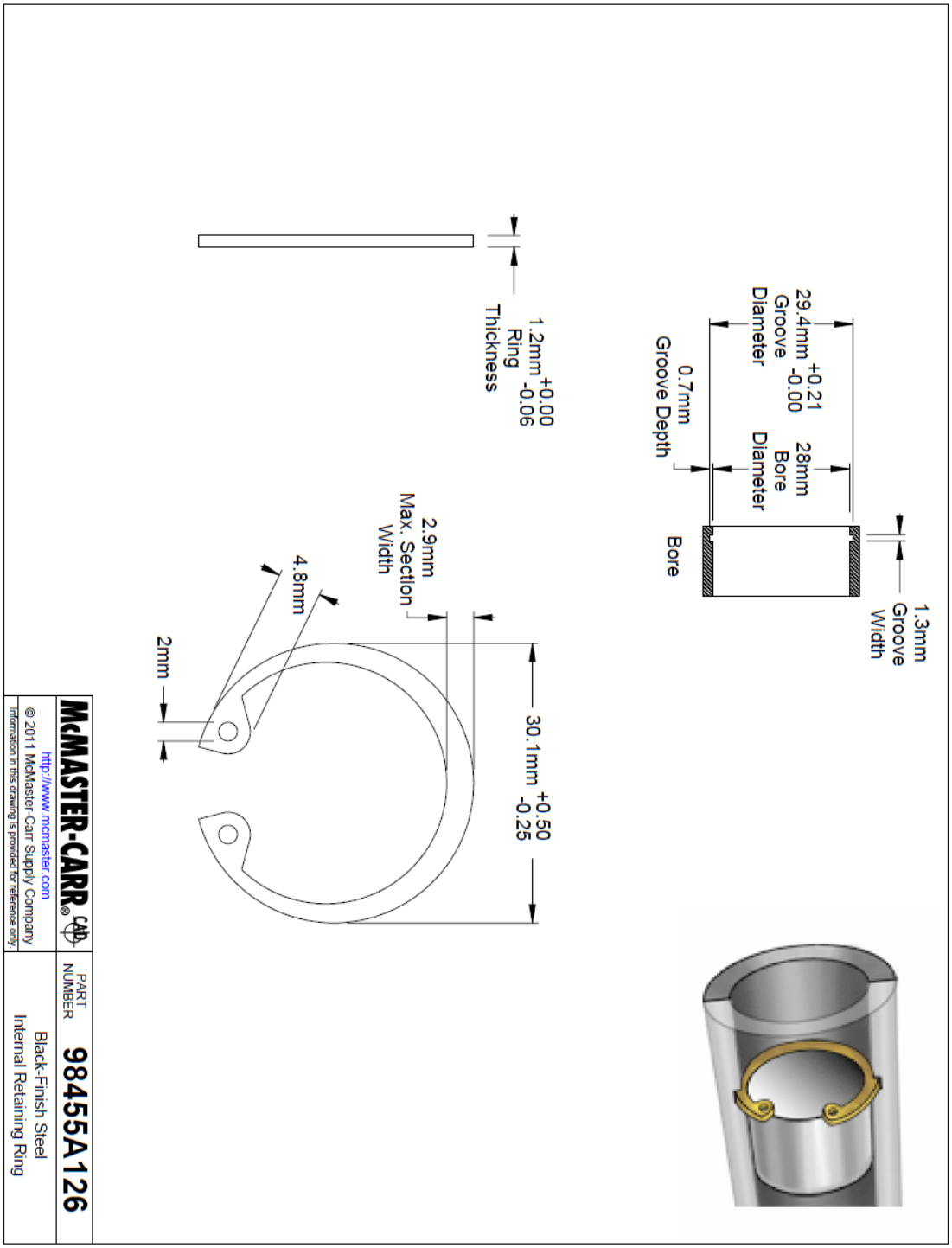
1.3mm
Groove
Width
29.4mm +0.21 -0.00
Groove
Diameter
28mm
Bore
Diameter
0.7mm
Groove Depth
Bore
1.2mm +0.00 -0.06
Ring
Thickness
2.9mm
Max. Section
Width
4.8mm
2mm
30.1mm +0.50 -0.25
McMASTER-CARR
http://www.mcmaster.com
© 2011 McMaster-Carr Supply Company
Information in this drawing is provided for reference only.
PART NUMBER
98455A126
Black-Finish Steel
Internal Retaining Ring

Appendix D

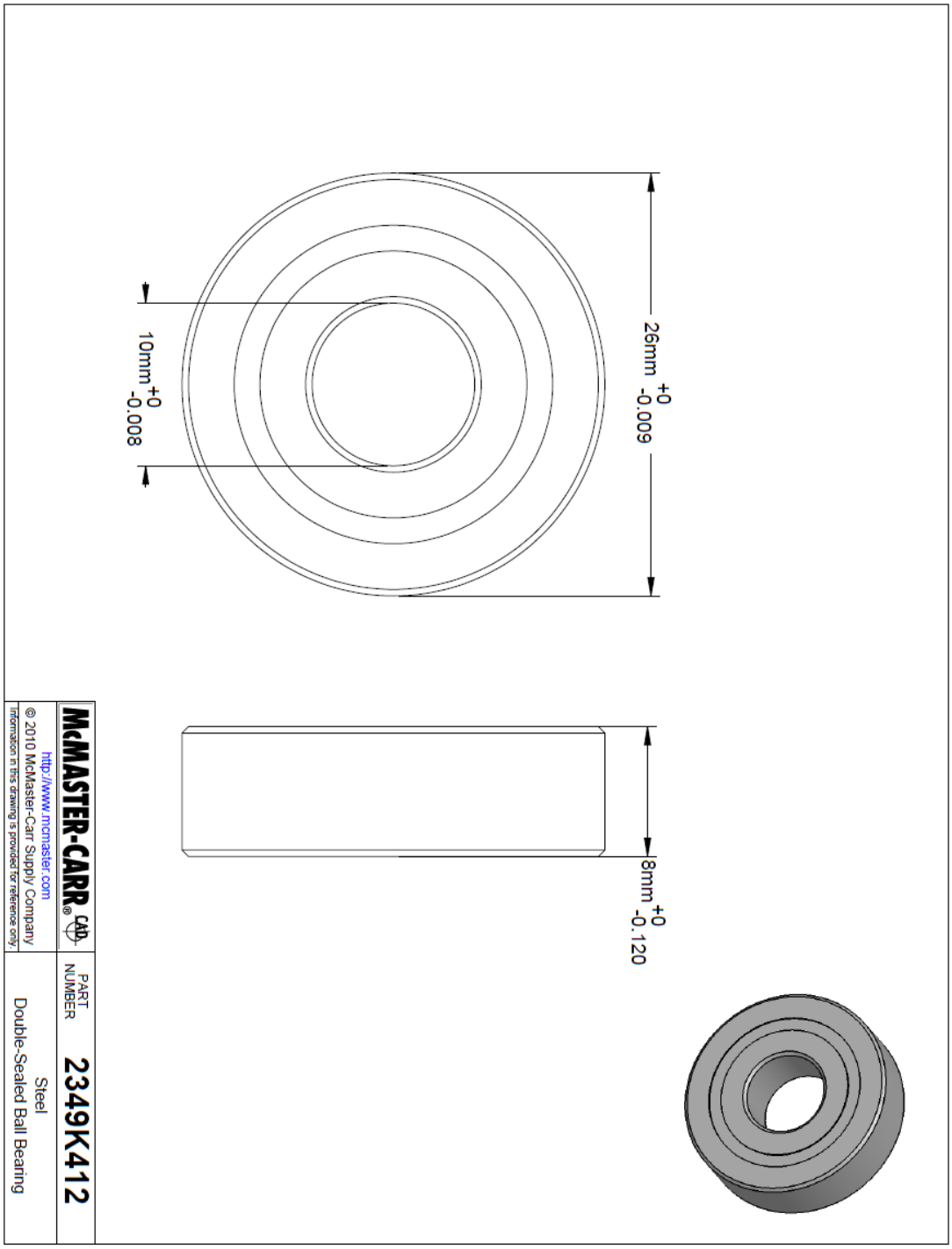
26mm +0 -0.009
10mm +0 -0.008
8mm +0 -0.120
McMASTER-CARR
http://www.mcmaster.com
© 2010 McMaster-Carr Supply Company
Information in this drawing is provided for reference only.
PART NUMBER
2349K412
Steel
Double-Sealed Ball Bearing